Mon. Not. R. astr. Soc. (1989) **236**, 653–708

The effective temperatures and colours of G and K stars

R. A. Bell *Astronomy Program, University of Maryland, College Park, Maryland 20742, USA*

B. Gustafsson *Uppsala Universitets Astronomiska Observatorium, Box 515, S-751 20 Uppsala, Sweden*

Accepted 1988 August 22. Received 1988 August 22; in original form 1988 April 14

Summary. Temperature scales are found for G and K dwarf and giant stars, using new tables of synthetic infrared colours as well as the infrared flux ratio method. The temperatures of 95 individual stars are given. The colours are presented for grids of flux constant, line blanketed models. One grid has been published previously, as have some colours for the visible region of the spectrum. The models of this grid are in the range $4000\ K < T_{eff} < 6000\ K$, $0.75 < \log g < 3.00$, $-3.0 < [A/H] < 0.0$. A grid of dwarf models, with the same temperature and abundance range but with $3.75 < \log g < 4.5$ is also used. The colours are computed from two series of overlapping synthetic spectra, which have been calculated with a resolution of 0.1 Å between 3000 and 12 000 Å and 1.0 Å between 0.9 and 6.0 μm.

The following colours and magnitudes are presented: Glass $J-H$, $H-K$, $K-L$ and K; Cohen, Frogel & Persson $J-H$, $H-K$, $K-L$ and K; Johnson $V-J$, $V-K$, $V-L$ and K; Cousins $V-R$, $R-I$; Johnson & Mitchell 13-colour and Wing's near-infrared eight-colour photometry. The colours are given relative to Vega. Near-infrared synthetic scans, using Oke's 50 Å bandpasses, are also given. In an appendix, transformation equations between several of the different systems are compared with those found from observational data.

1 Introduction

It is obvious from the recent literature (for example, Lambert & Ries 1981; Kjærgaard *et al.* 1982; Frisk *et al.* 1982) that the problem of determining red-giant temperatures is an important one that has still not been satisfactorily solved. It plays a vital role in the analysis of molecular lines and other temperature-sensitive spectral features, which are used to find stellar abundances and gravities. Recent advances in quantitative high-resolution stellar spectroscopy, which can in principle admit abundance analysis with an accuracy better than 0.1 dex for an individual element, have sharpened the requirements for accurate effective temperatures. The major aim of the present paper is the determination of the temperature scale of G and K stars. This problem has been treated in three different ways. First, the so-called infrared flux method of Blackwell & Shallis (1977) has been applied: the integrated fluxes of stars relative to their *K*-band fluxes were used as temperature indicators, calibrated with model-atmosphere calculations. Secondly, observed and computed colours have been compared. Finally, an attempt to establish a relation between spectral type and effective temperature by classification of synthetic spectrograms has been attempted, and will be discussed in a separate paper.

Observations of late G and K stars in the infrared are of great value for finding the temperatures of these cool stars, since they have their flux maxima in this wavelength region and their spectra are clean enough to provide well-defined continuum regions, in contrast to the visible region. For these reasons, broad-band near-IR colours are very good temperature criteria, being relatively independent of gravity and abundance (we define near-IR to refer to wavelengths between 0.7 and 1.0 μm). The flux curves are also quite temperature sensitive in the near-IR regions, in contrast to the longer wavelength regions. However, the use of all infrared observations to determine temperatures is non-trivial; the blocking from stellar and terrestrial spectral lines still presents serious problems that have to be overcome in accurate analyses.

The colours and flux ratios are given for the model atmospheres in the grid of yellow and red giant models published previously (Gustafsson *et al.* 1975, hereafter GBEN75; Bell *et al.* 1976, hereafter BEGN76). In addition, we also present infrared colours for a set of dwarf models, computed using the methods and programs of GBEN. Some colours have been published for these models by VandenBerg & Bell (1985, hereafter VB85) and Bell & VandenBerg (1987). Some information on the visible colours of the models is given. While most of this information is new, some is an improvement over the values given earlier in a compilation of model colours (Bell & Gustafsson 1978, hereafter BG78; Gustafsson & Bell 1979, hereafter GB79). The effect of telluric absorption lines has been included in the calculations, by multiplying the synthetic stellar spectra with the Kitt Peak winter atmospheric transmission computed by Manduca & Bell (1979). However, at least using the methods and programs of Manduca & Bell, the infrared magnitudes are not particularly dependent on the choice of site, provided they are individually normalized to Vega. For example, calculations for Mauna Kea give results which agree with the Kitt Peak winter magnitudes to better than 0.01 mag for Johnson *J*, *K* and *L*.

Synthetic spectra and colours have been computed for one other model, the Vega model of Dreiling & Bell (1980). The latter model has been used to establish the colour zero points, by requiring that the colours of Vega (HR 7001) be the colours of this model. (The same zero points were adopted by VB85.) The zero points are thus different from those used by BG78 and GB79, where ϕ^2 Ori (HR 1907, K0III) was used as the zero-point star. While the present treatment does rely more heavily on knowledge of the sensitivity functions of the various filter systems, the Vega model can be much more extensively tested than can the ϕ^2 Ori model. The Vega model does give a very good fit to the observations, while the blue and violet fluxes for red giant models are too bright, probably owing to inadequacies in the atomic and molecular line data which is available for the calculations. This problem exists for the ϕ^2 Ori model. However, more recent work on the sensitivity function of the *U* band of the *UBV* system does suggest that the deficiencies in *U–B* colours found by GB79 were exaggerated by the use of the Matthews & Sandage (1963) sensitivity function – see Bessell (1986a). The use of Vega as the zero-point star will allow these problems to be explored.

The colours presented by VB85 differ from those presented here in some respects. The synthetic spectra used by VB85 were computed using a turbulent velocity of 1 km s^{-1}, whereas those of the present paper (and BG78) use a Doppler Broadening Velocity (thermal and turbulent) of 2 km s^{-1} for lines other than those of C, N, O and their hydrides. This velocity is taken to be constant with optical depth. The Cousins' colours and Johnson *V* magnitudes were calculated by the same routines for VB85 and the present paper.

The sensitivity functions of the *R*, *I* passbands of the *UBVRI* system of Johnson appear to be poorly known, with Sopar & Malyuto (1974) suggesting the I_J band is about 1000 Å to the red of Johnson's profile. Our colours calculated using the Johnson profiles do not match the observations, whereas calculations in the same spectral region for other systems are satisfactory. For this reason we have found it necessary to discuss transformations between colour systems in detail.

The synthetic colours presented below have been computed under a variety of assumptions and approximations. For example, the model atmospheres are homogeneous and plane-parallel. The fluxes and colours are computed using LTE and, in general, using a limited list of atomic and molecular line data, containing about 125 000 lines altogether. A further 200 000 lines of TiO were added for the calculation of fluxes and colours for some of the 4000 K models, the data having been assembled by Lengyel-Frey (1977). It is known that some computed colours are erroneous; for example, the $B-V$ colour of the solar model (0.616) is bluer than the colour of the Sun [$0.63<(B-V)<0.69$, Hayes 1985]. It is clearly desirable to explore different ways of finding effective temperatures, in order to map out regions where particular colours give the most reliable results. *A priori*, one would expect that the well-defined narrow-band colours in the near infrared, and the IR broad-band colours, which are not so well defined but have a broader wavelength base, would be well suited, due to the small blocking of spectral lines, but this suitability remains to be proven.

For a few stars, e.g. Vega, angular diameters are known with sufficient precision that the flux measured at the Earth in a particular bandpass can be converted to the flux in that bandpass radiated by the star. Comparison with model fluxes then gives the stellar temperature. This approach is feasible for very few stars. In general, it is necessary to use the ratios of fluxes in different bandpasses, i.e. either to use colours or to use the ratio of the observed integrated flux to that observed in a particular bandpass. This latter bandpass is frequently chosen to be an infrared one, in order to exploit the relatively small sensitivity of the infrared flux to uncertainties in model atmospheres and opacities. The method (called the IR flux method or IRFM below) has been used for many different kinds of stars.

The strategy of the present study is as follows: We establish a set of comparison stars within the spectral interval G0–K5, and of luminosity class II–V. These stars are selected such that their IR colours are relatively well observed and their fundamental parameters, in most cases, relatively well known. A group of standard stars in the MK spectral classification system is also included. In practice, these requirements will limit us to essentially Population I stars, with some representation from Intermediate Population II.

For the stars in the set, we determine the effective temperatures by the IR flux method and, alternatively, from a comparison between suitable observed and calculated colours. After a discussion of the different temperature scales that result from this, a choice is made and established as our preferred scale – this is then used in further comparisons with observations and for calibrating additional photometric temperature indices and spectral types.

Photometric CO indices and *IRAS* fluxes of G–K stars will be treated in subsequent papers.

2 Calculations of synthetic spectra and colours

2.1 MODEL ATMOSPHERES

The model atmospheres used for this work were computed, including the effects of both atomic and molecular lines. Atomic lines with wavelengths <7200 Å were included, although the effects of lines shortward of 3000 Å were estimated from line data at longer wavelengths. The molecular systems considered included infrared CN and CO, as well as bands of C_2, CH, OH, NH and MgH at shorter wavelengths. The effects of water vapour have not been included in the calculations of the model atmospheres. Calculations of synthetic spectra, using Auman's (1967) opacities, confirm that this omission is justified for the models in our grid ($T_{\rm eff} \geq 4000$ K).

2.2 SYNTHETIC SPECTRUM CALCULATIONS

The models and synthetic spectra and colours were calculated with different overall heavy-element abundances M/H, but the abundances of all elements heavier than He were changed in unison. Thus, the non-solar C/Fe and N/Fe ratios found in red giants as a probable consequence of CNO burning and subsequent dredge-up (Lambert & Ries 1981; Kjærgaard *et al.* 1982) were not allowed for, nor were the tendencies for metal-poor stars to show abundances of O, Mg, Si and Ca relative to Fe to be greater than those of Population I (Clegg, Lambert & Tomkin 1981; Tomkin, Lambert & Balachandran 1985; Nissen, Edvardsson & Gustafsson 1985). The neglect of such non-solar abundance ratios on the infrared colours and fluxes are relatively small – some sample calculations with changes in C and N abundances were given in BG78. The effects on the effective temperature scales are discussed further below.

In previous work we have attempted to use mainly oscillator strengths which were based on laboratory measurements. Since accurate measurements are available for only a small number of lines, we have had to use them to obtain correction factors which we have applied to the more extensive series of measurements. We have also had to utilize stellar spectra, particularly the solar spectrum, to obtain additional line data. A study of the data available in the infrared showed a dearth of laboratory data when a synthetic spectrum was compared with the observed spectrum. In order to obtain the necessary data in a convenient manner, we have utilized the compilation of Kurucz & Peytremann (1975, KP), which gives wavelengths, identifications, lower excitation potentials and oscillator strengths for many lines. These calculated oscillator strengths have been compared with laboratory values by several workers, e.g. Smith (1976) and Blackwell, Petford & Shallis (1979). This showed that while many of the KP lines have oscillator strengths which are precise enough for our purposes, others do not. Consequently, in order to detect erroneous *gf*-values and to see if lines were missing, we computed a number of synthetic solar infrared spectra. The process of checking these spectra with the observed solar spectrum tracings would have been extremely tedious, since the observations were not available in digital form at the time that this work was done, and so we used the tabulation of solar-line wavelengths and intensities by Swensson *et al.* (1970).

A comparison of lines expected in the solar spectrum, computed using the KP list, with the identifications of Swensson *et al.* showed that about 130 lines with intensities greater than 10 (on the Swensson *et al.* scale) were missing from the KP list. The lower limit of 10 in intensity corresponds to an equivalent width of $W_\lambda = 10$ mÅ. 'Astrophysical oscillator strengths' for these lines were then determined from a comparison between observed and calculated solar lines, the latter being based on calculations with the HSRA solar model. These lines were then added to our list. No systematic attempt was made to refine the treatment of the weaker lines. The wavelength interval treated was 7200–12 000 Å. Beyond this wavelength, the KP lines were used without being checked.

In addition to the atomic lines, we have included molecular lines for CN, CO, SiO, OH, C_2, H_2O and TiO. Isotopic lines of CH, C_2, CO, CN and TiO were included, the isotopic abundance ratios of C and Ti being taken to have their terrestrial values. The molecular lines were treated individually in all cases, except for H_2O, where the data of Auman (1967) were used. While included in the synthetic spectrum program, water vapour lines do not affect the spectra of these relatively warm stars significantly and are not expected to have any influence on the temperature structures. The sources of molecular line data are given in Table 1.

Table 1. Molecular dissociation energies and oscillator strengths.

Molecule	D_0(ev)	Band	f_{00}	Reference
C_2	6.12	Swan	0.0262	
CH	3.47	A-X	0.0055	
		B-X	0.0041	
		C-X	0.0075	
CN	7.50	Red	0.0046	
		Violet	0.0662	
NH	3.80	A-X	0.0021	
OH	4.40	A-X	0.0018	
MgH	1.27	A-X	0.161	Balfour & Cartwright (1976)
TiO	6.78	α	0.077	Davis, Littleton & Phillips (1986, DLP86)
		β	0.255	DLP86
		γ	0.119	DLP86
		γ'	0.10	DLP86

The data is from Bell & Gustafsson (1978) except where otherwise indicated. The values for the TiO α and γ systems are for the $1-0$ and $2-0$ bands, respectively, converted to f_{00} using the zero rotation Franck-Condon factors of Bell *et al.* (1979).

A general discussion of the methods used to compute the synthetic spectra has been given by BG78, who also give the sources of the atomic and molecular lines. We have made no important changes to the computer program used for these calculations.

The dominant opacity source in the infrared is H^-. We have used the polynomial fits, given by Gray (1976) and Dreiling (unpublished) respectively, to the bound–free and free–free calculations of Geltman (1962) and Bell, Kingston & McIlveen (1975). The polynomial fit for the bound–free absorption agrees with the Doughty & Fraser (1966) results to within 2 per cent over the wavelength interval 4000–15 000 Å and to within 5 per cent of the results of Wishart (1979) between 3500 and 15 000 Å. The Bell, Kingston & McIlveen calculations are systematically smaller than those of Stilley & Calloway (1970), by about 4 per cent at 6300 K, while the difference with Doughty & Fraser (1966) is greater and shows a stronger wavelength dependence. In addition, the dipole velocity formula gives a cross-section which may be as much as 5 per cent smaller than that given by the dipole length formula. The effects of some of these uncertainties in the H^- free–free opacity upon the emergent fluxes of the models have been described by Frisk *et al.* (1982) and by Munduca, Bell & Gustafsson (1981), and are illustrated further in the present paper. The uncertainty in these values causes an error in the temperature deduced from near-infrared photometry for α Boo (HR 5340), for example, of 50 K.

The synthetic spectra were computed for the interval 0.3–1.2 μm, with a separation of 0.1 Å between successive flux calculations, and for the interval 0.9–6.0 μm, where a separation of 1.0 Å was used. The first was used for photometric systems in the visual and near infrared, while the second set was used for systems extending from the *J* band towards longer wavelengths.

2.3 COLOUR CALCULATIONS

The colours are computed from integrals of the form

$$\int F(\lambda)\, S(\lambda)\, A(\lambda)\, d\lambda,$$

where $F(\lambda)$ is the flux radiated by the model, $S(\lambda)$ is the sensitivity function of the telescope–filter–photometer system and $A(\lambda)$ is the transmission of the Earth's atmosphere. If needed, the contribution of interstellar reddening can also be included.

The sources of the sensitivity function data adopted for the various colour systems are:

(i) Johnson *JKL* – Johnson (1965);
(ii) Cousins *VRI* – Cousins (1980), with some tests using Bessell's (1983) values;
(iii) Glass *JHKL* – Glass (1973);
(iv) Wennfors *JHKL* – Wennfors (1986);
(v) Johnson, Mitchell and Latham (1967), and Johnson and Mitchell (1975), 13 colour – Johnson & Mitchell (1975), and
(vi) Frisk – Frisk (private communication).

In addition, a few test calculations were made using the Sopar & Malyuto (1974) representation of the Johnson *R* and *I* passbands.

We have used the treatment of Hayes & Latham (1975) to compute the atmospheric extinction due to Rayleigh scattering by molecules and scattering by aerosols. The effects of terrestrial line absorption at wavelengths greater than 7600 Å have been included, by using the Manduca & Bell (1979) computations of the winter extinction at Kitt Peak. The terrestrial spectrum has been computed using a single-layer approximation of the Earth's atmosphere (see Traub & Stier 1976) and the Air Force Cambridge Research Laboratory's atmospheric absorption line tape (McClatchey *et al.* 1973). The resultant transmission at the zenith is averaged over 100 Å intervals. In the present paper, we have not attempted to treat the line extinction in detail by computing colours at different air masses but have simply applied the zenith transmission of the Kitt Peak winter atmosphere to the individual sensitivity functions. This should give a reasonable correction for the absorption of stellar radiation by the O_2A band, the various H_2O bands and other features. In addition, a few calculations were carried out excluding the line absorption in the atmosphere. With the colours again normalized to Vega, it was found that only small differences (<0.02 mag.) occurred in $J-H$ and $H-K$ of the Caltech–CTIO system.

As noted above, ϕ^2 Ori was used to establish the zero points of the colours in previous work. This led to the colours of the Vega model being different from those of Vega. Since Dreiling & Bell (1980) have shown that their Vega model gives a good fit to the observed Vega fluxes in the visible and near-IR, the model colours should match the observations of Vega very well. In the following discussion we normalize the colours so that the fit of the model $T_{\rm eff}/\log g/[{\rm A/H}]=9650/3.9/0.0$ to Vega is perfect.

While the colours presented in this paper are based upon using Vega as the zero-point star, there is the possibility that this may cause systematic errors. If Vegas has $T_{\rm eff}=9350$ K, instead of 9650 K, the infrared colours which are presented subsequently will alter. However, the changes are small – $V-K$ will become bluer by 0.03 mag and $J-K$ by 0.015 mag. The data presented later show that the uncertainty of 250 K in the $T_{\rm eff}$ of Vega quoted by Dreiling & Bell produces colour changes which are small in comparison with the range in colour shown by G and K giants. The inconsistency in the relative $V-J$ and $V-K$ colours of Sirius and Vega, noted by Bell & Dreiling (1981) appears to have been removed by subsequent observations at the Anglo–Australian Observatory by D. A. Allen (private communication) and at Palomar by J. H. Elias *et al.* (private communication). However, the question of the absolute calibration of the infrared radiation from Vega has not yet been settled.

It has been argued (Leggett *et al.* 1986a) that the infrared colours of Vega agree with those of other A0V stars, but the significance of this is uncertain. Dreiling & Bell (1980) found Vega to be metal deficient, at least so far as iron and titanium are concerned. This result has recently been confirmed for iron by Gigas (1986). While the determination of the spectral type of Vega is not dependent on the strengths of iron lines, it seems possible that if Ca, Mg and Si are also deficient the actual determination of the spectral type of Vega will be affected by this abundance deficiency. The much higher metal abundance of Sirius causes it to have a later spectral type than Vega does, despite being hotter.

We have not studied the temperature differences that might exist between Vega and other A0V stars as a result of abundance differences. Clearly, Vega may be cooler than other A0V stars. However, since the infrared colours for early A stars are not very sensitive to temperature, as shown above, it is hard to confirm these temperature differences with infrared photometry.

There have been few published tests of the predictions of model stellar atmospheres in the infrared. The principal tests to date involve checks of models and observations of Vega. These have shown reasonably good agreement (e.g. Selby *et al.* 1983, and the comments on this work by Saxner & Hammarbäck 1985) but there may be discrepancies which are as large as 5 per cent in the fluxes. It is not certain whether the discrepancies are effects of the dust emission which is prominent at longer wavelengths (Aumann *et al.* 1984) or are due to errors in the measurements or a fundamental difficulty with the models. Blackwell *et al.* (1986) compare the Tenerife calibration with the Vega model in their analyses of α Boo and μ Her. The critical point for the present paper is at 2 μm, where one of the Mountain *et al.* (1985) calibration points agrees with the Vega model and the other is about 3 per cent greater.

Dr S. Ridgway kindly sent us KPNO FTS scans of a number of stars, including Vega. This gave us the opportunity to compare observed and computed Brackett-lines profiles for this object for Br γ, Br11, Br12, Br13 and Br14, the profiles being computed using the Stark-broadening coefficients of Edmonds, Schluter & Wells (1967). The fit is satisfactory. This data would be of value in testing future non-LTE model calculations for Vega. The Brackett lines have been included in the synthetic spectrum and colour calculations. They occur in the H bandpass and therefore affect the zero point of the H magnitudes.

2.4 COMPARISON OF OBSERVED AND COMPUTED FLUXES

In order to check the reliability of our flux calculations for both Vega and for the late-type stars, we have compared model and observed fluxes in the ultraviolet, visible and near-IR. Similar comparisons were made for longer wavelengths by Manduca *et al.* (1981). Cochran (1980) has observed several of the stars for which we subsequently derive effective temperatures. These observations are in the wavelength interval 4600–10 250 Å. In order to make the comparison at shorter wavelengths, we have used the data of Gunn & Stryker (1983).

Fig. 1 shows a comparison of the flux from the Vega model and the A0V star θ Vir (HR 4963). No attempt has been made to choose the best possible model for fitting the star, apart from Vega and θ Vir having the same spectral type. For the purposes of the present paper, the wavelength region of interest is from the V-band region to greater wavelengths, e.g. 4600 Å onwards. No significance is attached to the dip seen in the observations between 5000 and 5500 Å – this is believed to be a small error in the observations, on the basis of comparison of the Vega model to other A stars. The fit of the Paschen lines appears to be reasonably satisfactory and suggests that Vega can be used to normalize theoretical photometry, even in the region of the Paschen discontinuity around 9000 Å.

The models 5000/3.00/0.0, 4500/2.25/0.0 and 4000/1.50/0.0 are compared with the stars HD 152306, 91 Aqr (HR 8841) and α Tau (HR 1457) in Figs 2, 3 and 4 for the Gunn–Stryker and Cochran photometry. The choice of the stars to be compared with the models has been made on the basis of $B-V$ colour. In this sense one would expect a reasonably good fit. However, the alternative of choosing the stars on the basis of spectral type gives a misleading impression. This was shown by the comparison of θ^1 Tau (HR 1411) with 5000/3.00/0.0. The star has a very red $B-V$ (0.95) for its $V-K$ colour of 2.10. The models are found to be brighter in the ultraviolet than are the stars, as would be expected from experience with the Sun and other red giants (Gustafsson & Bell 1979).

2.5 THE INFLUENCE OF TiO LINES ON STELLAR COLOURS

The need to add TiO line data for the coolest (4000 K) giants was evident from the comparison of calculated fluxes with the observed fluxes published by Cochran (1980) and Gunn & Stryker (1983). Fig. 5 shows the necessity of including the effects of TiO in the giant star models with $T_{eff}=4000$ K, synthetic spectra computed both with and without TiO lines being plotted. Lines of the β system at 5500 Å, the γ' system at 6200 and 6600 Å, and the γ system at 7100 and 7600 Å, can be seen. These TiO lines were not included by BG78 and GB79 and affect the redder colours of the coolest stars. After studying the results of the molecular equilibria calculations, synthetic spectra were computed with TiO lines being included only for some trial calculations for the models with $T_{eff}=4000$ K and [A/H] = 0.0 and −0.5. The TiO systems included are from the α, β, γ and γ' systems. Lines of all five Ti isotopes are included, the relative abundances being in the terrestrial ratio. The relative strengths of the different band systems, i.e. the β, γ and γ' systems, seem to be rather well represented by the models, judging from Fig. 4. The δ and ϕ systems, which have lines in the 8800 and 10 000 Å regions, have not yet been included in the work.

In order to determine the influence of the TiO lines, the colours of spectra computed with and without TiO were compared. In general the effects are found to be quite small. However, in a few cases, e.g. the 7120 filter of the Wing system, the change resulting from the inclusion of TiO exceeds 0.1 mag. The colour and magnitude changes for the models 4000/0.75/0.0, 4000/2.25/0.0, 4000/0.75/−0.5 and 4000/2.25/−0.5 are given in Table 2 (*cf.* also Piccirillo, Bernat & Johnson 1981). Since some of the colours of solar abundance models in this table are quite strongly affected by the TiO lines, some models with $T_{eff}=4100$ and 4200 K were computed. None of the colours given in other tables are based on synthetic spectra which include the effects of TiO lines.

3 Selection of a sample of comparison stars

The sample of stars used for establishing the temperature scale and for further comparison with the computed colours consists of 95 bright giant, giant and dwarf stars which had been

Table 2. Colour and magnitude changes caused by the inclusion of TiO lines.

	Johnson			Cousins		Wing	
	V	B-V	V-R	V-I	R	7120	7810
4000/0.75/0.0	0.036	-0.057	-0.037	0.002	0.075	0.342	0.086
4000/1.50/0.0	0.048	-0.035	-0.032	0.005	0.078	0.342	0.094
4000/2.25/0.0	0.049	-0.064	-0.031	-0.005	0.090	0.382	0.110
4000/0.75/-0.5	0.000	-0.011	0.001	0.003	0.004	0.042	0.005
4000/1.50/-0.5	0.007	-0.011	-0.004	0.007	0.006	0.049	0.008
4000/2.25/-0.5	0.015	-0.010	-0.008	0.016	0.012	0.067	0.012

	Johnson and Mitchell 13 Colour					
	52	58	63	72	80	86
4000/0.75/0.0	0.021	0.045	0.074	0.104	0.034	0.003
4000/1.50/0.0	0.024	0.050	0.082	0.109	0.037	0.009
4000/2.25/0.0	0.017	0.058	0.086	0.125	0.043	0.010
4000/0.75/-0.5	0.003	0.002	0.005	0.008	0.000	0.000
4000/1.50/-0.5	0.017	0.003	0.005	0.011	0.002	0.000
4000/2.25/-0.5	0.031	0.008	0.010	0.018	0.004	0.000

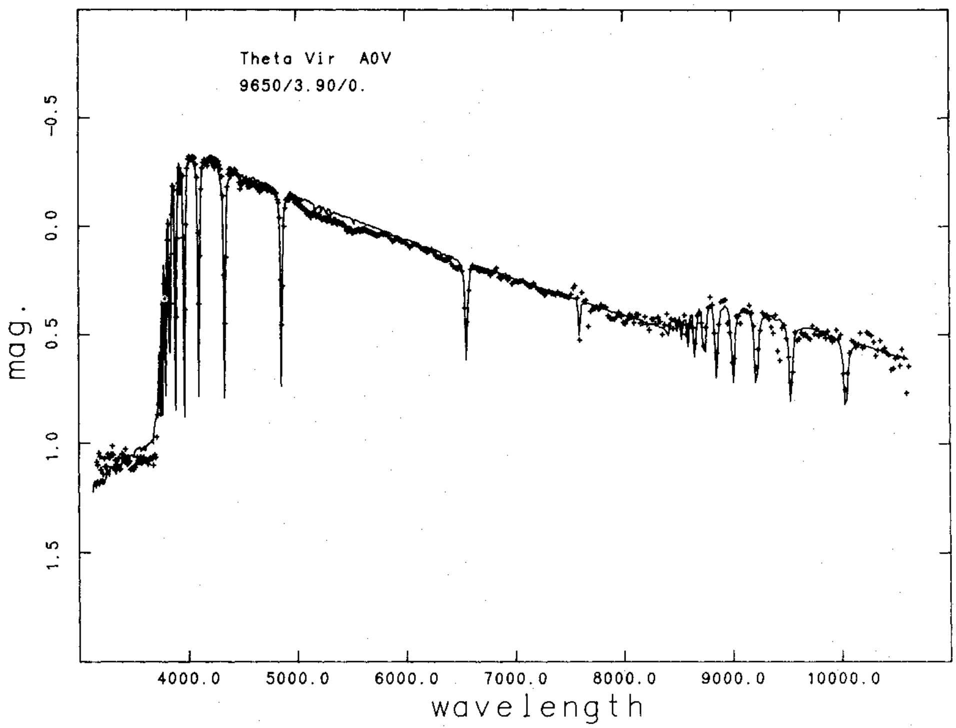

Figure 1. The fluxes of the model 9650/3.9/0.0 are compared with the Gunn & Stryker (1983) observations of the A0 *V* star *θ* Vir. The feature at 7700 Å, in this and in Figs 2–5, is the atmospheric *A* band.

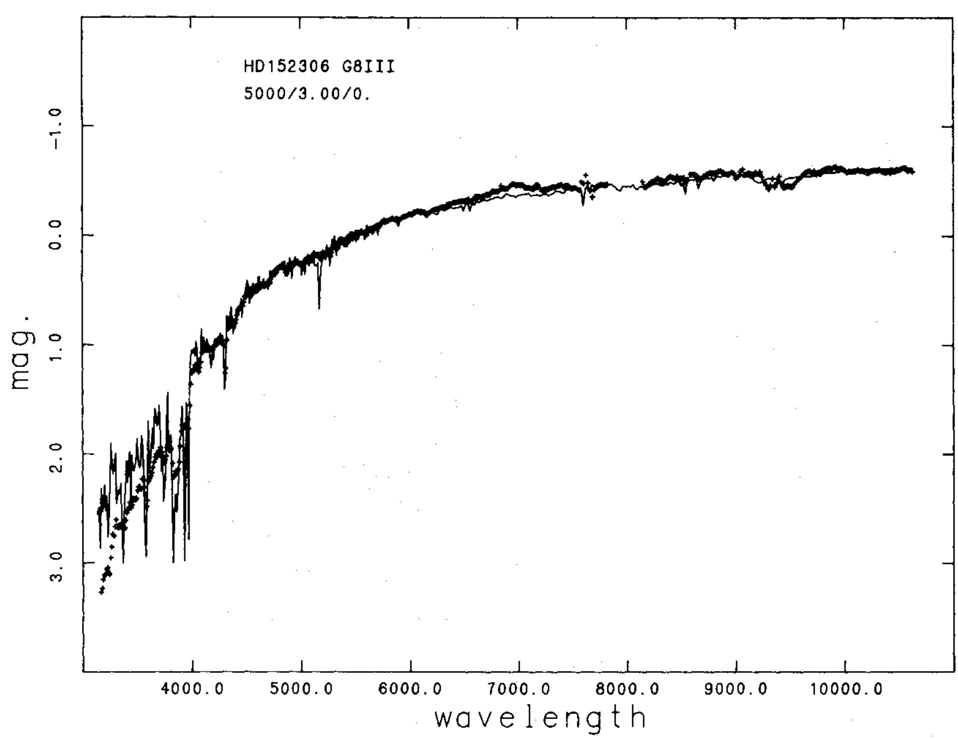

Figure 2. The fluxes of the model 5000/3.0/0.0 are compared with the Gunn & Stryker (1983) observations of the K0III star HD 152306.

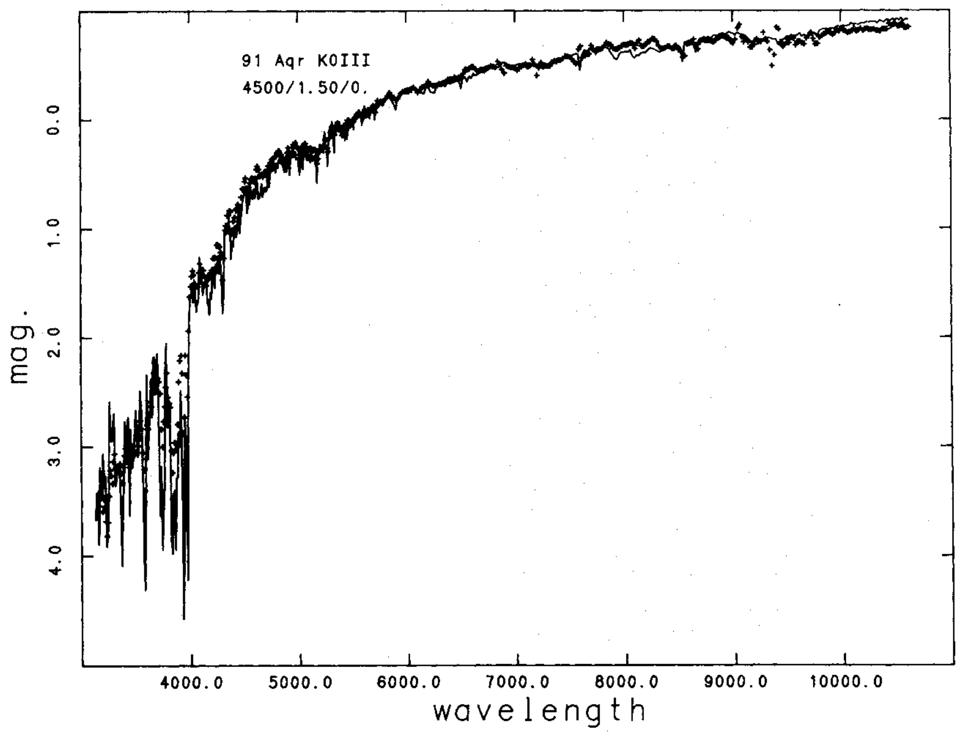

Figure 3. The fluxes of the model 4500/2.25/0.0 are compared with the Gunn & Stryker (1983) observations of the K2III star 91 Aqr.

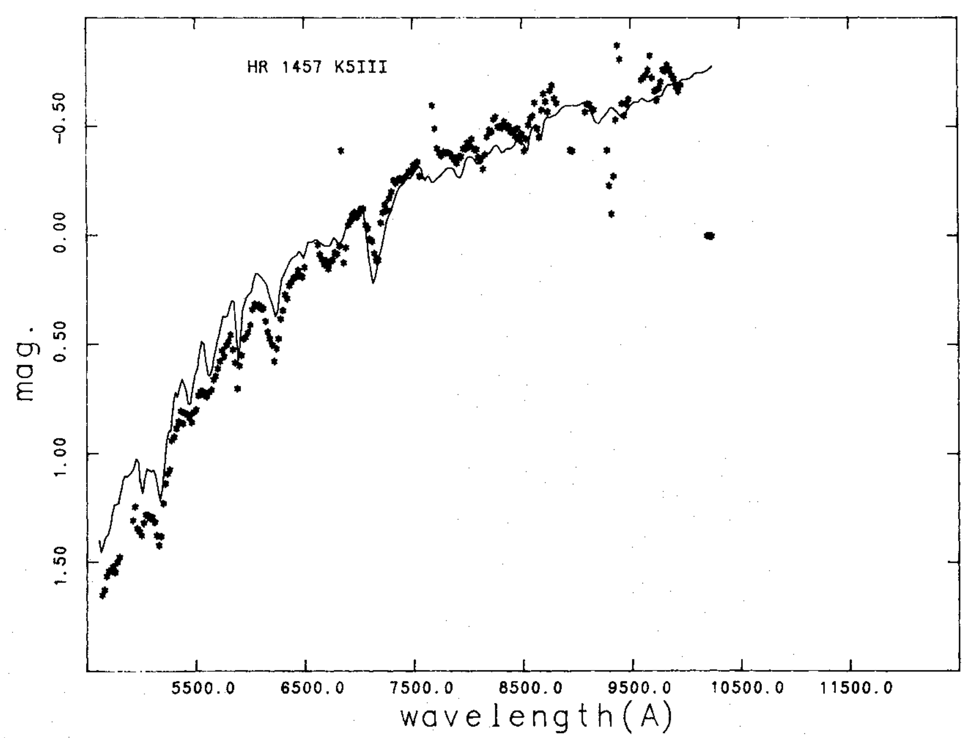

Figure 4. The fluxes of the model 4000/1.5/0.0 are compared with the Cochran (1980 observations of the K5III star α Tau.

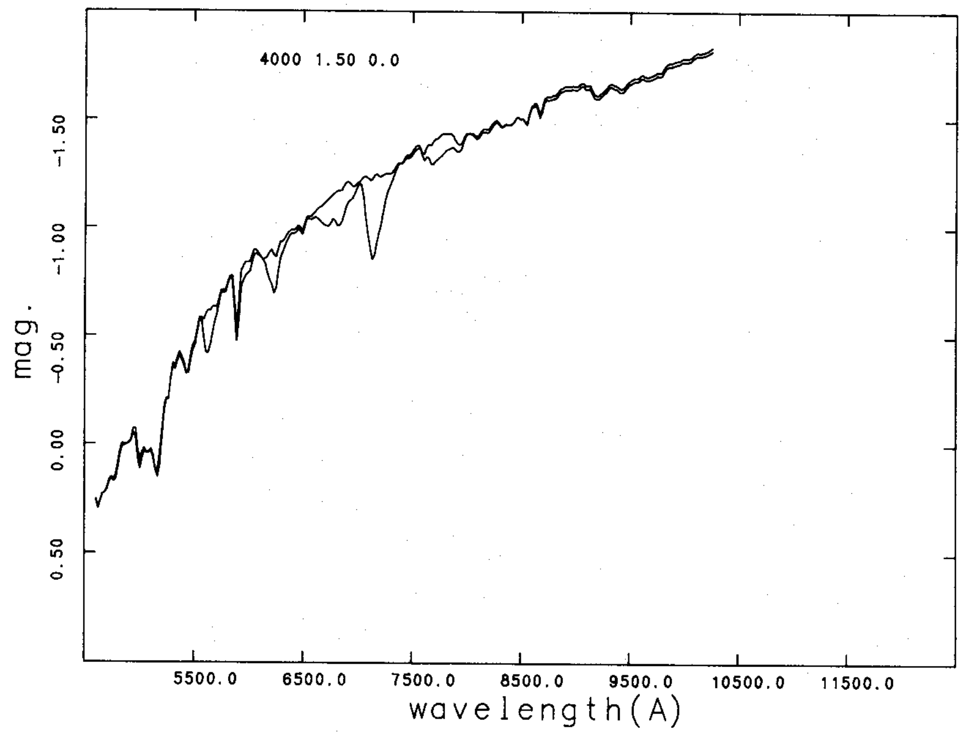

Figure 5. Synthetic spectra are compared for the model 4000/1.50/0.0. One has TiO lines included, the other does not. Lines of the β system at 5500, the γ' system at 6200 and 6600, and the γ system at 7100 and 7600 Å can be seen.

observed on the 13-colour system of Johnson, Mitchell & Latham (1967) and Johnson & Mitchell (1975) as well as in the Johnson *et al.* (1966) *JKL* system. The sample includes the G and K spectral classification standards of Keenan & McNeil (1976), the stars observed by the Kuiper Airborne Observatory by Strecker, Erickson & Witteborn (1979), and the stars with near-infrared colours in the systems of Wing (1971) and Frisk (1983), as well as α Boo and ϕ^2 Ori. The sample of dwarf stars was taken from Keenan & McNeil and from Frisk. The objects are listed in Table 3. Some of the stars in the sample have been observed by Glass (1974a,b). Unfortunately only a very few bright stars have been observed on the Caltech–CTIO system. These stars, and the mean colours published by Frogel *et al.* (1978) are discussed subsequently.

In selecting this comparison sample we also required that the gravity and overall metal abundance should be relatively well determined for most of the stars. These parameters were adopted from the spectroscopic and very narrow band analyses of Kjærgaard *et al.* (1982), Gustafsson, Kjærgaard & Andersen (1974), Nissen (1981), Frisk (1983), and, if not available in any of these sources, from the catalogue of Cayrel de Strobel *et al* (1985). If the star was not even listed there, but was found in the narrow-band determinations of Hansen & Kjærgaard (1971), we adopted their value for [Fe/H] (adjusted to a Hyades [Fe/H] = 0.16, following Gustafsson *et al.* 1974, in fair agreement with Branch, Lambert & Tomlin 1980 and with Cayrel, Cayrel de Strobel & Campbell 1985) and selected a surface gravity characteristic for the MK class in question, according to the log g values for the rest of the stars. For 20 of the stars no metal abundance determination was found in any of the sources listed – for these stars we assumed solar abundances. It will be seen below that this does not introduce any serious systematic errors in the comparisons between calculated and observed colours, which is due to the fact that the IR colours are not very sensitive to the metallicity.

Table 3. Standard stars in the T_{eff} determination.

Name	HR	Spectral Type	T_{eff} IRFM	T_{eff} adopted	F_{bol}	ϕ	log g	[Fe/H]	
η Cas	219	G0 V	5919	5839	119.3	1.76	4.4		D
χ^1 Ori	2047	G0 V		5842			4.41	-0.09	N
β CVn	4785	G0 V	5941	5861[1]	54.09	1.17	4.45	-0.25	N
β Com	4983	G0 V	6104	6024	55.09	1.12	4.47	0.27	C
16 Cyg A	7503	G1.5 V	5906	5826	11.33	0.54	4.30	0.00	C
70 Vir	5072	G2.5 Va		5602			3.75	-0.11	C
16 Cyg B	7504	G2.5 V	5744	5664[1]	9.31	0.52	4.40	0.00	C
κ^1 Cet	996	G5 V		5650			4.52	0.02	F
61 Vir	5019	G6 V		5650			4.5		
61 UMa	4496	G8 V	5632	5552	23.19	0.86	4.60	-0.14	C
σ Dra	7462	K0 V	5333	5253	42.49	1.29	4.50	-0.25	
o^2 Eri	1325	K1 V	5194	5114	56.09	1.57	4.65	-0.21	F
ε Eri	1084	K2 V	5236	5156	109.3	2.15	4.61	0.05	F
	753	K3 V		4775			4.6		
	8832	K3 V	4976	4896	22.42	1.08	4.50	0.00	C
61 Cyg A	8085	K5 V	4543	4463	39.43	1.73	4.50	-0.05	C
61 Cyg B	8086	K7 V	4332	4252[3]	25.33	1.53	4.60	-0.05	C
μ Her	6623	G5 IV-V	5607	5527	123.6	1.99	4.10	0.30	C
η Boo	5235	G0 IV	6128	6048	227.9	2.26	3.80	0.16	C
φ Vir	5409	G2 IV		5648			3.8		
β Aql	7602	G8 IV	5178	5098	105.0	2.16	3.56	-0.08	F
δ Eri	1136	K0 IV	5056	4976[1]	131.0	2.53	3.95	0.05	C
η Cep	7957	K0 IV	5076	4996	147.9	2.67	3.34	-0.17	F
κ CrB	5901	K1 IVa		4920			3.3		
24 UMa	3771	G4 III-IV	5359	5279	46.98	1.35	3.5	-0.08	F
δ CrB	5889	G5 III-IV		5608			3.10	-0.04	Fe-1
φ Cyg	7478	G8 III-IV		4976			3.2	-0.03	HK
θ Aqr	8499	G8 III-IV	5036	4956	73.58	1.91	2.80	-0.07	C
46 LMi	4247	K0 III-IV	4772	4692	112.4	2.64	3.0	-0.23	C
η Ser	6869	K0 III-IV	5029	4949	177.5	2.98	2.90	-0.08	CN1
γ Cep	8974	K1 III-IV		4904			3.10	0.04	KG
37 Lib	5777	K1 III-IV	4822	4742	52.36	1.76	3.20	-0.14	C
31 Com	4883	G0 III	5841	5761	30.50	0.91	3.00	-0.20	GKA
o UMa	3323	G5 IIIa	5256	5176	139.7	2.42	2.6	0.03	KG
υ^2 Eri	1464	G8 III	5054	4974	99.74	2.21			H
τ Aur	1995	g8 III	4996	4916	53.11	1.65		-0.35	HK
ε Vir	4932	G8 III	5132	5052	236.2	3.30	2.7	0.05	KG
β Boo	5602	G8 IIIa	5009	4929	134.4	2.61	2.30	0.04	KG Ba 0.4
δ Boo	5681	G8 III	4912	4832	142.3	2.80	2.60	-0.32	KG CN-1
71 Oph	6770	G8 III		5120			2.9	-0.21	
η Her	6220	G8 IIIb	4993	4913	131.9	2.61	2.70	-0.13	KG CN-1
μ Peg	8684	G8 III	5124	5044	131.6	2.47		-0.14	HK
ν Leo	4471	G8.5 III	4882	4802	67.56	1.95	2.80	-0.24	GKA CN-0.5
θ Lib	5908	G8.5 IIIb	4862	4782	81.82	2.17	2.90	-0.24	C
ε Tau	1409	G9.5 III	4976	4896	133.1	2.64	2.5	0.16	KG
ϕ^2 Ori	1907	K0 IIIb	4799	4719	86.55	2.29	2.7	-0.54	KG CN-2
δ Aur	2077	K0 III	4911	4831	114.0	2.51	2.8	0.02	GKA
β Gem	2990	K0 IIIb	4976	4896	1236.	8.04	2.8	-0.01	KG
α UMa	4301	K0 IIIa	4735	4655	720.2	6.79	2.2	-0.19	C
η Cyg	7615	K0 III	4967	4887	96.90	2.26	2.5	0.11	KG
ι Cep	8694	K0 III	4910	4830	146.0	2.84	2.7	0.11	KG
π^2 Uma	3403	K1 IIIb		4542			2.4		
39 Ari	824	K1 III	4716	4636	60.91	1.99		0.03	HK
ψ UMa	4335	K1 III	4622	4542	247.3	4.18	2.3	0.03	KG
λ Sgr	6913	K1 IIIb	4754	4674	282.1	4.21			
ξ^2 Ser	7150	K1 III	4723	4643	157.9	3.19			
72 Cyg	8255	K1 III	4795	4715	43.30	1.62	2.	0.25	C
α Ari	617	K2 III	4579	4499	652.0	6.91	2.5	-0.25	C
β Col	2040	K2 III	4599	4519	224.6	4.02			
χ UMa	4518	K2 III	4501	4421	144.0	3.36	2.00	-0.3	KG
ε Crv	4630	K2 III	4418	4338	294.4	4.99			
γ Com	4737	K2 III	4761	4681	69.83	2.09		0.17	HK CN+1
π Hya	5287	K2 III	4733	4653[2]	201.9	3.59			CN-0.5
α Boo	5340	K2 IIIp	4401	4321	5159.	21.07	1.8	-0.51	KG
α Ser	5854	K2 III	4636	4556	353.8	4.96	2.6	0.18	KG
ε CrB	5947	K2 III	4430	4350	99.98	2.90		-0.05	HK
κ Oph	6299	K2 III	4651	4571	209.2	3.79	2.50	-0.09	KG
β Oph	6603	K2 III	4683	4603	310.8	4.56	2.5	0.18	KG
51 And	464	K3 III	4505	4425	167.3	3.62	2.1	0.12	KG
ρ Boo	5429	K3 III	4383	4303	175.3	3.92	1.5	-0.50	KG
μ Aql	7429	K3 IIIb	4536	4456	69.71	2.30	2.2	0.08	C,HK
39 Cyg	7806	K3 III	4366	4286	84.60	2.74	1.9	0.09	HK
31 Leo	3980	K3.5 IIIb	4172	4092	108.6	3.41			Fe-1
μ Psc	434	K4 III	4126	4046	68.40	2.77		-0.50	HK,D

Table 3. – *continued*

Name	HR	Spectral Type	T_{eff} IRFM	T_{eff} adopted	F_{bol}	Φ	log g	[Fe/H]	
θ CMa	2574	K4 III	4070	3980	144.4	4.13	1.9	-0.03	C
β Cnc	3249	K4 III	4111	4031	234.9	5.17	1.87	-0.21	C Ba0.5
β UMi	5563	K4 III		4050			1.6	-0.14	KG
μ Hya	4094	K4.5 III	4108	4028	193.2	4.69		-0.20	HK
ζ^2 Sco	6271	K4 III		4164			1.8		
δ Psc	224	K5 III	3998	3918	117.9	3.87		-0.07	HK V?
α Tau	1457	K5 III	4023	3943	3422.	20.62	1.2	-0.10	C
γ Dra	6705	K5 III	4035	3955	890.6	10.45	1.55	-0.23	
α Hya	3748	K3 II-III	4221	4141	872.8	9.44	1.86	-0.19	C
ε Leo	3873	G1 II	5379	5299	194.2	2.72	2.4	-0.13	C
α Sge	7479	G1 IIb	5509	5429	52.39	1.35			
37 LMi	4166	G2 IIa		5590			2.0		
β Sct	7063	G4 IIa	4782	4702[2]	81.89	2.24			
θ Lyr	7314	K0 II	4581	4501	78.50	2.40	1.72	-0.20	C
σ Oph	6498	K2 II	4155	4075	109.4	3.45		0.01	C
π Her	6418	K3 IIab	4203	4123	293.8	5.52			

Column 6 is the apparent bolometric flux in units of 10^{-15} W cm^{-2}, while column 7 is the predicted angular diameter in units of milliarcsec.
Explanation of source/coding = final column: D (= Double) is from the Bright Star Catalogue (Hoffleit 1982); Fe-1, CN-0.5, etc. are from Keenan & McNeil (1976).
Sources for [Fe/H] values: C = Cayrel de Strobel *et al.* (1985); F = Frisk (1983); GKA = Gustafsson, Kjærgaard & Andersen (1974); HK = Hansen & Kjærgaard (1971); KG = Kjærgaard, Gustafsson, Walker & Hultquist (1982); N = Nissen (1981).
Notes on temperatures of individual stars suggested by colours: [1]T_{eff} higher by about 100 K for HR 1136, 4785 and 7504; [2]T_{eff} lower by about 100 K for HR 5287 and 7063; [3]The colours for the K7V star HR 8086 indicate T_{eff} = 4000 K. Comments on other stars are made in the text.

4 Stellar temperatures using the infrared flux method

4.1 METHOD

The infrared flux method is based upon measurements of the integrated stellar flux and a monochromatic flux, usually measured at infrared wavelengths in order to make the ratio of the two fluxes reasonably sensitive to effective temperature. The choice of this wavelength region also makes the flux ratio relatively independent of gravity and metal abundance and of uncertainties of the model atmospheres used in the analysis. This method has been applied to cool stars (e.g. Blackwell & Shallis 1977; Shallis & Blackwell 1979), to F dwarfs (Saxner & Hammarbäck 1985, hereafter SH85) and to hot stars. SH85 give a detailed list of references to application of this method. The present paper's approach closely follows that of SH85. In particular, we have used the 13-colour photometry of Johnson & Mitchell (1975) to find the integrated stellar fluxes between 3300 and 11 000 Å, satellite observations to find fluxes shortward of 3300 Å and Johnson *JKL* data (Johnson *et al.* 1966) to obtain the infrared fluxes. The infrared fluxes have been checked using the observations of Strecker *et al.* (1979). Model fluxes have also been used as checks.

The infrared reference band used by us is the Johnson *K* band at about 2.2 μm. This is a compromise, dictated by the lower accuracy and smaller number of photometric IR observations at longer wavelengths. The stellar effective temperatures derived using the flux of this passband are given in Table 3. Some of the model flux ratios on which these temperatures are based are given in Table 7.

4.2 FLUXES

The data on the UV fluxes of the stars were obtained from the *IUE* Ultraviolet Spectral Atla (Wu *et al.* 1983). The data for the stars in this Atlas with spectral types G and K, luminosit classes II–V and *V–K* colours available from Johnson *et al.* (1966) were used. Two measure ments were made – first the integrated flux between a short wavelength and 3200 Å, secondl the integrated flux between 3000 and 3200 Å. The short wavelength value was taken to b 2000 Å for the early G stars. However, the cooler stars emit negligible flux at this wavelengt and so the limit was increased to 2400 Å for these objects. The flux between 3000 an 3200 Å, calculated from the mean flux at 3100 Å, was used together with the flux in the 3 filter of the 13-colour system as interpolation points to find the contribution of the flux in th 3200–3367 Å region to the total flux.

In order to obtain UV fluxes for the stars which had not been observed with the *IUE*, th UV integrated fluxes were normalized to the same *V* magnitude and the resulting fluxe plotted versus *V–K*. A mean curve drawn through this data was used to supply fluxes for th stars not observed.

The UV fluxes are much more important for the determination of the temperatures of the (stars than the K stars. For example, the temperature of the G0V star HR 4785 is increased b 100 K when the UV fluxes are included in the manner described above. However, th temperature of α Boo (K2IIIp) changes by only 4 K.

We follow SH85 in adopting the relative calibration of the 13-colour system from Johnso & Mitchell (1975). This calibration and the calibration of the infrared passbands is given i Table 4. We also use the SH85 calibration of the 52 filter, i.e. the flux from a zero-magnitud star in the 52 passband is taken to be 4.34 E − 9 erg cm^{-2} $Å^{-1}$ s^{-1}), which is consistent wit the absolute Vega flux measured by Hayes (1985) at 5556 Å. The stellar fluxes in the 13 pass bands of the system were then computed for each star. The effective wavelengths of the 3 filter and the 110 filter are 3367 and 11 078 Å, respectively. The trapezoidal rule was the used to give the integrated flux between these wavelengths.

As a check on how accurately the integrations using the filter fluxes represented the overa flux, the same calculations were made using stellar model fluxes. The results were compare

Table 4. Flux calibration (in ergs cm^{-2} s^{-1} $Å^{-1}$) for an A0 V star of zero magnitude in each pass-band.

Filter (pass-band)	Flux
33	3.41–9
35	3.29–9
37	4.32–9
40	7.83–9
45	6.16–9
52	4.34–9
58	3.12–9
63	2.34–9
72	1.59–9
80	1.16–9
86	9.48–10
99	7.05–10
110	4.83–10
J	3.47–10
K	4.21–11
L	7.19–12

with direct integrations using fluxes computed at a separation of 0.1 Å. The results for the Vega model (9650/3.9/0.0) agreed to much better than 0.1 per cent. Denoting filter fluxes by F and direct integrations by T, the results are $(F-T)/T = -0.0004$, 0.0034, 0.0085 and 0.0148 for models with $T_{eff} = 5500$, 5000, 4500 and 4000 K. (The model fluxes discussed in this section were computed without allowing for TiO lines.) While the models do not fit the stellar fluxes, particularly at shorter wavelengths in the cooler stars, the correction factor needed to convert filter fluxes to true fluxes should still be valid to first order. The correction factor $(F-T)/T$, given as a function of $V-K$ by the models, was applied to the stellar filter fluxes as a function of the $V-K$ colour of the stars.

The infrared fluxes were found using the Johnson *et al.* (1966) broad-band *JKL* data. A number of stars in the sample were not observed in the L band. A plot of $V-K$ versus $V-L$ for the remaining stars showed very little scatter and so the missing $V-L$ values were obtained by interpolation in this plot. The SH85 calibrations of J, K and L in terms of absolute fluxes were used, as well as the SH85 effective wavelengths. The flux at wavelengths beyond 3.4 μm (the effective wavelength of the L band) was included by assuming that the stars radiate like black bodies at these wavelengths. This blackbody flux was normalized to the L band flux at 3.4 μm. The errors introduced by this approximation for the long-wavelength flux in the integrated fluxes can be estimated with model atmospheres to be less than 1 per cent of the flux beyond 3.4 μm, assuming that spectral lines can be ignored. Since the blackbody flux beyond 3.4 μm is less than 4 per cent of the total flux for the coolest stars, the resulting errors in the final effective temperatures are negligible.

The infrared flux data obtained using the NASA aircraft (Strecker *et al.* 1979) allow a check of the infrared fluxes found from the J, K and L magnitudes. These data have been corrected to outside the terrestrial atmosphere by Strecker *et al.* In order to increase the number of stars in the comparison of 'airborne' fluxes and 'colours' fluxes, we have included β And (HR 337), α U Ma (HR 4301) and β Dra (HR 6536), as well as α Tau (HR 1457), α Boo (HR 5340) and μ Her (HR 6623) which are in the sample of 95 stars. Table 5 gives the fluxes deduced for this sample from the K and L Johnson magnitudes and from the airborne data, the latter fluxes being weighted according to the sensitivity functions of the K and L passbands. The ratios of the fluxes for the 1.25–3.4 μm interval computed from the colours are also given in the table. In addition, to give some check of the J fluxes, the flux from the J magnitude is given, as is the flux from the 110 magnitude of the 13-colour photometry, and the flux at 1.25 μm from the airborne work.

Unfortunately, the airborne data do not extend to short enough wavelengths for the J magnitudes to be computed. It is seen that the J-band fluxes fall in between the 1.1 μm flux

Table 5. Comparison of observed fluxes using different measurements.

Star HR	337	1457	4301	5340	6536	6623
Name	β And	α Tau	α UMa	α Boo	β Dra	μ Her
Spectral Type	M0III	K5III	K0III	K2IIIp	G2II	G5IV
J flux from J mag.	7.38-10	1.89-09	3.31-10	2.58-09	1.05-10	4.66-11
1.1 μ m flux (110 mag)	8.03-10	2.15-09	3.67-10	2.85-09	1.20-10	5.22-11
1.25 μm flux (scans)	6.89-10	1.82-09	3.02-10	2.40-09	9.65-11	4.08-11
K flux from K mag.	2.27-10	5.61-10	7.66-11	6.67-10	2.07-11	8.24-12
K flux from scans	2.40-10	5.92-10	7.70-11	6.83-10	2.15-11	8.26-12
L flux from L mag.	4.25-11	1.14-10	1.48-11	1.30-10	3.88-12	1.54-12
L flux from scans	4.94-11	1.23-10	1.52-11	1.38-10	4.27-12	1.57-12
Integrated flux ratio (Color/scans)	1.05	1.05	1.20	1.12	1.24	1.31

The unit of flux is ergs $cm^{-2} s^{-1} Å^{-1}$.

(from the 110 filter of the 13-colour photometry) and airborne 1.25 μm flux, as expected, while the K-magnitude fluxes seem systematically lower by typically 3 per cent. If this is due to a systematic error in the K-band calibration, it would lead to our values of T_{eff}(IRFM) being overestimated by typically 30 K. The wavelength interval between J and K contains a significant amount of the integrated flux. Since the integrated flux ratio given in the bottom line of Table 5 appears to vary with T_{eff}, we computed the effective wavelengths of the filters, weighted according to model fluxes and allowing for absorption in the terrestrial atmosphere. The effective wavelength of the J filter changes by 125 Å as T_{eff} is altered from 4000 to 5000 K, while the K and L effective wavelengths change by much less. Comparing the model flux derived by trapezoidal integration using the mean J, K and L band fluxes (denoted by F) with the flux found by direct integration (denoted by T) gave a check of the accuracy of the integrations. The values of F/T, given in Table 6, are very similar to those of Table 5. In view of this, we established the mean variation of F/T with $V-K$, from the data of Table 6, and used this to correct the fluxes found from the J, K and L colours. There are several possible reasons for the fact that the F/T ratios deviate significantly from unity, one of them being quadrature errors, e.g. caused by the adoption of constant effective wavelengths independent of spectral type for the passbands. Some of the variation of F/T with effective temperature is presumably due to the increasing importance of the 1.6 μm peak with decreasing temperature. Errors in the photometry presumably cause some scatter in the results, e.g. the L-magnitude fluxes for HR 337 differ by 16 per cent, whereas those for α Tau differ by only 8 per cent. More details of the fit of scans and models can be seen in Manduca *et al.* (1981).

The integrated fluxes of the stars are given in Table 3.

4.3 THE REFERENCE BAND

A problem with the K band is the presence of a considerable fraction of the CO vibration–rotation first overtone lines within the photometric band. Although these lines are included in the synthetic-spectrum calculations, they may be affected by non-standard microturbulent velocity (deviating from our choices of DBV = 2 km s^{-1} and a turbulent velocity of 1 km s^{-1} for giants and dwarfs, respectively) or non-solar [C/Fe] ratios (*cf.* Lambert & Ries 1981, and Kjærgaard *et al.* 1982, who show that the carbon abundance is depleted in G and K giants by about 0.2 dex, probably as a result of CNO burning). The K magnitudes of the models 4000/1.50/0.0, 4500/2.25/0.0, 5000/3.0/0.0 and 5500/3.0/0.0 are increased by 0.072, 0.039, 0.025 and 0.014 mag respectively, due to line blocking. Most of the blocking is due to CO. In the extreme case of CO bands not being present in the spectrum of a star, the deduced value of the temperature would be about 90 K too low at a T_{eff} of 4000 K and the error would decrease at higher T_{eff}s. Since the CO lines are strong in cool stars, more typical changes in the effective temperatures are 45 K if DBV is changed to 3 km s^{-1} from the standard 2 km s^{-1}, or 25 K if the carbon abundance is decreased by 0.2 dex. The effect of similar changes in metal abundance on K magnitude, assuming that CNO scale with Fe, are in the thousandths of a magnitude, e.g. 0.003 mag at T_{eff} = 4000 K and log g = 1.5 and 0.002 mag at this gravity and

Table 6. Ratio of calculated fluxes

Model	4000/1.5/0.0	4500/2.25/0.0	5000/3.0/0.0	5500/3.0/0.0
Integrated flux ratio (colours/scans)	1.05	1.12	1.18	1.23

$T_{eff} = 4500$ K. This amounts to only 5–7 K and can be neglected. The temperatures found for the two metal-poor stars, ϕ^2 Ori and α Boo, will not be affected by their low ([M/H] ~ −0.5) metal abundances. Kjærgaard *et al.* (1982) find α Boo to be carbon poor by 0.16 dex but the correction of about 25 K derived above is an overestimate, since the high C^{13} abundance ($C^{12}/C^{13} = 7$, Day, Lambert & Sneden 1973) will increase the strength of the CO bands.

In the following section, temperatures are deduced from colours and these temperatures are not always consistent with those found from the IRFM. Furthermore, the question of the uncertainty in the H^- absorption coefficient suggests that other passbands be checked. The availability of 13-colour photometry suggests that one of these bands could serve as a reference. We consequently calculated flux ratios, using both the 99 and 110 bands as the reference passband. These flux ratios are given in Table 7. Unfortunately, the sensitivity of the IRFM becomes much lower when these passbands, located at shorter wavelengths, are used. The ratio of total flux to reference band flux varies by a factor of 2.35 between $T_{eff} = 5500$ and 4000 K when the *K* band is the reference band. When the 110 band is used, this ratio drops to 1.3 and when the 99 band is used, it becomes 1.15.

Some comparisons of the temperatures using the 110 and *K* bands as reference bands were made. A comparison for K2III stars (α Boo being excluded) showed that the *K* band (using the Doughty–Fraser H^- opacity) gave temperatures which were 33 K higher, but the individual differences, $T_{eff}(K) - T_{eff}(110)$, ranged from −309 to 341 K. Much of this scatter is ascribed to the uncertainties in the 110 magnitudes.

The point which is quite critical in the application of the IRFM is the accuracy of the *K*-band flux. (This is the point made by SH85 in the comparison of Vega models and Vega observations.) If, for example, the *K*-band filter were to be shifted 0.1 μm to longer wavelengths, then the mean flux in this band is reduced by about 18 per cent, the exact value

Table 7. Ratio of total flux to flux in a reference band.

Ratios for Johnson K band as reference

H^- Opacity Source

Model	Giant Stars Bell *et al.*	Doughty-Frazer
5500/3.00/0.0	1.384E+05	1.410E+05
5000/3.00/0.0	1.067E+05	1.091E+05
4500/2.25/0.0	0.7994E+05	0.8203E+05
4000/1.50/0.0	0.5830E+05	0.6018E+05

Model	Dwarf Stars Bell *et al.*	Doughty-Frazer
6000/4.50/0.0	1.782E+05	1.806E+05
5500/4.50/0.0	1.400E+05	1.421E+05
5000/4.50/0.0	1.077E+05	1.096E+05
4500/4.50/0.0	0.808E+05	0.825E+05

Ratios for Glass K band using Bell et al. opacity

Model	Giant Stars
5500/3.00/0.0	1.4783E+05
5000/3.00/0.0	1.1390E+05
4500/2.25/0.0	0.8512E+05
4000/1.50/0.0	0.6185E+05

Ratios for 98 and 110 pass bands

Model	98	110
5500/3.00/0.0	1.81E+04	2.30E+04
5000/3.00/0.0	1.70E+04	2.09E+04
4500/2.25/0.0	1.60E+04	1.89E+04
4000/1.50/0.0	1.57E+04	1.77E+04

depending on the model concerned. Such a change does affect the K-band magnitudes, but the change made is compensated for by the change made in the Vega model magnitude. However, a change of 18 per cent in flux ratio would alter the temperatures derived for cool stars by about 250 K at $T_{\rm eff}=4000$ K. This effect can be seen when the results of the IRFM obtained using Glass K magnitudes are compared with those from Johnson magnitudes. The effective wavelength of the Glass K filter is 0.03 μm longer than that of the Johnson K filter, and so the model fluxes on the Glass system are 7 per cent less than the fluxes on the Johnson system. However, the K magnitudes on the two systems are very similar, those on the Glass system averaging 0.01 mag fainter. The temperatures deduced from the IRFM using the Glass K magnitudes then average about 80 K less than those derived from the Johnson K magnitudes. In the following section, $T_{\rm eff}$(IRFM) is used to refer to results from the Johnson K magnitude, whereas the results from Glass are referred to in Section 5.

Bessell & Brett (1987) have studied transformation equations between infrared colour systems. They have used the Strecker *et al.* (1979) data and Wing's (1967) data for the computation of synthetic colours and find that the Johnson K filter should be shifted bluewards in order for the Johnson synthetic colours to match those of other systems. Calculations using data from Bessell (private communication) suggest that the shift is about 0.03 μm. If such a shift is appropriate, then the temperatures deduced from Johnson K magnitudes would be increased by about 80 K. We agree that the effective wavelength of the Glass K filter is 0.03 μm greater than that of Johnson K, but use Johnson's (1965) profile.

4.4 INTERSTELLAR REDDENING

We studied the effects of interstellar reddening in the following way. The stellar distances were computed using absolute magnitudes from Blaauw (1963) and Keenan (1985) and reddening estimates were then made on a statistical basis. Following Sturch (1966), the extinction for a star at galactic latitude b and distance r pc was taken to be A cosec $b[1-\exp(-r\sin b/124)]$, where the scale height of the dust is 124 pc and the reddening in the galactic plane is taken to be $A_{\rm v}=0.7$ mag kpc^{-1}. The interstellar reddening law used to find the reddening at other wavelengths is that used by Bell & VandenBerg (1987), which gives $E(U-B)/E(B-V)=0.764$, $A_{\rm v}/E(B-V)=3.15$ and $E(V-I)_{\rm c}/E(B-V)=1.21$, $(V-I)_{\rm c}$ being on the Cousins system. The law also gives good fits to the observed Thuan–Gunn reddening coefficients (Bell & VandenBerg 1987).

The most distant dwarfs in the sample are HR 7503 and 7504, at 19 pc. The dereddening correction would increase the derived values of $T_{\rm eff}$ by only 13 K. All of the giant stars are within 100 pc of the Sun. The temperature of the most distant one, HR 434, would be increased by 25 K if this dereddening correction were applied. The bright giant stars are all more than 100 pc from the Sun, HR 7479 being at 200 pc. The dereddening correction causes the temperature of this object to be increased by 150 K, with the greatest increase for the other bright giants being 85 K. In this work, we have applied dereddening corrections, following the approach described above, for the seven bright giants; for the rest of the stars the effects of reddening were neglected.

4.5 COMPARISON WITH OTHER DETERMINATIONS OF $T_{\rm eff}$(IRFM)

Blackwell and collaborators (Blackwell & Shallis 1977; Shallis & Selby 1979; Blackwell, Petford & Shallis 1980; Blackwell *et al.* 1986; Leggett *et al.* 1986b) have used the IRFM to derive effective temperatures for a number of G and K giants. Various infrared flux bands beyond 2 μm were used as the reference band in these papers. These authors have 16 stars in common with us – the results are compared in Table 8.

Table 8. Comparison between different effective temperature determinations for G and K giants based on the infrared-flux method.

Name	HR	Present work	BS77	BSS79	BPS80	L86	B86
α Ari	617	4499	4400				
α Tau	1457	3943	3820				
α Hya	3748	4141	3960		4073		
β Gem	2990	4896	4760				
α UMa	4301	4655	4760		4512		
β CVn	4785	5861		5670	5671		
ε Vir	4932	5052				4990	
β Com	4983	6024				5720	
α Boo	5340	4321	4410		4420		4230,4307
β Boo	5602	4929		5150	5215		
δ Boo	5681	4832		4840	4907		
α Ser	5854	4556	4400		4494		
ε CrB	5947	4350				4280	
μ Her	6623	5527		5750	5678		5510,5605
γ Dra	6705	3955	3820			3940	
β Aql	7602	5098		5110	5159	4980	

BS77 is Blackwell & Shallis (1977); BSS79 is Blackwell, Shallis & Selby (1979); BPS80 is Blackwell, Petford & Shallis (1980); L86 is Leggett *et al.* (1986b); B86 is Blackwell *et al.* (1986). The two results for these last authors result from the use of two different Vega calibrations (see text). The values given in column 3 are based on the IRFM but corrected according to Section 6.

It is seen that Blackwell & Shallis (1977) have obtained somewhat lower T_{eff}s for many stars. There is an indication that the temperature difference increases with decreasing T_{eff} – it amounts to about 120 K for the coolest K giants. Blackwell & Shallis present diagrams showing the angular diameters one would obtain, using the IRFM with different choices of reference bands. It is noteworthy that the *K*-band fluxes according to these plots tend to produce smaller diameters, i.e., higher T_{eff}s, than fluxes at longer wavelengths. The size of this effect is quantitatively consistent with the effective temperature difference between us and Blackwell & Shallis; note also that the effect is not present in the diagram of Blackwell & Shallis for α Boo, for which they obtain a higher T_{eff}. The difference found by Blackwell & Shallis in the determinations of angular diameters, and thus temperatures, derived with the *K* and the *L* bands as reference bands, respectively, would vanish if the more recent absolute calibration by SH85 were used.

The effective temperatures determined by Blackwell *et al.* (1979) were based on the *K* band as reference band and agree better with our T_{eff}(IRFM) values, as expected, with the exception of HR 4785 (G0V). In the determinations of Blackwell *et al.* (1980) it is again obvious that the stars for which the *K* band was used as a reference (HR 5671, 5215, 4907, 5678, 5159) are in better agreement with our estimates, while for the other stars, where the *L* band was used, Blackwell *et al.* obtain lower values. Leggett *et al.* (1986b) also find systematically lower values than ours (again with the *L* band as a reference).

The greatest difference relative to previous T_{eff} determinations with the infrared flux method is that of β Com (HR 4983), where we find a temperature 300 K higher than that of Leggett *et al.* (1986b). The reason for this discrepancy is not known. We note, however, that the $(b-y)$ and $H\beta$ indices for this star indicate a temperature close to 6000 K, according to the calibrations of Saxner & Hammarbäck (1985). These calibrations are, however, based on a temperature scale established with basically the same method as ours.

In their most recent work, Blackwell *et al.* (1986) have derived results for α Boo and μ Her, based on (a) their own absolute calibration of Vega derived from observations made at Tenerife

(Mountain *et al.* 1985) and (b) the Dreiling & Bell (1980) Vega model atmosphere absolute calibration. The T_{eff} values have been derived using a number of reference wavelengths, with the goal of seeing if all these wavelengths give the same T_{eff}. The results are inconclusive, with the Vega model giving a better result for α Boo and a poorer one for μ Her. Blackwell *et al.* give $T_{eff}(\mathrm{IRFM})(K) = 4230 \pm 80$ and 4307 ± 80 for α Boo, and 5510 ± 110 and 5605 ± 110 for μ Her, the calibrations being the Tenerife one and the Vega model one, respectively. The adopted values obtained in the present paper, after the correction of Section 8 has been applied, are 4321 and 5527 K, respectively.

We conclude that our effective temperatures are consistent with those of Blackwell and collaborators, provided that the differences in absolute flux calibration are taken into account; also more recent calibrations than that of Johnson (1966) leads to an improved consistency between effective temperatures derived with different infrared reference bands.

However, we conclude that it cannot be excluded that our choice of the K band and the uncertainties in the calibration of that may lead to T_{eff}(IRFM) values which are systematically somewhat high.

4.6 SYSTEMATIC ERRORS IN THE T_{eff}(IRFM)

The effective temperatures derived with the IRFM for our sample are listed in Table 3. These temperatures may be in error due to random errors in the observed fluxes (magnitudes). For the hottest stars the errors in the ultraviolet fluxes may contribute significantly to the errors in the integrated fluxes; for most of the stars, however, the errors in the IR fluxes are more important. A typical error of 0.03 mag in the observed magnitudes as well as in the reference K band corresponds to errors in T_{eff} of about 45 K.

The most important sources of systematic error, which in the zero-order approximation shift the zero-point of the temperature scale, are the integration uncertainties in the total flux, the calibration of the 52- and infrared magnitudes and the model-atmosphere fluxes.

Our IR fluxes were calculated with the H^- absorption data of Doughty, Fraser & McEachran (1966) and Doughty & Fraser (1966), consistent with the data used for the model atmospheres. In addition, we have calculated the IR fluxes with the free–free H^- data of Bell *et al.* (1979). The latter fluxes give flux ratios F_{tot}/F_{ref} lower by about 3 per cent (*cf.* Table 7). Typical errors in the effective temperatures T_{eff}(IRFM), owing to uncertainties in the H^- data, may thus amount to about 40 K.

The relative errors in the integrated fluxes, including the calibration errors, are estimated to contribute an uncertainty to the flux ratio F_{tot}/F_{ref} of less than 4 per cent (*cf.* also the discussion of Saxner & Hammarbäck 1985). Possible errors in the calibration of the reference K-band flux and errors in the calculated fluxes in this band, owing to uncertainties in CO band strength, H^- opacity and K-band transmission function, may lead to errors in the flux ratio of about twice as much. Altogether, we find that a total systematic error of about 150 K in T_{eff}(IRFM) is possible – an error twice as great does, however, not seem probable.

The model atmospheres used here are consistent with those of BEGN76, described in detail by GBEN75. It was shown by GB79 that these plane-parallel LTE models did not reproduce the violet–ultraviolet fluxes of the G–K stars very well. This discrepancy was explained tentatively by a hypothetical 'veil' of numerous very faint atomic lines, which were, and are, not included in our line lists. Later research has verified this presumption (Magain 1983; Kurucz 1986). This opacity probably does not affect the red–infrared part of the spectrum directly. However, the effects on the model atmospheres might be of some importance. The back-warming which would be produced by the veiling opacity would heat the deeper layers of the atmospheres where the continuum fluxes are formed.

The problem was investigated by Magain (1983), who derived an approximate expression for the extra opacity, assuming it to be due to a veil of weak Fe I lines of rather high excitation, with a wavelength dependence such that the solar-model flux agreed with the observed one. Magain also showed that our model atmosphere program, with this extra opacity added, gives good agreement between calculated and observed ultraviolet and blue colours in the *UBV* and Geneva systems.

Magain used fluxes calculated directly through the 100-Å wide Opacity Distribution Functions of the model atmosphere code. A similar study, based on the more accurate fluxes from the synthetic spectrum program, shows that the opacity corrections adopted by Magain are overestimated. However, we have adopted his recipe to estimate an upper limit to the errors caused by this missing opacity.

A temperature sequence of models was calculated with this extra opacity added. The temperature increase around $\tau_{Ross} = 0.67$ due to the extra back-warming was found to be around 60 K and is only weakly dependent on effective temperature. The extra blocking in the ultraviolet and blue increased the flux in the K band by 0.8 per cent ($T_{eff} = 6000$ K) to 11.7 per cent ($T_{eff} = 4000$ K), corresponding to an effective temperature increase of typically 20 K. The effective temperatures derived from the infrared colours were, however, found to decrease by about 55 K, this decrease being almost independent of the colour index used.

Other systematic errors in the model atmospheres may also be of importance. One should note, however, that a major objective of the present study is to establish a relation between the model atmospheres of the Bell *et al.* grid and the stars, such that the characteristic temperature of the line-forming region can be estimated from colours, for applications in abundance analyses etc. In this situation T_{eff} is merely a label on the model which should be chosen such that the temperature structure of the layers where weak lines are formed are reproduced by the model reasonably well. Whether this label is an adequate measure of the total flux or not is actually less important for such an application. It is noteworthy that the infrared flux method stresses the defining property of T_{eff} as a flux measure, while the colours give a more direct measure of the temperature in the flux-forming layers. We shall see later that some inconsistency may exist between these different T_{eff} estimates – an inconsistency which might contain information about further shortcomings of the model atmospheres.

5 Effective temperatures from colours

In order to check the temperature scale established with the IRFM, as well as the accuracy of the calculated infrared colours, we have derived effective temperatures by interpolation in our grids of calculated colours for a number of colour systems. This was done for all stars in our standard sample that had been observed in the system in question, taking the gravity and metal abundance given in Table 3 into account. The results are displayed in Figs 6–16, where the differences $\Theta(\text{colour}) = T_{eff}(\text{colour}) - T_{eff}(\text{IRFM})$ are plotted. These results will be commented on below for each colour system.

The bulk of the colour calculations were made using spectra computed using the Bell *et al.* (1975) H^- absorption coefficients. In addition, in view of the differences in the calculated infrared fluxes caused by the use of different opacities, we computed colours from a few giant model spectra calculated using Doughty & Fraser (1966) absorption coefficients.

Since the model atmospheres, as well as the T_{eff}(IRFM) values, are based on the Doughty & Fraser data, the use of the Bell *et al.* data in the colour calculations introduces some inconsistencies. These are, however, not very important since they only cause minor errors in the T_{eff}(colour) estimates. A comparison of the Glass colours (see below) showed that the $J–H$ colour was always bluer when computed with the Doughty & Fraser opacities, the blueness ranging from 0.013 mag at 5500 K to 0.025 at 4000 K. This corresponds to the use of the Doughty & Fraser opacities giving lower T_{eff} values, the difference being about 50 K at all T_{eff}. The changes in other colours are less than 0.002 mag for $H-K$ and 0.004 mag for $K-L$, while the K magnitude is 0.02 mag fainter at 5500 K and 0.033 mag fainter at 4000 K. This will give T_{eff} values from $V-K$ about 25 K cooler when the Doughty & Frazer absorption coefficients are used. Owing to the general similarity of the filters of the different infrared colour systems, similar T_{eff} changes are expected for other colour systems.

5.1 THE JOHNSON BROAD-BAND SYSTEM

The synthetic colours for this system and the Johnson V and K magnitudes are given in Table 9.

It has been generally assumed that a colour such as $V-K$ is independent of abundance. The data of Table 9 show that this is generally true. However, at $T_{eff}=4000$ K, $V-K$ shows a very complex behaviour for the [A/H] $= -3.0$ models. These are redder than models of other abundance at the lower gravities and bluer at higher gravities. The reason for this is the effect which convection in the H_2 dissociation zone has on the model structure (*cf.* GBEN figs 4 and 13). The TiO bands also affect the V magnitude in the coolest [A/H] $= 0.0$ models.

As is seen in Fig. 6, the Johnson $(V-K)$ observations tend to give lower effective temperatures than the IRFM by typically 100 K for the cooler stars – for the hotter stars $\Theta(V-K)$ seems closer to zero, and is even positive for the G dwarfs. On the other hand, in Fig. 7 $\Theta(J-K)$ is systematically positive by more than 100 K. The greater scatter in Fig. 7 is mainly the result of the smaller temperature sensitivity of $J-K$. The different tendencies for $V-K$ and $J-K$ are further illustrated in Fig. 8, where our standards and some representative models are plotted in the two-colour diagram. It is seen that there is a zero-point difference and a small difference in slope between the theoretical and observed two-colour relations – these discrepancies may be caused by errors in any of the magnitudes involved. Thus, an extra absorption in V (by 0.15 mag, increasing to 0.35 mag for the coolest stars) or in K (by 0.07 to 0.15 mag) or too much (terrestrial?) absorption in J (by 0.05 to 0.10 mag) would explain them. We consider the error of the magnitude required in V as much less probable than the two other possibilities. Alternatively, if a 300 K cooler model were adopted for Vega, the temperature adopted from $V-K$ would become cooler, by about 40 K at 6000 K and 20 K at 4000 K. The corresponding numbers found using $J-K$ are 75 and 35 K, respectively.

For a star with $T_{eff}=4500$ K, an error in the calculated K magnitude of the size suggested would, when corrected for, lead to a reduction of $T_{eff}(J-K)$ by typically 300 K, while $T_{eff}(V-K)$ would be reduced by less than 50 K. However, such a correction, if due simply to an error in the calculation of K-band flux, would cause the temperatures derived from the IRFM to increase, by perhaps 150 K, and therefore remain inconsistent with $T_{eff}(V-K)$. The only manner in which $T_{eff}(V-K)$ could be made consistent with T_{eff}(IRFM) is by arguing that the effective wavelength for the K passband given by Johnson is wrong. It is noteworthy that T_{eff}(IRFM) would then decrease by about 150 K and thus become roughly consistent with both $T_{eff}(V-K)$ and $T_{eff}(J-K)$. An equally likely possibility would be a failure in the J-magnitude calculations, caused by the difficulties in considering terrestrial extinction in this passband. An error of the size mentioned above would obviously bring the $T_{eff}(J-K)$ scale to agreement with $T_{eff}(V-K)$. Another, at least partial, explanation for the discrepancy in the $(V-K)-(J-K)$ diagram could be a 'zero-point error' in, for example, $J-K$, reflecting the difficulties in spanning the wide range in T_{eff} from A0V stars to G and K stars with model atmospheres and synthetic colours for broad-band systems. In conclusion, however, we find that the agreement in the temperature scales derived from $V-K$ and $J-K$ with the T_{eff}(IRFM) scale is acceptable.

Table 9.

			Johnson					Glass				
T	log g	[A/H]	J-K	K-L	L-M	K	V-K	J-H	H-K	K-L	K	V-K
4000	0.75	-0.0	1.017	0.090	-0.375	1.090	3.391	0.832	0.171	0.113	1.083	3.398
4000	0.75	-0.5	1.039	0.079	-0.329	1.084	3.394	0.864	0.157	0.101	1.077	3.401
4000	0.75	-1.0	1.044	0.071	-0.293	1.077	3.413	0.875	0.151	0.093	1.072	3.418
4000	0.75	-2.0	1.026	0.070	-0.226	1.067	3.494	0.849	0.160	0.091	1.062	3.499
4000	0.75	-3.0	0.973	0.084	-0.208	1.069	3.492	0.773	0.182	0.106	1.060	3.582
4000	1.50	-0.0	1.035	0.080	-0.338	1.089	3.399	0.858	0.163	0.103	1.082	3.406
4000	1.50	-0.5	1.052	0.072	-0.299	1.086	3.390	0.881	0.154	0.094	1.080	3.396
4000	1.50	-1.0	1.057	0.066	-0.268	1.082	3.390	0.887	0.153	0.088	1.077	3.395
4000	1.50	-2.0	1.037	0.076	-0.213	1.085	3.399	0.850	0.170	0.095	1.079	3.405
4000	1.50	-3.0	0.973	0.108	-0.179	1.114	3.426	0.757	0.198	0.127	1.108	3.432
4000	2.25	-0.0	1.055	0.073	-0.309	1.089	3.413	0.880	0.158	0.095	1.083	3.419
4000	2.25	-0.5	1.062	0.067	-0.276	1.088	3.399	0.891	0.155	0.089	1.082	3.405
4000	2.25	-1.0	1.065	0.065	-0.253	1.087	3.388	0.890	0.158	0.086	1.082	3.393
4000	2.25	-2.0	1.034	0.086	-0.199	1.105	3.346	0.835	0.183	0.104	1.099	3.352
4000	2.25	-3.0	0.939	0.134	-0.145	1.171	3.286	0.709	0.213	0.150	1.164	3.293
4000	3.00	-0.0	1.061	0.069	-0.288	1.092	3.431	0.889	0.158	0.090	1.084	3.439
4000	3.00	-0.5	1.068	0.065	-0.264	1.091	3.413	0.894	0.158	0.085	1.085	3.419
4000	3.00	-1.0	1.065	0.066	-0.241	1.094	3.392	0.883	0.166	0.086	1.088	3.398
4000	3.00	-2.0	0.985	0.113	-0.162	1.154	3.278	0.771	0.198	0.129	1.147	3.285
4000	3.00	-3.0	0.875	0.195	-0.055	1.233	3.179	0.637	0.230	0.182	1.226	3.186
4500	0.75	-0.0	0.784	0.071	-0.339	0.923	2.641	0.695	0.105	0.074	0.922	2.642
4500	0.75	-0.5	0.790	0.060	-0.296	0.917	2.652	0.670	0.101	0.082	0.912	2.657
4500	0.75	-1.0	0.790	0.052	-0.261	0.910	2.669	0.674	0.098	0.074	0.906	2.673
4500	0.75	-2.0	0.783	0.041	-0.201	0.893	2.715	0.655	0.110	0.063	0.890	2.718
4500	0.75	-3.0	0.783	0.045	-0.080	0.884	2.735	0.644	0.121	0.057	0.881	2.738
4500	1.50	-0.0	0.799	0.063	-0.306	0.921	2.649	0.652	0.112	0.094	0.917	2.653
4500	1.50	-0.5	0.807	0.055	-0.271	0.919	2.652	0.687	0.101	0.077	0.915	2.656
4500	1.50	-1.0	0.808	0.049	-0.243	0.916	2.657	0.689	0.101	0.070	0.912	2.661
4500	1.50	-2.0	0.799	0.046	-0.195	0.909	2.673	0.664	0.118	0.066	0.905	2.677
4500	1.50	-3.0	0.788	0.058	-0.081	0.906	2.681	0.636	0.134	0.069	0.902	2.685
4500	2.25	-0.0	0.799	0.059	-0.276	0.922	2.661	0.677	0.107	0.080	0.917	2.666
4500	2.25	-0.5	0.816	0.052	-0.250	0.922	2.660	0.695	0.105	0.074	0.922	2.660
4500	2.25	-1.0	0.818	0.048	-0.227	0.921	2.659	0.695	0.106	0.068	0.917	2.663
4500	2.25	-2.0	0.804	0.057	-0.185	0.926	2.648	0.657	0.130	0.075	0.921	2.653
4500	2.25	-3.0	0.774	0.083	-0.077	0.939	2.627	0.607	0.150	0.091	0.934	2.632
4500	3.00	-0.0	0.815	0.055	-0.255	0.924	2.677	0.692	0.106	0.075	0.919	2.682
4500	3.00	-0.5	0.822	0.049	-0.233	0.924	2.673	0.697	0.107	0.070	0.920	2.677
4500	3.00	-1.0	0.823	0.049	-0.212	0.926	2.666	0.692	0.113	0.068	0.922	2.670
4500	3.00	-2.0	0.798	0.070	-0.171	0.944	2.629	0.640	0.141	0.087	0.939	2.634
4500	3.00	-3.0	0.750	0.107	-0.063	0.976	2.582	0.572	0.162	0.113	0.970	2.588
5000	1.50	-0.0	0.617	0.043	-0.249	0.775	2.105	0.529	0.070	0.064	0.771	2.109
5000	1.50	-0.5	0.621	0.035	-0.216	0.772	2.112	0.535	0.069	0.055	0.769	2.115
5000	1.50	-1.0	0.627	0.028	-0.184	0.767	2.122	0.535	0.074	0.047	0.765	2.124
5000	1.50	-2.0	0.635	0.029	-0.075	0.761	2.134	0.534	0.083	0.040	0.759	2.136
5000	1.50	-3.0	0.636	0.030	-0.053	0.762	2.134	0.535	0.084	0.040	0.760	2.136
5000	2.25	-0.0	0.628	0.041	-0.233	0.777	2.121	0.541	0.070	0.061	0.773	2.125
5000	2.25	-0.5	0.633	0.035	-0.205	0.777	2.125	0.546	0.070	0.053	0.774	2.128
5000	2.25	-1.0	0.639	0.029	-0.177	0.774	2.133	0.546	0.075	0.047	0.772	2.135
5000	2.25	-2.0	0.644	0.033	-0.076	0.770	2.138	0.537	0.090	0.043	0.768	2.140
5000	2.25	-3.0	0.643	0.035	-0.053	0.772	2.136	0.534	0.092	0.044	0.769	2.139
5000	3.00	-0.0	0.637	0.039	-0.216	0.779	2.137	0.547	0.072	0.058	0.776	2.140
5000	3.00	-0.5	0.641	0.034	-0.192	0.781	2.139	0.551	0.073	0.052	0.778	2.142
5000	3.00	-1.0	0.647	0.031	-0.169	0.780	2.144	0.549	0.084	0.049	0.781	2.143
5000	3.00	-2.0	0.642	0.044	-0.076	0.783	2.135	0.525	0.100	0.052	0.780	2.138
5000	3.00	-3.0	0.637	0.050	-0.054	0.787	2.125	0.514	0.106	0.058	0.784	2.128
5500	1.50	-0.0	0.474	0.023	-0.178	0.641	1.671	0.402	0.055	0.042	0.639	1.673
5500	1.50	-0.5	0.483	0.019	-0.131	0.640	1.682	0.408	0.058	0.034	0.638	1.684
5500	1.50	-1.0	0.491	0.019	-0.094	0.642	1.692	0.415	0.064	0.032	0.644	1.690
5500	1.50	-2.0	0.499	0.021	-0.052	0.646	1.702	0.423	0.059	0.030	0.645	1.703
5500	1.50	-3.0	0.502	0.022	-0.042	0.648	1.704	0.426	0.058	0.030	0.647	1.705
5500	2.25	-0.0	0.486	0.022	-0.171	0.643	1.694	0.417	0.051	0.040	0.641	1.696
5500	2.25	-0.5	0.495	0.019	-0.128	0.644	1.705	0.423	0.055	0.033	0.642	1.707

Table 9. – *continued*

			Johnson					Glass				
T	log g	[A/H]	J-K	K-L	L-M	K	V-K	J-H	H-K	K-L	K	V-K
5500	2.25	-1.0	0.503	0.017	-0.091	0.645	1.717	0.429	0.062	0.030	0.647	1.715
5500	2.25	-2.0	0.510	0.020	-0.048	0.650	1.725	0.435	0.058	0.029	0.648	1.727
5500	2.25	-3.0	0.514	0.021	-0.039	0.652	1.728	0.439	0.058	0.028	0.651	1.729
5500	3.00	-0.0	0.489	0.023	-0.165	0.648	1.714	0.425	0.050	0.039	0.645	1.717
5500	3.00	-0.5	0.504	0.019	-0.124	0.649	1.727	0.433	0.054	0.033	0.647	1.729
5500	3.00	-1.0	0.513	0.018	-0.088	0.650	1.737	0.437	0.063	0.030	0.652	1.735
5500	3.00	-2.0	0.518	0.021	-0.047	0.654	1.744	0.440	0.062	0.029	0.653	1.745
5500	3.00	-3.0	0.521	0.022	-0.039	0.657	1.746	0.443	0.062	0.029	0.655	1.748
6000	2.25	-0.0	0.372	0.011	-0.121	0.529	1.335	0.314	0.043	0.026	0.528	1.336
6000	2.25	-0.5	0.382	0.011	-0.091	0.535	1.351	0.324	0.042	0.024	0.534	1.352
6000	2.25	-1.0	0.389	0.011	-0.068	0.540	1.362	0.332	0.047	0.023	0.543	1.359
6000	2.25	-2.0	0.395	0.016	-0.033	0.547	1.372	0.339	0.040	0.023	0.546	1.373
6000	2.25	-3.0	0.399	0.015	-0.032	0.548	1.375	0.343	0.040	0.022	0.548	1.375
6000	3.00	-0.0	0.383	0.010	-0.117	0.530	1.366	0.328	0.039	0.024	0.529	1.367
6000	3.00	-0.5	0.393	0.010	-0.088	0.537	1.382	0.338	0.039	0.022	0.536	1.383
6000	3.00	-1.0	0.400	0.011	-0.065	0.542	1.394	0.345	0.039	0.021	0.541	1.395
6000	3.00	-2.0	0.407	0.015	-0.032	0.549	1.405	0.352	0.038	0.021	0.548	1.406
6000	3.00	-3.0	0.411	0.013	-0.029	0.550	1.410	0.356	0.038	0.020	0.550	1.410
4500	4.50	0.0	0.819	0.074	-0.058	0.925	2.75	0.629	0.093	0.047	0.899	2.78
4500	4.50	-0.5	0.821	0.072	-0.043	0.926	2.73	0.626	0.097	0.046	0.902	2.75
4500	4.50	-1.0	0.803	0.086	-0.024	0.943	2.68	0.597	0.110	0.058	0.916	2.71
4500	4.50	-2.0	0.734	0.135	0.025	1.002	2.57	0.498	0.142	0.103	0.972	2.60
4500	4.50	-3.0	0.687	0.167	0.063	1.043	2.50	0.432	0.160	0.133	1.012	2.54
5000	4.50	0.0	0.645	0.059	-0.038	0.781	2.18	0.484	0.060	0.033	0.757	2.20
5000	4.50	-0.5	0.648	0.055	-0.024	0.783	2.17	0.486	0.063	0.030	0.759	2.20
5000	4.50	-1.0	0.646	0.059	-0.015	0.788	2.16	0.474	0.073	0.033	0.764	2.18
5000	4.50	-2.0	0.612	0.090	0.016	0.816	2.11	0.419	0.096	0.062	0.789	2.13
5000	4.50	-3.0	0.592	0.105	0.041	0.831	2.08	0.391	0.103	0.075	0.804	2.11
5500	4.50	0.0	0.510	0.042	-0.021	0.653	1.76	0.374	0.035	0.017	0.630	1.78
5500	4.50	-0.5	0.517	0.037	-0.009	0.655	1.76	0.378	0.038	0.013	0.633	1.78
5500	4.50	-1.0	0.518	0.039	-0.001	0.658	1.76	0.372	0.046	0.015	0.635	1.78
5500	4.50	-2.0	0.508	0.053	0.016	0.668	1.74	0.352	0.057	0.028	0.644	1.76
5500	4.50	-3.0	0.507	0.058	0.019	0.673	1.74	0.348	0.060	0.032	0.648	1.76
6000	4.50	0.0	0.403	0.026	-0.004	0.537	1.42	0.285	0.017	0.003	0.515	1.44
6000	4.50	-0.5	0.411	0.024	0.004	0.543	1.43	0.292	0.018	0.001	0.521	1.45
6000	4.50	-1.0	0.415	0.024	0.010	0.546	1.43	0.294	0.020	0.001	0.524	1.45
6000	4.50	-2.0	0.418	0.027	0.014	0.553	1.44	0.296	0.023	0.003	0.530	1.46
6000	4.50	-3.0	0.422	0.026	0.013	0.555	1.44	0.299	0.024	0.002	0.533	1.47
6500	4.50	0.0	0.323	0.019	0.005	0.446	1.16	0.218	0.004	-0.004	0.425	1.18
6500	4.50	-0.5	0.328	0.017	0.011	0.452	1.16	0.226	0.002	-0.006	0.430	1.19
6500	4.50	-1.0	0.331	0.017	0.013	0.455	1.17	0.229	0.002	-0.006	0.433	1.19
6500	4.50	-2.0	0.336	0.016	0.013	0.459	1.17	0.234	0.002	-0.007	0.438	1.19
6500	4.50	-3.0	0.336	0.015	0.013	0.460	1.17	0.236	0.001	-0.008	0.438	1.20

The two colour scales bracket the IRFM scale; however, there are some indications from the colours that $T_{\rm eff}$(IRFM) could be somewhat reduced, in accordance with the discussion above.

The neglect of TiO-band absorption in the 4000 K, solar abundance model colours of Table 9 will cause too low values of $T_{\rm eff}$ to be deduced. The error for $T_{\rm eff}$ from $V-K$ will be about 30 K, whereas that from $V-J$ will be about 50 K. These errors will be negligible for stars more metal poor than $[A/H]=-0.5$ but will, of course, be much more serious for metal-rich stars. Since the K magnitudes of the Wennfors, Glass and Caltech–CTIO systems are virtually identical to those of the Johnson system, similar temperature errors will occur if $V-K$ or $V-J$ on these systems is used to derive $T_{\rm eff}$.

5.2 THE WENNFORS *JHK* COLOURS

The synthetic Wennfors colours and K magnitudes are given in Table 10. Eighteen giants from the standard stars were measured by Wennfors (1986), with small internal errors. It should be

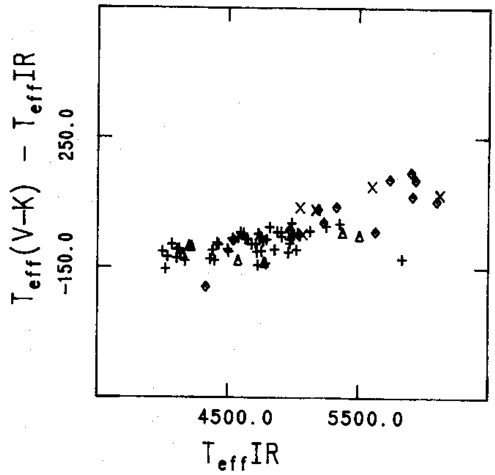

Figure 6. The differences between the effective temperatures deduced from Johnson *V–K* and from the IRFM are plotted versus $T_{\rm eff}$(IRFM). The stellar luminosity class coding is: II, triangles; III, plus signs; IV, crosses; and V, diamonds. This symbolism is used in Figs 6–19.

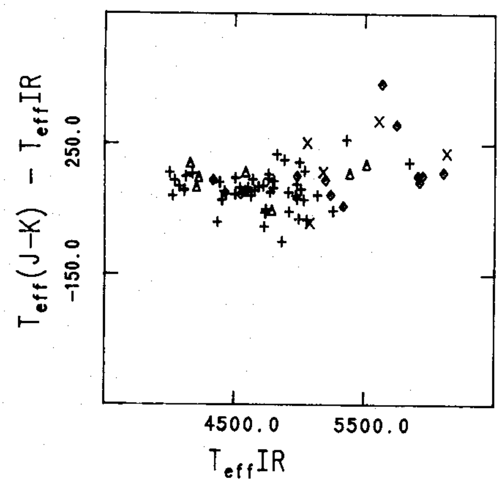

Figure 7. The differences between the effective temperatures deduced from Johnson *J–K* and from the IRFM are plotted versus $T_{\rm eff}$(IRFM).

noted that Wennfors' passbands are well defined and in particular that the *J* band, in contrast to Johnson's *J*, avoids the terrestrial absorption band longwards of 1.34 μm. As is seen in Fig. 9, $\Theta(J-K)_{\rm w}$ is around -100 K, and thus supports a lower $T_{\rm eff}$ than $T_{\rm eff}$(IRFM). The results are thus compatible with those of Johnson's *V–K* but not those from Johnson's *J–K*. The Wennfors *J–K* colour gives rather lower $T_{\rm eff}$s.

5.3 THE GLASS *JHK* COLOURS

The synthetic Glass colours for giants star models are given in Table 9. The number of stars in common with Glass is only 11; however, the scatter is small enough for a systematic tendency to be visible (Fig. 10). It is seen that, in contrast to the Cousins system (see below), $\Theta(J-K)_{\rm G}$ suggests that $T_{\rm eff}$(IRFM) should be increased by somewhat less than 100 K. $\Theta(J-H)_{\rm G}$ indicates an even greater positive correction to $T_{\rm eff}$(IRFM).

It was noted earlier that the $T_{\rm eff}$ given by the IRFM when the Glass *K* magnitude was used is about 80 K less than that found using the Johnson *K* magnitude. Since the *V–K* colours on the Glass and Johnson systems differ by only 0.01 mag on average for the stars in our sample,

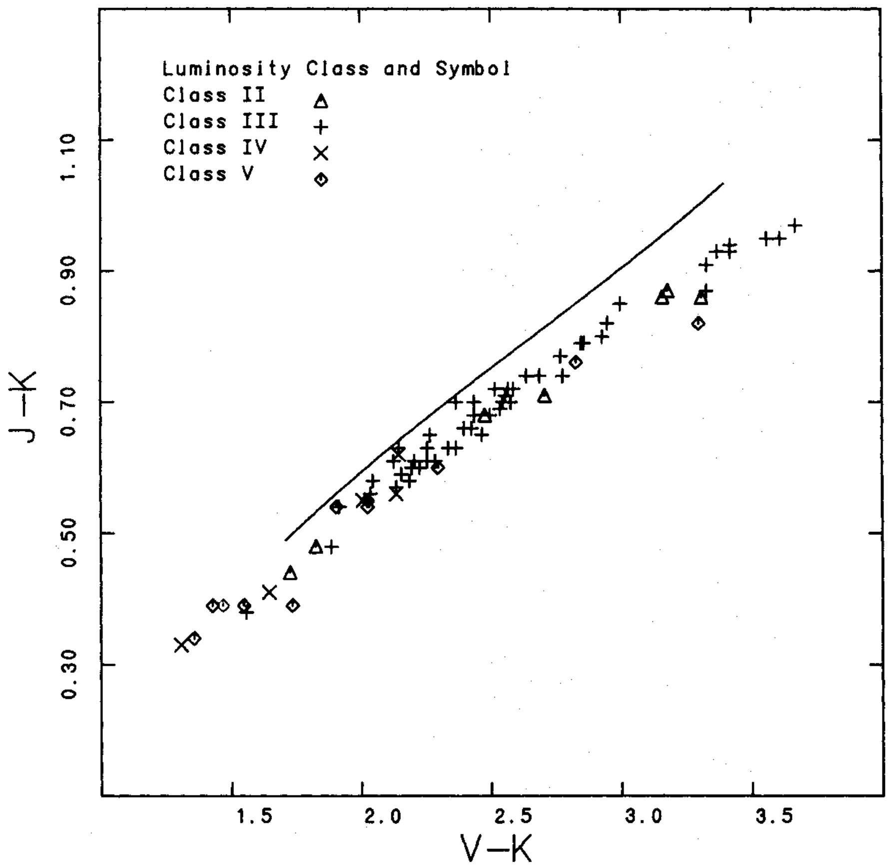

Figure 8. Johnson J–K is plotted versus V–K for stars and for Population I giant star models.

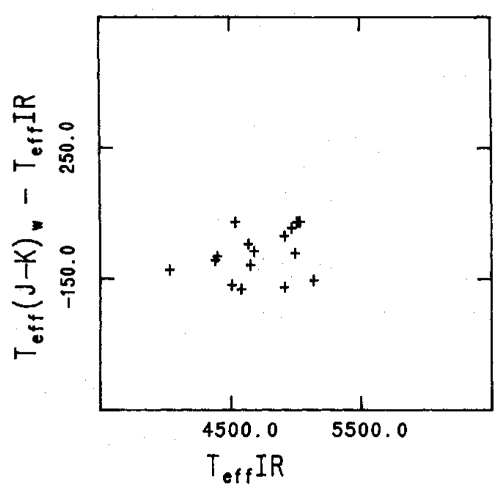

Figure 9. The differences between the effective temperatures deduced from Wenfors $J-K$ and from the IRFM are plotted versus T_{eff}(IRFM).

while the model colours are almost identical, this suggests that the T_{eff} error found by using $(V–K)_G$ [taken to be the error in $(V–K)_J$ in Table 16], would be consistent with that found using T_{eff}(IRFM) with Glass K magnitudes.

5.4 THE COUSINS *VRI* COLOURS

The synthetic Cousins colours and R magnitudes for the giant star models are given in Table 11. The colours for the dwarf models have been published by VandenBerg & Bell (1985),

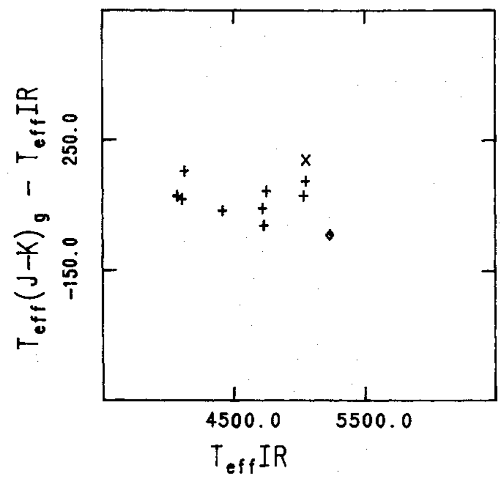

Figure 10. The differences between the effective temperatures deduced from Glass $J-K$ and from the IRFM are plotted versus T_{eff}(IRFM).

Table 10a.

				Wennfors				Caltech-CTIO				
T	log g	[A/H]	I-J	J-H	H-K	K	V-K	J-H	H-K	K-L	K	V-K
4000	0.75	-0.0	0.360	0.801	0.203	1.037	3.444	0.846	0.151	0.105	1.072	3.409
4000	0.75	-0.5	0.425	0.833	0.174	1.039	3.439	0.872	0.136	0.095	1.069	3.409
4000	0.75	-1.0	0.417	0.852	0.155	1.040	3.450	0.883	0.128	0.089	1.065	3.425
4000	0.75	-2.0	0.395	0.834	0.148	1.045	3.516	0.857	0.135	0.090	1.060	3.501
4000	0.75	-3.0	0.370	0.761	0.160	1.057	3.585	0.780	0.156	0.111	1.062	3.580
4000	1.50	-0.0	0.370	0.835	0.181	1.042	3.446	0.872	0.140	0.096	1.073	3.415
4000	1.50	-0.5	0.415	0.859	0.160	1.047	3.429	0.891	0.131	0.090	1.073	3.403
4000	1.50	-1.0	0.409	0.870	0.149	1.050	3.422	0.896	0.129	0.085	1.072	3.400
4000	1.50	-2.0	0.392	0.836	0.155	1.065	3.419	0.858	0.144	0.096	1.078	3.406
4000	1.50	-3.0	0.367	0.745	0.174	1.107	3.433	0.764	0.171	0.133	1.111	3.429
4000	2.25	0.0	0.412	0.858	0.165	1.049	3.453	0.891	0.134	0.090	1.076	3.426
4000	2.25	-0.5	0.407	0.874	0.152	1.055	3.432	0.902	0.130	0.086	1.077	3.410
4000	2.25	-1.0	0.402	0.876	0.149	1.059	3.416	0.900	0.132	0.085	1.078	3.397
4000	2.25	-2.0	0.387	0.823	0.164	1.088	3.363	0.844	0.155	0.107	1.099	3.352
4000	2.25	-3.0	0.347	0.700	0.187	1.167	3.290	0.716	0.184	0.159	1.168	3.289
4000	3.00	0.0	0.405	0.872	0.157	1.055	3.468	0.900	0.132	0.087	1.079	3.444
4000	3.00	-0.5	0.401	0.881	0.149	1.062	3.442	0.905	0.132	0.084	1.081	3.423
4000	3.00	-1.0	0.396	0.872	0.151	1.071	3.415	0.894	0.139	0.087	1.086	3.400
4000	3.00	-2.0	0.363	0.761	0.176	1.143	3.289	0.780	0.170	0.135	1.149	3.283
4000	3.00	-3.0	0.324	0.629	0.205	1.232	3.180	0.644	0.202	0.193	1.232	3.180
4500	0.75	-0.0	0.371	0.625	0.135	0.879	2.685	0.699	0.077	0.072	0.918	2.646
4500	0.75	-0.5	0.360	0.652	0.112	0.881	2.688	0.672	0.087	0.077	0.905	2.664
4500	0.75	-1.0	0.344	0.663	0.099	0.882	2.697	0.676	0.083	0.071	0.901	2.678
4500	0.75	-2.0	0.316	0.653	0.094	0.883	2.725	0.659	0.091	0.064	0.890	2.718
4500	0.75	-3.0	0.308	0.644	0.096	0.884	2.735	0.648	0.100	0.061	0.883	2.736
4500	1.50	0.0	0.366	0.650	0.123	0.883	2.687	0.653	0.099	0.087	0.908	2.662
4500	1.50	-0.5	0.357	0.671	0.106	0.888	2.683	0.688	0.086	0.073	0.909	2.662
4500	1.50	-1.0	0.344	0.679	0.099	0.891	2.682	0.692	0.085	0.068	0.908	2.665
4500	1.50	-2.0	0.320	0.660	0.103	0.897	2.685	0.667	0.099	0.068	0.905	2.677
4500	1.50	-3.0	0.308	0.633	0.111	0.906	2.681	0.639	0.114	0.073	0.905	2.682
4500	2.25	-0.0	0.303	0.668	0.113	0.890	2.693	0.685	0.090	0.075	0.911	2.672
4500	2.25	-0.5	0.352	0.682	0.103	0.894	2.688	0.699	0.077	0.071	0.917	2.665
4500	2.25	-1.0	0.341	0.686	0.100	0.900	2.680	0.698	0.089	0.067	0.914	2.666
4500	2.25	-2.0	0.321	0.652	0.114	0.915	2.659	0.661	0.110	0.077	0.922	2.652
4500	2.25	-3.0	0.303	0.604	0.128	0.938	2.628	0.611	0.129	0.097	0.937	2.629
4500	3.00	0.0	0.353	0.679	0.107	0.894	2.707	0.695	0.089	0.072	0.914	2.687
4500	3.00	-0.5	0.345	0.688	0.102	0.901	2.696	0.701	0.089	0.068	0.917	2.680
4500	3.00	-1.0	0.337	0.685	0.104	0.908	2.684	0.696	0.095	0.068	0.920	2.672
4500	3.00	-2.0	0.317	0.635	0.124	0.936	2.637	0.644	0.121	0.090	0.940	2.633
4500	3.00	-3.0	0.291	0.570	0.141	0.974	2.584	0.575	0.141	0.121	0.974	2.584

Table 10a – *continued*

				Wennfors				Caltech-CTIO				
T	log g	[A/H]	I-J	J-H	H-K	K	V-K	J-H	H-K	K-L	K	V-K
5000	1.50	0.0	0.299	0.522	0.076	0.748	2.132	0.528	0.060	0.060	0.766	2.114
5000	1.50	-0.5	0.285	0.534	0.066	0.753	2.131	0.535	0.057	0.054	0.766	2.118
5000	1.50	-1.0	0.275	0.538	0.063	0.756	2.133	0.536	0.060	0.048	0.764	2.125
5000	1.50	-2.0	0.267	0.539	0.064	0.759	2.136	0.535	0.068	0.043	0.760	2.135
5000	1.50	-3.0	0.265	0.541	0.063	0.762	2.134	0.536	0.068	0.043	0.762	2.134
5000	2.25	0.0	0.301	0.534	0.073	0.752	2.146	0.540	0.058	0.058	0.769	2.129
5000	2.25	-0.5	0.288	0.544	0.067	0.758	2.144	0.546	0.058	0.052	0.771	2.131
5000	2.25	-1.0	0.279	0.547	0.066	0.763	2.144	0.547	0.062	0.048	0.771	2.136
5000	2.25	-2.0	0.269	0.540	0.072	0.768	2.140	0.538	0.074	0.045	0.769	2.139
5000	2.25	-3.0	0.266	0.538	0.073	0.772	2.136	0.535	0.077	0.047	0.771	2.137
5000	3.00	-0.0	0.300	0.541	0.072	0.757	2.159	0.546	0.060	0.056	0.772	2.144
5000	3.00	-0.5	0.289	0.549	0.068	0.765	2.155	0.551	0.060	0.052	0.776	2.144
5000	3.00	-1.0	0.281	0.549	0.071	0.768	2.156	0.551	0.060	0.050	0.781	2.143
5000	3.00	-2.0	0.267	0.527	0.084	0.781	2.137	0.526	0.085	0.056	0.782	2.136
5000	3.00	-3.0	0.262	0.516	0.089	0.787	2.125	0.515	0.090	0.063	0.786	2.126
5500	1.50	0.0	0.228	0.412	0.047	0.632	1.680	0.401	0.045	0.042	0.638	1.674
5500	1.50	-0.5	0.224	0.421	0.044	0.636	1.686	0.408	0.046	0.036	0.639	1.683
5500	1.50	-1.0	0.224	0.428	0.042	0.641	1.693	0.417	0.043	0.032	0.646	1.688
5500	1.50	-2.0	0.224	0.436	0.041	0.647	1.701	0.423	0.047	0.033	0.646	1.702
5500	1.50	-3.0	0.224	0.440	0.040	0.648	1.704	0.426	0.046	0.032	0.648	1.704
5500	2.25	0.0	0.236	0.425	0.046	0.631	1.706	0.416	0.042	0.039	0.640	1.697
5500	2.25	-0.5	0.231	0.433	0.043	0.638	1.711	0.423	0.044	0.034	0.642	1.707
5500	2.25	-1.0	0.229	0.440	0.042	0.644	1.718	0.431	0.041	0.033	0.649	1.713
5500	2.25	-2.0	0.229	0.446	0.042	0.649	1.726	0.435	0.046	0.031	0.650	1.725
5500	2.25	-3.0	0.228	0.450	0.041	0.653	1.727	0.439	0.046	0.030	0.652	1.728
5500	3.00	-0.0	0.215	0.433	0.046	0.637	1.725	0.425	0.041	0.039	0.644	1.718
5500	3.00	-0.5	0.235	0.440	0.045	0.643	1.733	0.432	0.043	0.034	0.647	1.729
5500	3.00	-1.0	0.233	0.446	0.045	0.647	1.740	0.439	0.042	0.033	0.654	1.733
5500	3.00	-2.0	0.230	0.449	0.047	0.654	1.744	0.440	0.050	0.031	0.654	1.744
5500	3.00	-3.0	0.230	0.452	0.047	0.656	1.747	0.442	0.050	0.031	0.656	1.747
6000	2.25	0.0	0.183	0.334	0.029	0.528	1.336	0.313	0.034	0.027	0.528	1.336
6000	2.25	-0.5	0.186	0.344	0.027	0.535	1.351	0.323	0.033	0.026	0.535	1.351
6000	2.25	-1.0	0.188	0.352	0.026	0.541	1.361	0.334	0.029	0.026	0.544	1.358
6000	2.25	-2.0	0.189	0.359	0.025	0.547	1.372	0.339	0.031	0.024	0.547	1.372
6000	2.25	-3.0	0.189	0.363	0.024	0.549	1.374	0.342	0.030	0.023	0.549	1.374
6000	3.00	0.0	0.191	0.344	0.029	0.528	1.368	0.327	0.031	0.025	0.529	1.367
6000	3.00	-0.5	0.193	0.355	0.027	0.535	1.384	0.337	0.030	0.023	0.536	1.383
6000	3.00	-1.0	0.195	0.362	0.026	0.541	1.395	0.344	0.030	0.022	0.542	1.394
6000	3.00	-2.0	0.195	0.369	0.025	0.549	1.405	0.351	0.030	0.023	0.549	1.405
6000	3.00	-3.0	0.195	0.373	0.025	0.550	1.410	0.355	0.029	0.022	0.551	1.409

while the R magnitudes are given by Bell & VandenBerg (1987). The results for similar models are not identical, in part due to the difference in turbulent broadening of the lines, i.e. a microturbulent velocity of 1 km s^{-1} for the dwarfs and a total, depth-independent, turbulent velocity of 2.0 km s^{-1} for the giants.

Thirty-five of the standard stars were observed by Cousins (almost all of them being giants) and $\Theta(R-I)_c$ and $\Theta(V-I)_c$ are shown in Figs 11 and 12. These colours give systematic and mutually consistent evidence for the fact that the IRFM temperature scale may be too high by about 180 K. The result is similar for $(V-R)_c$.

As noted previously, we have used the Cousins (1981) response functions. Bessell (1983) has discussed the accuracy of these response functions and has also published response functions. Bessell (1986b) has found that his response functions yield bluer colours than do those of Cousins. Our comparisons of the synthetic colours show that, at $T_{eff}=4000$ K, our calculations using Bessell's (1986b) response functions give colours which are 0.012 mag bluer in $V-R$ and 0.039 mag bluer in $V-I$, in agreement with Bessell's own conclusions. If these synthetic colours were used to derive T_{eff}, the values would be lower, by about 60 K at 4000 K, and the discrepancy with the IRFM would be greater.

Table 10b.

			Wennfors				Caltech-CTIO			
T	log g	[A/H]	I-J	J-H	H-K	V-K	J-H	H-K	K-L	V-K
4500	4.50	-0.0	0.345	0.637	0.109	2.676	0.704	0.087	0.068	2.760
4500	4.50	-0.5	0.340	0.635	0.109	2.648	0.699	0.092	0.068	2.737
4500	4.50	-1.0	0.328	0.607	0.119	2.591	0.670	0.104	0.082	2.693
4500	4.50	-2.0	0.292	0.510	0.148	2.441	0.571	0.134	0.133	2.578
4500	4.50	-3.0	0.268	0.446	0.166	2.354	0.505	0.151	0.166	2.511
5000	4.50	-0.0	0.299	0.497	0.077	2.131	0.553	0.062	0.054	2.189
5000	4.50	-0.5	0.292	0.500	0.078	2.120	0.554	0.065	0.052	2.181
5000	4.50	-1.0	0.283	0.489	0.085	2.095	0.542	0.075	0.057	2.167
5000	4.50	-2.0	0.258	0.436	0.106	2.016	0.488	0.096	0.089	2.113
5000	4.50	-3.0	0.246	0.410	0.113	1.981	0.461	0.103	0.104	2.086
5500	4.50	-0.0	0.252	0.393	0.053	1.725	0.439	0.043	0.039	1.764
5500	4.50	-0.5	0.245	0.398	0.053	1.725	0.443	0.046	0.036	1.767
5500	4.50	-1.0	0.240	0.393	0.060	1.713	0.437	0.053	0.039	1.763
5500	4.50	-2.0	0.229	0.374	0.071	1.683	0.418	0.064	0.053	1.745
5500	4.50	-3.0	0.227	0.370	0.074	1.677	0.414	0.067	0.057	1.743
6000	4.50	-0.0	0.209	0.311	0.033	1.399	0.348	0.029	0.026	1.424
6000	4.50	-0.5	0.208	0.318	0.033	1.407	0.355	0.030	0.023	1.433
6000	4.50	-1.0	0.206	0.320	0.036	1.408	0.357	0.033	0.024	1.437
6000	4.50	-2.0	0.205	0.322	0.038	1.412	0.359	0.035	0.026	1.443
6000	4.50	-3.0	0.205	0.325	0.039	1.417	0.361	0.036	0.025	1.449
6500	4.50	-0.0	0.180	0.249	0.021	1.147	0.280	0.020	0.018	1.162
6500	4.50	-0.5	0.181	0.256	0.019	1.155	0.287	0.019	0.016	1.169
6500	4.50	-1.0	0.181	0.260	0.019	1.159	0.290	0.018	0.016	1.172
6500	4.50	-2.0	0.180	0.265	0.019	1.165	0.295	0.018	0.015	1.178
6500	4.50	-3.0	0.180	0.266	0.018	1.166	0.297	0.018	0.014	1.178

The TiO-band studies suggest that the Cousins colours $V-R$ and $R-I$ must be used with caution for stars with solar abundance and $T_{eff} \sim 4000$ K. The $V-R$ range between models with $T_{eff} = 4000$ and 4500 K, $\log g = 1.50$ and [A/H] = 0.0 is only 0.17 mag so that the shift of $V-R$ of 0.03 mag caused by TiO cannot be neglected. The $V-I$ colour should be much better because of the compensating effects in the two passbands and the broader base in wavelength. However, as is also the case with the Wing system (discussed below), the observational results suggest that the TiO effects predicted by the models may well be too large.

The problem of defining the broad-band colours in a way suitable for theoretical calibration is non-trivial and involves accurate measurements of filter transmission profiles, detector sensitivity and the wavelength dependence of atmospheric transmission. These problems are considerably reduced for narrow-band systems, provided that they span a wavelength interval that is broad enough. Several such systems have been used in the near infrared and some colours that have been measured are suitable for temperature determinations.

5.5 THE JML 13-COLOUR PHOTOMETRY

The 13-colour photometry of Johnson *et al.* (1967) and Johnson & Mitchell (1975) is very useful in the problem of determining stellar temperatures. The synthetic photometry is given in Table 12.

In the previous section this photometry serves as an essential source of data for determining the integrated fluxes of stars. The passbands are sufficiently well separated in wavelength that the resultant colours vary strongly with T_{eff}. The passbands shortward of 5200 Å are not suitable for this purpose since they are affected by line blocking and consequently depend upon stellar abundances and gravities. However, six passbands still remain for analysis; a seventh, the 6300 Å band, is omitted since it was found to give results inconsistent with the other bands; Cousins (1981) has found a similar problem with this passband. He points out

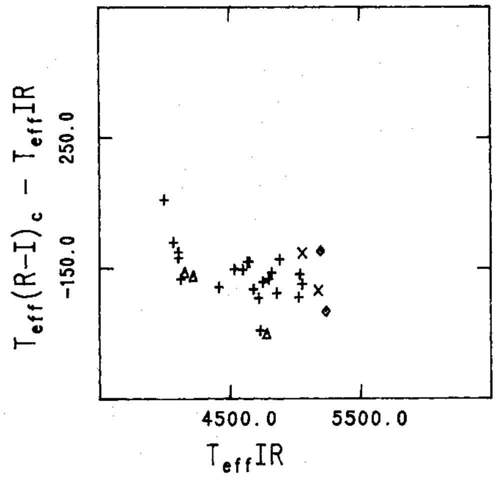

Figure 11. The differences between the effective temperatures deduced from Cousins $R-I$ and from the IRFM are plotted versus T_{eff}(IRFM).

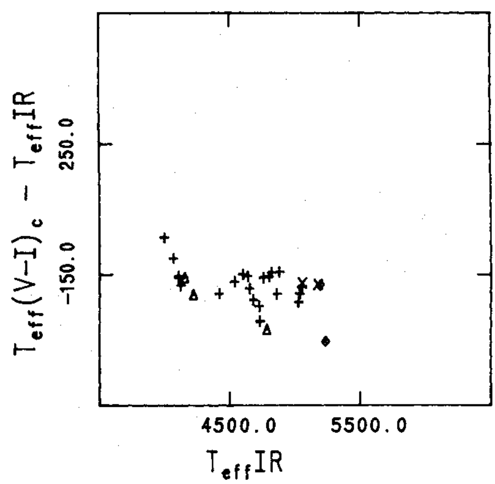

Figure 12. The differences between the effective temperatures deduced from Cousins $V-I$ and from the IRFM are plotted versus T_{eff}(IRFM).

that the long-wavelength side of this band is cathode limited, not filter limited, and consequently temperature dependent. An error would have crept in if the cathode response were measured at a different temperature than that used for the stellar work.

Eighty-five of our standard stars have been observed in the JML system. For these stars, we derived effective temperatures from all 15 colour combinations of the six passbands. For each star an average temperature was derived, and the scatter around these averages, allowing for a zero-point shift individual to each colour, was adopted as a measure of the power of each colour as a temperature criterion. Not unexpectedly, the colours with the longest wavelength bases were found to give the best temperature determinations. We found the indices 58–99 and 72–110 to be the best ones, with the smallest scatter for the first mentioned. $\Theta(58-99)$ is plotted relative to T_{eff}(IRFM) in Fig. 13. It is seen that the IRFM scale is essentially confirmed. A small negative shift, less than -70 K, could, however, be present. Fig. 14 shows that the 72–110 index suggests an upward revision of the IRFM scale by about 100 K. This latter index also indicates a luminosity dependence – the correction for the dwarfs and subgiants is much less, or even negative. It should be noted that the direction of this luminosity dependence is reversed with respect to that indicated by the Johnson $(V-K)$ colour (Fig. 6). The scatter in

Table 11. The Cousins' system.

T_{eff}	Log g	[A/H]	V-R	V-I	R-I	R
4000	0.75	-0.0	0.765	1.435	0.670	3.714
4000	0.75	-0.5	0.746	1.426	0.680	3.723
4000	0.75	-1.0	0.744	1.440	0.697	3.731
4000	0.75	-2.0	0.791	1.536	0.745	3.745
4000	0.75	-3.0	0.868	1.672	0.804	3.741
4000	1.50	-0.0	0.760	1.436	0.676	3.728
4000	1.50	-0.5	0.736	1.417	0.681	3.735
4000	1.50	-1.0	0.722	1.411	0.689	3.740
4000	1.50	-2.0	0.729	1.440	0.711	3.737
4000	1.50	-3.0	0.789	1.543	0.754	3.724
4000	2.25	-0.0	0.766	1.449	0.683	3.743
4000	2.25	-0.5	0.740	1.425	0.685	3.749
4000	2.25	-1.0	0.721	1.408	0.687	3.751
4000	2.25	-2.0	0.705	1.401	0.695	3.734
4000	2.25	-3.0	0.745	1.473	0.728	3.687
4500	0.75	-0.0	0.596	1.119	0.523	2.967
4500	0.75	-0.5	0.585	1.127	0.543	2.976
4500	0.75	-1.0	0.586	1.150	0.564	2.980
4500	0.75	-2.0	0.608	1.207	0.599	2.983
4500	0.75	-3.0	0.616	1.228	0.612	2.985
4500	1.50	-0.0	0.585	1.114	0.528	2.985
4500	1.50	-0.5	0.569	1.111	0.542	2.995
4500	1.50	-1.0	0.562	1.117	0.556	3.001
4500	1.50	-2.0	0.570	1.148	0.578	2.997
4500	1.50	-3.0	0.581	1.172	0.591	2.988
4500	2.25	-0.0	0.585	1.122	0.537	3.001
4500	2.25	-0.5	0.566	1.112	0.546	3.012
4500	2.25	-1.0	0.554	1.108	0.555	3.017
4500	2.25	-2.0	0.550	1.117	0.568	3.010
4500	2.25	-3.0	0.563	1.142	0.580	2.986
4500	3.00	-0.0	0.595	1.142	0.547	3.014
4500	3.00	-0.5	0.573	1.125	0.552	3.024
4500	3.00	-1.0	0.557	1.114	0.557	3.029
4500	3.00	-2.0	0.546	1.110	0.564	3.015
4500	3.00	-3.0	0.561	1.139	0.579	2.980
5000	1.50	-0.0	0.476	0.915	0.438	2.408
5000	1.50	-0.5	0.460	0.914	0.454	2.419
5000	1.50	-1.0	0.452	0.916	0.464	2.429
5000	1.50	-2.0	0.446	0.919	0.473	2.440
5000	1.50	-3.0	0.442	0.916	0.475	2.446
5000	2.25	-0.0	0.474	0.915	0.442	2.428
5000	2.25	-0.5	0.457	0.912	0.455	2.442
5000	2.25	-1.0	0.448	0.911	0.463	2.453
5000	2.25	-2.0	0.441	0.911	0.470	2.460
5000	2.25	-3.0	0.436	0.909	0.473	2.463
5000	3.00	-0.0	0.475	0.922	0.447	2.445
5000	3.00	-0.5	0.459	0.916	0.458	2.460
5000	3.00	-1.0	0.448	0.912	0.464	2.471
5000	3.00	-2.0	0.441	0.911	0.470	2.469
5000	3.00	-3.0	0.438	0.910	0.473	2.466
5500	1.50	-0.0	0.379	0.749	0.370	1.938
5500	1.50	-0.5	0.365	0.743	0.377	1.957
5500	1.50	-1.0	0.358	0.739	0.382	1.975
5500	1.50	-2.0	0.350	0.735	0.386	1.996
5500	1.50	-3.0	0.345	0.732	0.387	2.004
5500	2.25	-0.0	0.382	0.756	0.374	1.960
5500	2.25	-0.5	0.369	0.750	0.381	1.981
5500	2.25	-1.0	0.361	0.747	0.385	1.999
5500	2.25	-2.0	0.353	0.743	0.390	2.019
5500	2.25	-3.0	0.349	0.741	0.391	2.029
5500	3.00	-0.0	0.387	0.765	0.378	1.981
5500	3.00	-0.5	0.373	0.758	0.385	2.003
5500	3.00	-1.0	0.365	0.755	0.389	2.021
5500	3.00	-2.0	0.358	0.751	0.394	2.038
5500	3.00	-3.0	0.354	0.749	0.395	2.047

Table 11. – *continued*

T_{eff}	Log g	[A/H]	V-R	V-I	R-I	R
6000	2.25	-0.0	0.300	0.607	0.307	1.573
6000	2.25	-0.5	0.290	0.602	0.311	1.600
6000	2.25	-1.0	0.285	0.599	0.314	1.621
6000	2.25	-2.0	0.279	0.598	0.319	1.643
6000	2.25	-3.0	0.276	0.595	0.320	1.652
6000	3.00	-0.0	0.309	0.624	0.315	1.595
6000	3.00	-0.5	0.300	0.619	0.319	1.624
6000	3.00	-1.0	0.295	0.617	0.322	1.644
6000	3.00	-2.0	0.289	0.616	0.327	1.667
6000	3.00	-3.0	0.286	0.614	0.328	1.677

Figs 13 and 14 essentially corresponds to the observational errors. In conclusion, we find that the JML system seems to roughly verify the IRFM scale.

The two-colour diagram, (58–99) versus (72–110) (Fig. 15), shows the effect discussed in the previous paragraph. The slope of the line computed for solar abundance giant branch models matches that found from the stars in a fairly satisfactory manner. However, it is offset from the observations, with either (58–99) being too blue or (72–110) being too red, or both. This offset is 0.07 in (72–110) or 0.1 in (58–99) at $T_{\rm eff}=5500$ K, and increases to 0.1 in (72–110) or 0.15 in (58–99) at 4000 K. If we assume, following the subsequent discussion in Section 6, that the temperature scale from (58–99) is essentially correct, then the change of about 0.07–0.10 mag in (72–110) corresponds to the temperature found from (72–110) being about 250 K too high. If a systematic change of about 0.08 mag is made to the computed (72–110) colours, the temperatures deduced from the (58–99), (72–110) diagram and from the (72–110) colour alone would be in reasonable accord with the revised $T_{\rm eff}$(IRFM) described in Section 6. The fact that (58–99) and (72–110) were the two JML indices found to give the least scatter in temperature determinations probably explains the relatively small scatter in Fig. 15.

Both (58–99) and (72–110) must be treated with caution when used as temperature indicators for stars with TiO lines in their spectra. The 72 magnitude, from the data of Table 2, is strongly affected, although use of the (72–110) colour might be partly compensated for by the TiO ϕ system, with lines in the 11 000 Å region.

5.7 THE WING EIGHT-COLOUR PHOTOMETRY

The Wing (1971) synthetic photometry is given in Table 13. For 32 of our standard stars measurements in the eight-colour system were available from Wing (1971). The system contains two 'continuum points', centred at 7810 Å and 10 540 Å, which are only slightly affected by CN (see Wing *et al.* 1985). In fact, our calculations prove that the $m(7810)-m(10540)=78-110$ colour is indeed very little gravity and metallicity dependent – we find $|\partial(78-110)/\partial(\log g)|<0.004$ mag and $|\partial(78-110)/\partial[{\rm Fe/H}]|<0.012$ mag. This property, the high observational accuracy of the observations available and the independence of the IRFM determinations make this photometry one of the most important checks on the IRFM effective temperature scale. We have used the 78–110 colour to derive the effective temperatures – the resulting $\Theta(78-110)$ values are shown in Fig. 16. It is seen that a correction of the IRFM scale downwards is again suggested – the results of the 78–110 colour are compatible with those of the Johnson's $V-K$, the Wennfors *JHK* and the JML 58–99 colour.

TiO lines affect the magnitudes calculated for the 7120 and 7810 Å passbands of the Wing system. The temperature error to be expected for the stars with $T_{\rm eff}=4000$ K and solar

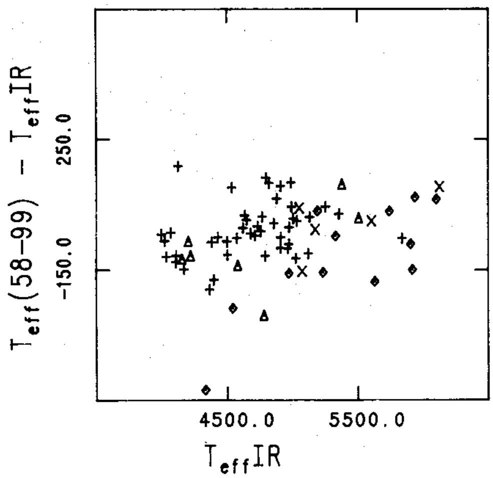

Figure 13. The differences between the effective temperatures deduced from Johnson and Mitchell 58–99 and from the IRFM are ploted versus T_{eff}(IRFM).

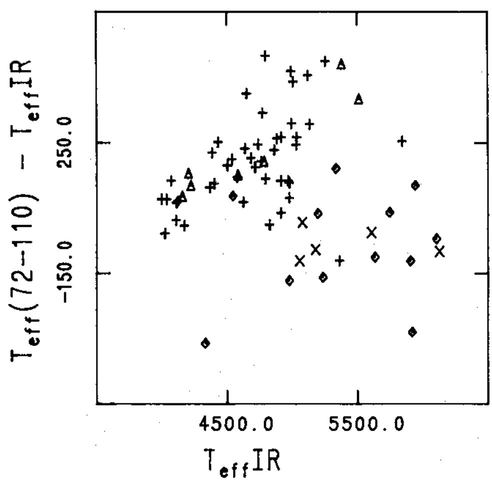

Figure 14. The differences between the effective temperatures deduced from Johnson and Mitchell 72–110 and from the IRFM are plotted versus T_{eff}(IRFM).

abundances is possibly as high as 150 K, although the results shown in Fig. 16 suggest that this is an overestimate.

5.8 THE PHOTOMETRY OF FRISK

Frisk (1983) obtained photometry in three bands, centred at 5930 Å, 7800 Å and 10640 Å, respectively. However, only nine stars were observed that are in common with our standard sample for which T_{eff}(IRFM) are available. Both the indices $m(5930)-m(7800)$ and $m(5930)-m(10\,640)$ lead to temperatures in reasonable accord with the IRFM, with $\langle\Theta\rangle$ around -50 K. It should be noted that Frisk's stars are mainly dwarfs and subgiants.

5.9 THE CALTECH–CTIO PHOTOMETRY

As noted earlier, photometry on the Caltech–CTIO system is not available for the majority of the stars in our sample. The synthetic photometry is given in Table 10. Observational data for

Table 12a. Johnson & Mitchell 13-colour giant stars.

T_{eff}	log g	[A/H]	33-52	35-52	37-52	40-52	45-52	52-58	52-63	52-72	52-80	52-86	52-99	52-110
4000	0.75	-0.0	2.920	2.797	3.163	2.184	0.652	0.781	1.106	1.558	1.845	1.987	2.310	2.640
4000	0.75	-0.5	2.840	2.524	2.761	1.905	0.676	0.729	1.048	1.511	1.806	1.962	2.270	2.595
4000	0.75	-1.0	2.870	2.379	2.509	1.830	0.716	0.695	1.022	1.498	1.802	1.960	2.265	2.586
4000	0.75	-2.0	2.877	2.276	2.212	1.882	0.814	0.706	1.072	1.582	1.913	2.074	2.381	2.700
4000	1.50	-0.0	2.269	2.212	2.600	1.834	0.552	0.782	1.013	1.516	1.915	2.064	2.375	2.702
4000	1.50	-0.5	2.225	2.007	2.322	1.638	0.588	0.713	1.029	1.493	1.793	1.945	2.252	2.576
4000	1.50	-1.0	2.219	1.858	2.075	1.570	0.604	0.672	0.989	1.457	1.764	1.917	2.222	2.544
4000	1.50	-2.0	2.429	1.841	1.864	1.592	0.694	0.643	0.980	1.461	1.782	1.937	2.240	2.562
4000	1.50	-3.0	2.637	1.978	1.858	1.744	0.810	0.683	1.059	1.572	1.911	2.070	2.374	2.694
4000	2.25	-0.0	1.876	1.852	2.263	1.602	0.534	0.794	1.120	1.590	1.892	2.038	2.349	2.675
4000	2.25	-0.5	1.821	1.664	1.993	1.467	0.521	0.717	1.035	1.500	1.806	1.954	2.263	2.587
4000	2.25	-1.0	1.794	1.524	1.813	1.385	0.530	0.677	0.991	1.457	1.767	1.916	2.222	2.546
4000	2.25	-2.0	1.989	1.505	1.628	1.401	0.596	0.626	0.949	1.416	1.733	1.883	2.186	2.509
4000	2.25	-3.0	2.288	1.681	1.641	1.555	0.731	0.639	0.996	1.488	1.817	1.971	2.265	2.576
4500	0.75	-0.0	2.198	1.973	2.225	1.626	0.575	0.612	0.856	1.206	1.426	1.541	1.785	2.062
4500	0.75	-0.5	2.085	1.745	1.872	1.491	0.570	0.564	0.817	1.185	1.415	1.534	1.770	2.038
4500	0.75	-1.0	2.029	1.599	1.615	1.395	0.583	0.540	0.804	1.187	1.432	1.550	1.784	2.047
4500	0.75	-2.0	1.903	1.417	1.324	1.319	0.619	0.531	0.820	1.225	1.495	1.611	1.848	2.114
4500	0.75	-3.0	1.689	1.283	1.166	1.256	0.628	0.523	0.824	1.235	1.511	1.631	1.866	2.134
4500	1.50	-0.0	1.771	1.623	1.927	1.475	0.534	0.586	0.830	1.184	1.408	1.525	1.766	2.041
4500	1.50	-0.5	1.639	1.410	1.617	1.318	0.522	0.539	0.787	1.153	1.386	1.505	1.740	2.009
4500	1.50	-1.0	1.570	1.243	1.364	1.234	0.521	0.511	0.766	1.141	1.385	1.503	1.736	2.002
4500	1.50	-2.0	1.541	1.092	1.106	1.174	0.553	0.494	0.765	1.153	1.416	1.531	1.765	2.032
4500	1.50	-3.0	1.418	1.016	0.996	1.146	0.576	0.489	0.775	1.169	1.438	1.556	1.788	2.056
4500	2.25	-0.0	1.445	1.389	1.746	1.366	0.500	0.572	0.821	1.181	1.411	1.528	1.767	2.040
4500	2.25	-0.5	1.320	1.148	1.432	1.224	0.488	0.527	0.777	1.145	1.384	1.501	1.737	2.006
4500	2.25	-1.0	1.250	0.998	1.192	1.128	0.484	0.498	0.750	1.123	1.371	1.487	1.721	1.988
4500	2.25	-2.0	1.222	0.842	0.964	1.074	0.508	0.473	0.736	1.115	1.374	1.488	1.723	1.991
4500	2.25	-3.0	1.208	0.826	0.890	1.081	0.546	0.472	0.749	1.135	1.400	1.515	1.745	2.011
4500	3.00	-0.0	1.256	1.229	1.615	1.279	0.463	0.574	0.829	1.197	1.435	1.548	1.788	2.059
4500	3.00	-0.5	1.133	1.017	1.357	1.161	0.456	0.532	0.784	1.157	1.401	1.515	1.753	2.022
4500	3.00	-1.0	1.050	0.855	1.148	1.078	0.455	0.500	0.754	1.127	1.378	1.492	1.729	1.997
4500	3.00	-2.0	1.061	0.736	0.917	1.028	0.485	0.469	0.730	1.106	1.364	1.477	1.711	1.979
4500	3.00	-3.0	1.083	0.730	0.842	1.046	0.534	0.469	0.747	1.132	1.396	1.510	1.737	1.998
5000	1.50	-0.0	1.322	1.112	1.213	1.114	0.438	0.467	0.672	0.967	1.153	1.236	1.424	1.650
5000	1.50	-0.5	1.205	0.925	0.959	0.984	0.426	0.428	0.635	0.943	1.144	1.225	1.412	1.635
5000	1.50	-1.0	1.082	0.785	0.783	0.898	0.421	0.404	0.616	0.929	1.140	1.221	1.408	1.633
5000	1.50	-2.0	0.847	0.603	0.569	0.794	0.416	0.379	0.599	0.913	1.130	1.216	1.400	1.629
5000	1.50	-3.0	0.719	0.508	0.481	0.741	0.412	0.364	0.587	0.900	1.119	1.207	1.389	1.619
5000	2.25	-0.0	1.063	0.943	1.141	1.057	0.420	0.460	0.665	0.962	1.150	1.235	1.422	1.650
5000	2.25	-0.5	0.920	0.733	0.876	0.934	0.407	0.422	0.629	0.936	1.138	1.222	1.407	1.633
5000	2.25	-1.0	0.816	0.573	0.687	0.853	0.403	0.397	0.608	0.918	1.130	1.213	1.399	1.626
5000	2.25	-2.0	0.605	0.393	0.486	0.757	0.402	0.373	0.590	0.902	1.119	1.205	1.389	1.619
5000	2.25	-3.0	0.474	0.297	0.400	0.710	0.401	0.358	0.579	0.890	1.108	1.197	1.378	1.610
5000	3.00	-0.0	0.884	0.820	1.095	1.023	0.406	0.455	0.664	0.963	1.155	1.241	1.428	1.656
5000	3.00	-0.5	0.755	0.619	0.852	0.913	0.395	0.420	0.629	0.937	1.141	1.226	1.412	1.638
5000	3.00	-1.0	0.639	0.458	0.667	0.835	0.391	0.397	0.608	0.918	1.130	1.214	1.401	1.629
5000	3.00	-2.0	0.493	0.286	0.464	0.760	0.398	0.373	0.590	0.902	1.119	1.205	1.389	1.619
5500	1.50	-0.0	1.092	0.829	0.746	0.832	0.352	0.360	0.528	0.780	0.945	0.998	1.153	1.340
5500	1.50	-0.5	0.929	0.687	0.555	0.723	0.338	0.333	0.502	0.758	0.932	0.988	1.141	1.331
5500	1.50	-1.0	0.796	0.585	0.429	0.641	0.327	0.316	0.487	0.744	0.921	0.982	1.131	1.325
5500	1.50	-2.0	0.620	0.457	0.292	0.551	0.314	0.294	0.470	0.726	0.905	0.971	1.117	1.314
5500	1.50	-3.0	0.549	0.392	0.237	0.519	0.310	0.282	0.460	0.715	0.895	0.963	1.108	1.306
5500	2.25	-0.0	0.835	0.648	0.680	0.792	0.342	0.361	0.532	0.786	0.952	1.007	1.158	1.348
5500	2.25	-0.5	0.685	0.496	0.494	0.696	0.332	0.334	0.505	0.763	0.939	0.996	1.146	1.338
5500	2.25	-1.0	0.548	0.384	0.368	0.622	0.323	0.317	0.490	0.750	0.928	0.989	1.137	1.333
5500	2.25	-2.0	0.365	0.243	0.228	0.537	0.313	0.296	0.474	0.733	0.914	0.979	1.125	1.324
5500	2.25	-3.0	0.294	0.174	0.173	0.506	0.311	0.284	0.465	0.723	0.904	0.971	1.116	1.317
5500	3.00	-0.0	0.634	0.509	0.663	0.777	0.337	0.364	0.538	0.794	0.962	1.019	1.168	1.359
5500	3.00	-0.5	0.497	0.353	0.482	0.690	0.329	0.336	0.511	0.771	0.949	1.007	1.156	1.350
5500	3.00	-1.0	0.365	0.231	0.354	0.625	0.322	0.320	0.496	0.757	0.938	0.999	1.147	1.345
5500	3.00	-2.0	0.179	0.079	0.208	0.545	0.316	0.300	0.480	0.741	0.924	0.989	1.135	1.335
5500	3.00	-3.0	0.107	0.007	0.151	0.515	0.317	0.288	0.471	0.731	0.915	0.982	1.126	1.329

Table 12a – *continued*

T_{eff}	log g	[A/H]	33-52	35-52	37-52	40-52	45-52	52-58	52-63	52-72	52-80	52-99	52-110	
6000	2.25	-0.0	0.727	0.545	0.411	0.584	0.271	0.281	0.417	0.627	0.767	0.805	0.930	1.091
6000	2.25	-0.5	0.598	0.448	0.290	0.506	0.258	0.263	0.400	0.612	0.756	0.799	0.922	1.086
6000	2.25	-1.0	0.493	0.371	0.208	0.451	0.250	0.250	0.390	0.601	0.748	0.794	0.915	1.082
6000	2.25	-2.0	0.376	0.275	0.117	0.394	0.244	0.233	0.377	0.588	0.737	0.787	0.905	1.076
6000	2.25	-3.0	0.332	0.229	0.079	0.373	0.242	0.224	0.369	0.580	0.729	0.780	0.898	1.071
6000	3.00	-0.0	0.505	0.370	0.406	0.589	0.273	0.287	0.428	0.644	0.787	0.824	0.945	1.110
6000	3.00	-0.5	0.378	0.265	0.286	0.519	0.264	0.269	0.412	0.629	0.778	0.819	0.938	1.106
6000	3.00	-1.0	0.272	0.182	0.203	0.468	0.258	0.257	0.402	0.619	0.770	0.814	0.932	1.103
6000	3.00	-2.0	0.155	0.080	0.113	0.416	0.253	0.241	0.389	0.608	0.760	0.808	0.924	1.098
6000	3.00	-3.0	0.109	0.030	0.075	0.397	0.253	0.233	0.382	0.600	0.753	0.803	0.919	1.094

Table 12b. Johnson & Mitchell 13-colour dwarf stars.

T_{eff}	log g	[A/H]	33-52	35-52	37-52	40-52	45-52	52-58	52-63	52-72	52-80	52-99	52-110	
4500	3.00	.0	1.264	1.135	1.547	1.175	.377	.648	.889	1.256	1.496	1.611	1.818	2.023
4500	3.00	-.5	1.172	.946	1.316	1.080	.384	.599	.840	1.210	1.455	1.570	1.774	1.977
4500	3.00	-1.0	1.116	.807	1.130	1.020	.400	.556	.799	1.171	1.424	1.537	1.740	1.941
4500	3.00	-2.0	1.176	.721	.928	.998	.459	.499	.748	1.124	1.385	1.495	1.696	1.895
4500	3.75	.0	1.227	1.122	1.545	1.120	.333	.688	.938	1.313	1.558	1.669	1.879	2.081
4500	3.75	-.5	1.147	.955	1.357	1.038	.339	.642	.889	1.263	1.514	1.625	1.832	2.033
4500	3.75	-1.0	1.092	.818	1.189	.984	.354	.600	.846	1.220	1.475	1.586	1.791	1.992
4500	3.75	-2.0	1.151	.728	.992	.993	.440	.530	.784	1.163	1.424	1.534	1.733	1.928
4500	4.50	.0	1.277	1.199	1.616	1.105	.295	.735	.998	1.381	1.632	1.739	1.951	2.153
4500	4.50	-.5	1.207	1.048	1.460	1.032	.300	.694	.950	1.330	1.584	1.691	1.901	2.102
4500	4.50	-1.0	1.191	.936	1.315	.996	.328	.650	.905	1.285	1.541	1.649	1.855	2.053
4500	4.50	-2.0	1.243	.821	1.084	1.029	.447	.559	.823	1.210	1.474	1.583	1.778	1.966
5000	3.00	.0	.911	.742	1.061	.979	.362	.488	.681	.982	1.176	1.263	1.417	1.581
5000	3.00	-.5	.811	.562	.838	.886	.366	.445	.642	.949	1.154	1.238	1.391	1.551
5000	3.00	-1.0	.723	.422	.667	.822	.373	.414	.613	.924	1.138	1.220	1.373	1.533
5000	3.00	-2.0	.593	.274	.483	.759	.394	.381	.586	.899	1.117	1.201	1.351	1.512
5000	3.75	.0	.849	.707	1.084	.949	.330	.516	.714	1.017	1.215	1.301	1.456	1.620
5000	3.75	-.5	.758	.541	.886	.871	.340	.471	.670	.979	1.185	1.270	1.423	1.584
5000	3.75	-1.0	.691	.412	.727	.816	.353	.436	.637	.948	1.162	1.245	1.399	1.559
5000	3.75	-2.0	.605	.280	.533	.779	.394	.395	.602	.916	1.135	1.218	1.368	1.527
5000	4.50	.0	.851	.741	1.155	.934	.293	.559	.764	1.073	1.275	1.359	1.516	1.677
5000	4.50	-.5	.768	.583	.975	.864	.304	.513	.717	1.028	1.237	1.320	1.481	1.642
5000	4.50	-1.0	.725	.473	.835	.827	.328	.473	.677	.990	1.204	1.286	1.441	1.601
5000	4.50	-2.0	.666	.338	.615	.808	.396	.416	.629	.948	1.167	1.250	1.397	1.552
5500	3.00	.0	.648	.442	.647	.762	.316	.379	.539	.799	.968	1.025	1.139	1.265
5500	3.00	-.5	.538	.303	.482	.685	.316	.347	.509	.770	.948	1.006	1.120	1.247
5500	3.00	-1.0	.416	.197	.361	.624	.316	.327	.491	.753	.935	.994	1.108	1.238
5500	3.00	-2.0	.201	.062	.226	.551	.317	.304	.472	.734	.918	.982	1.093	1.225
5500	3.75	.0	.553	.378	.673	.755	.304	.396	.560	.820	.991	1.049	1.163	1.290
5500	3.75	-.5	.453	.235	.504	.686	.310	.361	.527	.789	.969	1.027	1.142	1.269
5500	3.75	-1.0	.351	.126	.385	.638	.315	.338	.505	.769	.952	1.011	1.126	1.256
5500	3.75	-2.0	.142	-.015	.230	.574	.325	.312	.483	.747	.932	.995	1.105	1.238
5500	4.50	.0	.515	.376	.738	.762	.286	.424	.592	.854	1.026	1.085	1.201	1.328
5500	4.50	-.5	.431	.237	.577	.702	.296	.385	.554	.818	.998	1.057	1.172	1.300
5500	4.50	-1.0	.353	.131	.451	.660	.309	.358	.528	.793	.977	1.036	1.151	1.280
5500	4.50	-2.0	.172	-.010	.272	.609	.335	.325	.500	.766	.952	1.014	1.123	1.252
6000	3.00	.0	.485	.310	.402	.585	.262	.295	.423	.643	.789	.825	.912	1.009
6000	3.00	-.5	.370	.221	.291	.516	.258	.275	.405	.624	.773	.813	.898	.998
6000	3.00	-1.0	.266	.150	.216	.466	.255	.262	.394	.612	.764	.807	.890	.993
6000	3.00	-2.0	.153	.064	.134	.418	.255	.246	.381	.600	.754	.800	.882	.988
6000	3.75	.0	.352	.188	.398	.586	.262	.309	.442	.665	.814	.851	.935	1.034
6000	3.75	-.5	.239	.087	.280	.525	.262	.287	.421	.644	.797	.837	.920	1.022
6000	3.75	-1.0	.124	.005	.197	.482	.262	.271	.408	.630	.785	.828	.910	1.014
6000	3.75	-2.0	-.012	-.092	.103	.435	.265	.254	.393	.617	.773	.820	.900	1.008
6000	4.50	.0	.270	.122	.419	.597	.256	.329	.467	.692	.843	.881	.965	1.064
6000	4.50	-.5	.168	.013	.301	.548	.262	.302	.441	.667	.822	.862	.945	1.048

Table 12b – *continued*

T_{eff}	log g	[A/H]	33-52	35-52	37-52	40-52	45-52	52-58	52-63	52-72	52-80	52-99	52-110	
6000	4.50	-1.0	.057	-.077	.204	.507	.267	.284	.424	.650	.806	.849	.931	1.035
6000	4.50	-2.0	-.100	-.186	.088	.458	.275	.262	.405	.632	.790	.837	.915	1.022
6500	3.00	.0	.429	.310	.277	.442	.207	.234	.332	.515	.635	.660	.729	.802
6500	3.00	-.5	.348	.252	.208	.387	.202	.219	.319	.499	.621	.649	.716	.792
6500	3.00	-1.0	.287	.206	.158	.351	.199	.208	.309	.489	.615	.648	.709	.790
6500	3.00	-2.0	.227	.152	.104	.319	.200	.194	.298	.477	.602	.635	.698	.780
6500	3.75	.0	.253	.139	.264	.459	.216	.248	.354	.544	.670	.693	.756	.834
6500	3.75	-1.0	.158	.071	.189	.409	.213	.232	.339	.527	.654	.681	.742	.823
6500	3.75	-1.0	.086	.018	.135	.375	.212	.219	.328	.515	.644	.673	.732	.815
6500	3.75	-2.0	.015	-.045	.076	.344	.214	.206	.316	.504	.633	.666	.723	.809
6500	4.50	.0	.126	.014	.256	.478	.221	.265	.377	.572	.703	.726	.786	.866
6500	4.50	-.5	.019	-.070	.169	.433	.222	.245	.358	.551	.683	.710	.768	.851
6500	4.50	-1.0	-.070	-.135	.102	.398	.223	.231	.345	.538	.670	.700	.756	.841
6500	4.50	-2.0	-.154	-.207	.032	.365	.227	.215	.331	.524	.658	.691	.744	.832
7000	3.00	.0	.458	.370	.251	.336	.153	.176	.242	.385	.476	.493	.553	.601
7000	3.00	-.5	.411	.335	.202	.294	.149	.164	.232	.373	.466	.485	.543	.593
7000	3.00	-1.0	.380	.310	.166	.267	.148	.154	.225	.365	.459	.479	.536	.588
7000	3.00	-2.0	.347	.280	.130	.244	.148	.144	.216	.356	.452	.473	.529	.584
7000	3.75	.0	.244	.172	.225	.360	.167	.192	.269	.422	.522	.534	.582	.637
7000	3.75	-.5	.188	.129	.175	.323	.165	.180	.257	.409	.510	.525	.571	.630
7000	3.75	-1.0	.150	.098	.140	.299	.165	.170	.250	.401	.503	.520	.565	.625
7000	3.75	-2.0	.110	.059	.102	.277	.166	.160	.241	.393	.496	.515	.558	.621
7000	4.50	.0	.061	-.004	.182	.381	.180	.209	.294	.456	.562	.574	.614	.674
7000	4.50	-.5	-.009	-.057	.124	.346	.180	.194	.280	.441	.549	.565	.601	.664
7000	4.50	-1.0	-.055	-.096	.084	.323	.181	.184	.272	.432	.540	.559	.594	.659
7000	4.50	-2.0	-.104	-.143	.041	.302	.183	.173	.262	.423	.533	.553	.587	.654

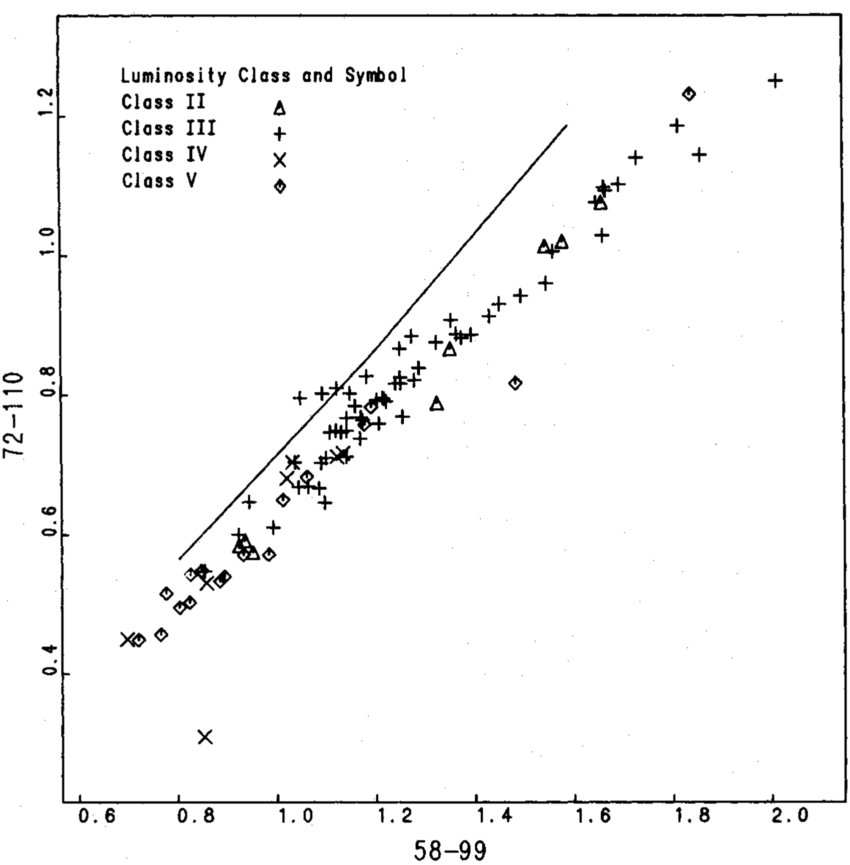

Figure 15. Johnson and Mitchell 58–99 is plotted versus 72–110 for stars and for Population I giant star models.

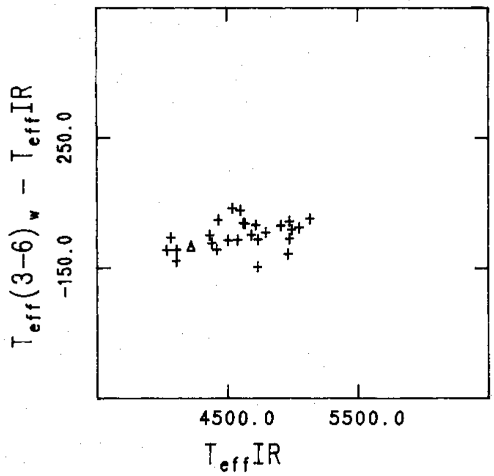

Figure 16. The differences between the effective temperatures deduced from Wing 7810 – 10 540 and from the IRFM are plotted versus T_{eff}(IRFM).

Table 13. Wing filter system.

T_{eff}	log g	[A/H]	7120	7540	7810	8120	10395	10525	10810	10975
4000	0.75	-0.0	2.233	2.229	2.223	2.365	2.481	2.478	2.549	2.651
4000	0.75	-0.5	2.243	2.239	2.237	2.351	2.494	2.493	2.553	2.647
4000	0.75	-1.0	2.242	2.243	2.246	2.330	2.497	2.499	2.551	2.633
4000	0.75	-2.0	2.235	2.235	2.239	2.276	2.473	2.479	2.523	2.572
4000	1.50	-0.0	2.244	2.245	2.247	2.350	2.505	2.504	2.568	2.645
4000	1.50	-0.5	2.248	2.256	2.261	2.342	2.517	2.518	2.573	2.643
4000	1.50	-1.0	2.250	2.262	2.269	2.330	2.522	2.525	2.573	2.634
4000	1.50	-2.0	2.239	2.250	2.259	2.292	2.504	2.510	2.553	2.591
4000	1.50	-3.0	2.210	2.212	2.218	2.237	2.454	2.463	2.504	2.528
4000	2.25	-0.0	2.248	2.260	2.268	2.339	2.524	2.525	2.583	2.637
4000	2.25	-0.5	2.255	2.271	2.281	2.337	2.535	2.537	2.588	2.637
4000	2.25	-1.0	2.259	2.277	2.287	2.331	2.539	2.542	2.588	2.631
4000	2.25	-2.0	2.242	2.259	2.271	2.300	2.521	2.528	2.569	2.599
4000	2.25	-3.0	2.183	2.192	2.202	2.223	2.458	2.468	2.511	2.535
4500	0.75	-0.0	1.554	1.577	1.581	1.778	1.986	1.990	2.073	2.213
4500	0.75	-0.5	1.545	1.580	1.596	1.741	1.999	2.007	2.078	2.195
4500	0.75	-1.0	1.534	1.578	1.602	1.697	2.000	2.011	2.073	2.161
4500	0.75	-2.0	1.521	1.565	1.594	1.640	1.982	1.997	2.051	2.086
4500	0.75	-3.0	1.520	1.560	1.590	1.630	1.973	1.988	2.039	2.067
4500	1.50	-0.0	1.563	1.595	1.605	1.775	2.008	2.013	2.092	2.214
4500	1.50	-0.5	1.562	1.603	1.623	1.750	2.024	2.032	2.100	2.203
4500	1.50	-1.0	1.557	1.605	1.632	1.720	2.029	2.040	2.101	2.179
4500	1.50	-2.0	1.545	1.593	1.624	1.673	2.016	2.031	2.084	2.121
4500	1.50	-3.0	1.532	1.577	1.609	1.651	1.999	2.014	2.066	2.093
4500	2.25	-0.0	1.567	1.609	1.625	1.765	2.026	2.033	2.107	2.210
4500	2.25	-0.5	1.572	1.619	1.642	1.749	2.041	2.050	2.115	2.202
4500	2.25	-1.0	1.574	1.624	1.652	1.730	2.048	2.059	2.118	2.186
4500	2.25	-2.0	1.562	1.613	1.646	1.695	2.039	2.053	2.107	2.142
4500	2.25	-3.0	1.535	1.584	1.616	1.660	2.013	2.029	2.080	2.107
4500	3.00	-0.0	1.570	1.619	1.641	1.750	2.040	2.049	2.119	2.200
4500	3.00	-0.5	1.579	1.630	1.657	1.742	2.053	2.064	2.126	2.195
4500	3.00	-1.0	1.584	1.637	1.666	1.733	2.060	2.072	2.130	2.184
4500	3.00	-2.0	1.569	1.621	1.654	1.703	2.049	2.063	2.117	2.149
4500	3.00	-3.0	1.528	1.577	1.610	1.654	2.013	2.030	2.083	2.110
5000	1.50	-0.0	1.002	1.081	1.115	1.255	1.628	1.643	1.721	1.830
5000	1.50	-0.5	1.007	1.089	1.132	1.226	1.640	1.658	1.728	1.802
5000	1.50	-1.0	1.015	1.096	1.142	1.212	1.647	1.666	1.731	1.779
5000	1.50	-2.0	1.026	1.103	1.152	1.212	1.653	1.673	1.734	1.767
5000	1.50	-3.0	1.032	1.109	1.158	1.218	1.657	1.677	1.736	1.770

Table 13 – *continued*

T_{eff}	log g	[A/H]	7120	7540	7810	8120	10395	10525	10810	10975
5000	2.25	-0.0	1.022	1.101	1.135	1.270	1.645	1.660	1.738	1.841
5000	2.25	-0.5	1.030	1.111	1.154	1.247	1.660	1.677	1.747	1.820
5000	2.25	-1.0	1.040	1.120	1.167	1.238	1.669	1.688	1.753	1.802
5000	2.25	-2.0	1.047	1.125	1.173	1.234	1.673	1.693	1.754	1.787
5000	2.25	-3.0	1.050	1.127	1.176	1.236	1.675	1.695	1.754	1.787
5000	3.00	-0.0	1.036	1.116	1.152	1.277	1.659	1.674	1.752	1.845
5000	3.00	-0.5	1.048	1.128	1.171	1.261	1.674	1.691	1.761	1.830
5000	3.00	-1.0	1.058	1.138	1.184	1.255	1.684	1.703	1.768	1.816
5000	3.00	-2.0	1.056	1.134	1.183	1.244	1.683	1.703	1.764	1.796
5500	1.50	-0.0	0.549	0.662	0.719	0.812	1.312	1.336	1.413	1.479
5500	1.50	-0.5	0.571	0.678	0.739	0.817	1.327	1.353	1.425	1.474
5500	1.50	-1.0	0.592	0.695	0.757	0.832	1.341	1.366	1.436	1.480
5500	1.50	-2.0	0.614	0.714	0.777	0.851	1.358	1.382	1.449	1.492
5500	1.50	-3.0	0.623	0.723	0.785	0.859	1.364	1.389	1.454	1.497
5500	2.25	-0.0	0.571	0.681	0.738	0.833	1.331	1.354	1.432	1.500
5500	2.25	-0.5	0.595	0.700	0.759	0.839	1.348	1.372	1.445	1.494
5500	2.25	-1.0	0.615	0.716	0.777	0.852	1.362	1.386	1.456	1.499
5500	2.25	-2.0	0.636	0.735	0.797	0.870	1.378	1.402	1.468	1.509
5500	2.25	-3.0	0.646	0.744	0.806	0.879	1.385	1.409	1.473	1.515
5500	3.00	-0.0	0.591	0.699	0.755	0.851	1.346	1.369	1.448	1.516
5500	3.00	-0.5	0.615	0.719	0.778	0.858	1.365	1.388	1.462	1.512
5500	3.00	-1.0	0.635	0.735	0.795	0.870	1.379	1.403	1.473	1.515
5500	3.00	-2.0	0.653	0.751	0.812	0.884	1.392	1.416	1.482	1.522
5500	3.00	-3.0	0.663	0.760	0.821	0.893	1.399	1.423	1.487	1.528
6000	2.25	-0.0	0.209	0.339	0.410	0.498	1.064	1.094	1.174	1.232
6000	2.25	-0.5	0.241	0.364	0.437	0.523	1.086	1.115	1.192	1.247
6000	2.25	-1.0	0.264	0.384	0.457	0.542	1.102	1.131	1.206	1.260
6000	2.25	-2.0	0.286	0.404	0.477	0.562	1.119	1.147	1.219	1.273
6000	2.25	-3.0	0.295	0.412	0.485	0.570	1.126	1.154	1.224	1.278
6000	3.00	-0.0	0.228	0.355	0.426	0.514	1.082	1.111	1.191	1.249
6000	3.00	-0.5	0.261	0.382	0.453	0.538	1.105	1.133	1.210	1.264
6000	3.00	-1.0	0.284	0.401	0.473	0.557	1.121	1.149	1.223	1.276
6000	3.00	-2.0	0.307	0.422	0.494	0.578	1.138	1.166	1.237	1.289
6000	3.00	-3.0	0.317	0.432	0.503	0.587	1.146	1.173	1.243	1.295

this system are given by Frogel *et al.* (1978) in terms of mean colours as a function of spectral type, based upon data on the Johnson system.

5.10 PHOTOMETRY IN 50 Å BAND PASSES

While not discussed in this paper, photometry on Oke's (1964) system is given in Table 14, for dwarfs, and Table 15, for giants. The giant model material replaces that in BG78.

6 The adopted temperature scale

In the discussion of temperature determinations from different colour systems we found that, by and large, they seem to confirm the temperature scale established with the IRFM. Admittedly, the $T_{\rm eff}$ values determined from the Johnson broad-band colours and from the JML system are not entirely independent of those determined by the IRFM, since the photometric magnitudes were used to obtain the integrated flux and the *K*-band flux of the stars. However, central temperature criteria such as the gradients in the near infrared, as measured by e.g. the 58–99 JML colour, only play an indirect and less important role in the IRFM.

As a rough measure of the deviation of the effective temperatures derived from the colours from the temperatures derived from the IRFM we have just taken the mean difference

$$\delta = T_{\rm eff}(\text{colour}) - T_{\rm eff}(\text{IRFM})$$

Table 14a. The Oke fluxes for dwarfs.

			Wavelength									
T_{eff}	log g	[A/H]	3390	3448	3509	3571	3636	3704	4032	4167	4255	4464
4500	3.00	0.0	2.886	2.695	2.498	2.979	2.352	2.378	1.357	1.404	1.239	0.819
4500	3.00	-0.5	2.744	2.493	2.271	2.651	2.141	2.131	1.255	1.227	1.162	0.763
4500	3.00	-1.0	2.645	2.346	2.117	2.375	1.995	1.950	1.185	1.104	1.109	0.726
4500	3.00	-2.0	2.643	2.260	2.044	2.090	1.897	1.776	1.151	1.029	1.062	0.704
4500	3.75	0.0	2.890	2.710	2.491	2.993	2.430	2.442	1.359	1.322	1.244	0.825
4500	3.75	-0.5	2.771	2.531	2.295	2.709	2.224	2.229	1.261	1.182	1.172	0.770
4500	3.75	-1.0	2.682	2.388	2.145	2.453	2.064	2.049	1.188	1.084	1.122	0.728
4500	3.75	-2.0	2.662	2.286	2.062	2.150	1.929	1.855	1.169	1.043	1.090	0.716
4500	4.50	0.0	2.991	2.825	2.584	3.105	2.623	2.595	1.403	1.275	1.290	0.854
4500	4.50	-0.5	2.891	2.661	2.407	2.866	2.415	2.407	1.306	1.167	1.215	0.797
4500	4.50	-1.0	2.839	2.548	2.285	2.642	2.246	2.237	1.244	1.104	1.167	0.763
4500	4.50	-2.0	2.784	2.404	2.171	2.280	2.033	1.975	1.229	1.089	1.134	0.752
5000	3.00	0.0	2.362	2.123	1.995	2.348	1.859	1.780	1.037	1.127	0.977	0.620
5000	3.00	-0.5	2.222	1.951	1.801	2.020	1.699	1.586	0.954	0.940	0.910	0.578
5000	3.00	-1.0	2.104	1.810	1.666	1.765	1.578	1.446	0.895	0.832	0.857	0.549
5000	3.00	-2.0	1.917	1.640	1.533	1.511	1.427	1.299	0.843	0.755	0.760	0.519
5000	3.75	0.0	2.342	2.110	1.965	2.352	1.871	1.825	1.046	1.111	0.995	0.630
5000	3.75	-0.5	2.210	1.944	1.782	2.050	1.707	1.634	0.965	0.948	0.939	0.587
5000	3.75	-1.0	2.110	1.813	1.654	1.805	1.583	1.492	0.908	0.842	0.881	0.554
5000	3.75	-2.0	1.964	1.666	1.538	1.542	1.438	1.334	0.870	0.785	0.817	0.533
5000	4.50	0.0	2.398	2.175	2.016	2.435	1.981	1.948	1.082	1.094	1.026	0.655
5000	4.50	-0.5	2.277	2.016	1.840	2.158	1.803	1.756	0.997	0.957	0.972	0.606
5000	4.50	-1.0	2.198	1.902	1.724	1.938	1.677	1.614	0.944	0.877	0.938	0.575
5000	4.50	-2.0	2.059	1.746	1.603	1.634	1.499	1.417	0.912	0.823	0.868	0.558
5500	3.00	0.0	1.976	1.760	1.666	1.808	1.568	1.409	0.773	0.767	0.721	0.462
5500	3.00	-0.5	1.833	1.618	1.525	1.573	1.446	1.278	0.703	0.652	0.652	0.430
5500	3.00	-1.0	1.682	1.489	1.417	1.419	1.342	1.175	0.648	0.587	0.587	0.403
5500	3.00	-2.0	1.432	1.333	1.282	1.248	1.185	1.053	0.584	0.521	0.486	0.368
5500	3.75	0.0	1.909	1.694	1.591	1.791	1.514	1.400	0.783	0.794	0.754	0.471
5500	3.75	-0.5	1.776	1.549	1.445	1.544	1.385	1.259	0.717	0.678	0.699	0.438
5500	3.75	-1.0	1.648	1.424	1.336	1.375	1.277	1.155	0.672	0.617	0.644	0.413
5500	3.75	-2.0	1.387	1.263	1.204	1.178	1.112	1.019	0.616	0.550	0.531	0.384
5500	4.50	0.0	1.911	1.698	1.587	1.848	1.539	1.452	0.814	0.828	0.798	0.491
5500	4.50	-0.5	1.793	1.558	1.443	1.602	1.402	1.306	0.750	0.715	0.748	0.455
5500	4.50	-1.0	1.688	1.443	1.338	1.424	1.290	1.196	0.706	0.653	0.695	0.432
5500	4.50	-2.0	1.437	1.286	1.213	1.198	1.119	1.043	0.661	0.592	0.588	0.407
6000	3.00	0.0	1.718	1.578	1.521	1.530	1.438	1.239	0.551	0.501	0.472	0.331
6000	3.00	-0.5	1.578	1.465	1.422	1.407	1.346	1.143	0.486	0.436	0.406	0.301
6000	3.00	-1.0	1.464	1.377	1.344	1.319	1.265	1.074	0.438	0.395	0.359	0.278
6000	3.00	-2.0	1.346	1.293	1.246	1.214	1.163	0.997	0.396	0.352	0.320	0.251
6000	3.75	0.0	1.609	1.454	1.388	1.439	1.323	1.176	0.569	0.532	0.521	0.344
6000	3.75	-0.5	1.470	1.332	1.280	1.294	1.221	1.072	0.510	0.464	0.458	0.316
6000	3.75	-1.0	1.338	1.231	1.193	1.187	1.130	0.994	0.468	0.424	0.404	0.294
6000	3.75	-2.0	1.189	1.135	1.090	1.063	1.013	0.906	0.428	0.379	0.349	0.269
6000	4.50	0.0	1.556	1.389	1.313	1.420	1.268	1.144	0.595	0.571	0.574	0.361
6000	4.50	-0.5	1.429	1.263	1.198	1.253	1.155	1.040	0.545	0.505	0.521	0.334
6000	4.50	-1.0	1.295	1.158	1.108	1.126	1.055	0.951	0.505	0.462	0.463	0.314
6000	4.50	-2.0	1.110	1.047	1.000	0.976	0.923	0.844	0.465	0.412	0.384	0.288
6000	5.25	0.0	1.573	1.397	1.314	1.486	1.294	1.194	0.642	0.624	0.633	0.387
6000	5.25	-0.5	1.460	1.274	1.197	1.307	1.172	1.077	0.590	0.555	0.587	0.359
6000	5.25	-1.0	1.329	1.166	1.102	1.155	1.054	0.971	0.547	0.504	0.515	0.336
6000	5.25	-2.0	1.115	1.042	0.988	0.969	0.905	0.841	0.508	0.449	0.426	0.312
6500	3.00	0.0	1.608	1.528	1.497	1.471	1.418	1.168	0.363	0.320	0.274	0.219
6500	3.00	-0.5	1.516	1.452	1.426	1.397	1.350	1.105	0.307	0.276	0.232	0.190
6500	3.00	-1.0	1.453	1.400	1.369	1.340	1.293	1.062	0.269	0.245	0.209	0.170
6500	3.00	-2.0	1.389	1.346	1.299	1.270	1.227	1.008	0.239	0.210	0.191	0.148
6500	3.75	0.0	1.447	1.355	1.321	1.318	1.258	1.085	0.397	0.355	0.323	0.240
6500	3.75	-1.0	1.339	1.266	1.241	1.228	1.179	1.015	0.345	0.310	0.275	0.213
6500	3.75	-1.0	1.263	1.207	1.180	1.161	1.115	0.965	0.310	0.280	0.246	0.194
6500	3.75	-2.0	1.187	1.147	1.105	1.080	1.040	0.905	0.281	0.246	0.225	0.173

Table 14 – *continued*

T_{eff}	log g	[A/H]	3390	3448	3509	3571	3636	3704	4032	4167	4255	4464
						Wavelength						
6500	4.50	0.0	1.344	1.232	1.189	1.222	1.142	1.001	0.433	0.396	0.383	0.263
6500	4.50	-0.5	1.217	1.127	1.096	1.107	1.049	0.920	0.384	0.349	0.330	0.237
6500	4.50	-1.0	1.120	1.055	1.028	1.021	0.972	0.858	0.349	0.316	0.289	0.217
6500	4.50	-2.0	1.025	0.987	0.946	0.924	0.886	0.789	0.320	0.280	0.257	0.195
7000	3.00	0.0	1.601	1.546	1.522	1.489	1.448	1.185	0.195	0.172	0.126	0.108
7000	3.00	-0.5	1.550	1.502	1.474	1.443	1.401	1.146	0.149	0.137	0.100	0.085
7000	3.00	-1.0	1.517	1.474	1.438	1.410	1.368	1.117	0.121	0.110	0.086	0.069
7000	3.00	-2.0	1.480	1.441	1.397	1.369	1.330	1.082	0.100	0.082	0.073	0.052
7000	3.75	0.0	1.399	1.344	1.324	1.304	1.263	1.081	0.240	0.209	0.167	0.136
7000	3.75	-0.5	1.338	1.292	1.269	1.248	1.208	1.037	0.198	0.177	0.141	0.115
7000	3.75	-1.0	1.300	1.260	1.229	1.207	1.168	1.006	0.173	0.154	0.127	0.100
7000	3.75	-2.0	1.254	1.220	1.180	1.156	1.122	0.967	0.153	0.127	0.114	0.084
7000	4.50	0.0	1.231	1.170	1.149	1.148	1.100	0.944	0.281	0.250	0.215	0.165
7000	4.50	-0.5	1.155	1.106	1.085	1.076	1.036	0.890	0.241	0.217	0.185	0.144
7000	4.50	-1.0	1.106	1.066	1.039	1.024	0.988	0.853	0.217	0.194	0.167	0.130
7000	4.50	-2.0	1.050	1.020	0.983	0.964	0.932	0.808	0.198	0.168	0.152	0.113

Table 14b. The Oke fluxes for dwarfs.

T_{eff}	log g	[A/H]	4566	4785	5000	5263	5556	5882	6055	6370	6800	7100
					Wavelength							
4500	3.00	0.0	0.638	0.510	0.465	0.260	0.000	-0.045	-0.229	-0.284	-0.419	-0.446
4500	3.00	-0.5	0.592	0.471	0.411	0.230	0.000	-0.075	-0.215	-0.288	-0.412	-0.455
4500	3.00	-1.0	0.565	0.442	0.367	0.204	0.000	-0.093	-0.204	-0.290	-0.407	-0.461
4500	3.00	-2.0	0.575	0.427	0.321	0.173	0.000	-0.116	-0.198	-0.294	-0.409	-0.473
4500	3.75	0.0	0.610	0.554	0.512	0.261	0.000	-0.010	-0.237	-0.306	-0.433	-0.475
4500	3.75	-0.5	0.572	0.508	0.455	0.233	0.000	-0.047	-0.221	-0.302	-0.421	-0.472
4500	3.75	-1.0	0.550	0.470	0.405	0.209	0.000	-0.072	-0.209	-0.297	-0.413	-0.469
4500	3.75	-2.0	0.580	0.445	0.342	0.179	0.000	-0.109	-0.203	-0.301	-0.418	-0.482
4500	4.50	0.0	0.593	0.612	0.576	0.270	0.000	0.053	-0.252	-0.331	-0.454	-0.505
4500	4.50	-0.5	0.562	0.563	0.517	0.243	0.000	0.004	-0.234	-0.320	-0.438	-0.493
4500	4.50	-1.0	0.558	0.520	0.460	0.220	0.000	-0.039	-0.221	-0.312	-0.429	-0.488
4500	4.50	-2.0	0.610	0.474	0.367	0.187	0.000	-0.106	-0.214	-0.316	-0.438	-0.506
5000	3.00	0.0	0.495	0.338	0.309	0.194	0.000	-0.065	-0.174	-0.210	-0.309	-0.321
5000	3.00	-0.5	0.455	0.322	0.274	0.166	0.000	-0.076	-0.160	-0.215	-0.303	-0.333
5000	3.00	-1.0	0.434	0.310	0.248	0.145	0.000	-0.083	-0.151	-0.215	-0.298	-0.338
5000	3.00	-2.0	0.434	0.310	0.225	0.123	0.000	-0.091	-0.144	-0.215	-0.296	-0.341
5000	3.75	0.0	0.483	0.355	0.330	0.201	0.000	-0.047	-0.174	-0.216	-0.313	-0.329
5000	3.75	-0.5	0.448	0.333	0.290	0.173	0.000	-0.063	-0.161	-0.218	-0.305	-0.336
5000	3.75	-1.0	0.429	0.316	0.260	0.150	0.000	-0.073	-0.152	-0.217	-0.301	-0.340
5000	3.75	-2.0	0.441	0.319	0.233	0.127	0.000	-0.088	-0.147	-0.219	-0.302	-0.347
5000	4.50	0.0	0.473	0.384	0.369	0.212	0.000	-0.018	-0.178	-0.228	-0.321	-0.345
5000	4.50	-0.5	0.442	0.352	0.322	0.184	0.000	-0.042	-0.165	-0.225	-0.312	-0.346
5000	4.50	-1.0	0.432	0.335	0.286	0.161	0.000	-0.058	-0.156	-0.222	-0.306	-0.345
5000	4.50	-2.0	0.458	0.335	0.247	0.134	0.000	-0.086	-0.153	-0.227	-0.313	-0.360
5500	3.00	0.0	0.366	0.242	0.218	0.139	0.000	-0.059	-0.125	-0.158	-0.221	-0.239
5500	3.00	-0.5	0.339	0.231	0.192	0.117	0.000	-0.062	-0.113	-0.155	-0.213	-0.238
5500	3.00	-1.0	0.324	0.223	0.175	0.103	0.000	-0.064	-0.107	-0.153	-0.208	-0.236
5500	3.00	-2.0	0.312	0.220	0.157	0.086	0.000	-0.065	-0.101	-0.150	-0.205	-0.234
5500	3.75	0.0	0.363	0.248	0.227	0.143	0.000	-0.052	-0.128	-0.163	-0.227	-0.244
5500	3.75	-0.5	0.339	0.237	0.200	0.121	0.000	-0.056	-0.116	-0.160	-0.218	-0.243
5500	3.75	-1.0	0.327	0.230	0.181	0.106	0.000	-0.060	-0.109	-0.157	-0.213	-0.241
5500	3.75	-2.0	0.323	0.229	0.163	0.089	0.000	-0.066	-0.104	-0.154	-0.210	-0.241
5500	4.50	0.0	0.363	0.260	0.244	0.153	0.000	-0.037	-0.132	-0.169	-0.233	-0.250
5500	4.50	-0.5	0.340	0.245	0.213	0.129	0.000	-0.046	-0.120	-0.165	-0.224	-0.248
5500	4.50	-1.0	0.334	0.240	0.193	0.113	0.000	-0.053	-0.113	-0.161	-0.219	-0.247
5500	4.50	-2.0	0.340	0.243	0.172	0.094	0.000	-0.066	-0.109	-0.161	-0.219	-0.250
6000	3.00	0.0	0.258	0.167	0.149	0.099	0.000	-0.041	-0.080	-0.101	-0.137	-0.150
6000	3.00	-0.5	0.237	0.157	0.131	0.082	0.000	-0.042	-0.073	-0.099	-0.132	-0.146

Table 14b – *continued*

T_{eff}	log g	[A/H]	Wavelength 4566	4785	5000	5263	5556	5882	6055	6370	6800	7100
6000	3.00	-1.0	0.224	0.151	0.119	0.072	0.000	-0.042	-0.069	-0.096	-0.129	-0.143
6000	3.00	-2.0	0.213	0.149	0.105	0.059	0.000	-0.041	-0.065	-0.095	-0.127	-0.142
6000	3.75	0.0	0.264	0.176	0.158	0.102	0.000	-0.039	-0.085	-0.109	-0.148	-0.160
6000	3.75	-0.5	0.246	0.166	0.138	0.085	0.000	-0.041	-0.078	-0.106	-0.142	-0.156
6000	3.75	-1.0	0.235	0.161	0.125	0.074	0.000	-0.043	-0.073	-0.103	-0.138	-0.153
6000	3.75	-2.0	0.227	0.160	0.111	0.062	0.000	-0.044	-0.070	-0.102	-0.136	-0.154
6000	4.50	0.0	0.269	0.184	0.168	0.108	0.000	-0.032	-0.091	-0.117	-0.157	-0.170
6000	4.50	-0.5	0.254	0.175	0.147	0.090	0.000	-0.037	-0.082	-0.113	-0.150	-0.165
6000	4.50	-1.0	0.247	0.171	0.133	0.079	0.000	-0.040	-0.077	-0.110	-0.146	-0.162
6000	4.50	-2.0	0.242	0.171	0.119	0.065	0.000	-0.046	-0.074	-0.108	-0.144	-0.162
6000	5.25	0.0	0.272	0.193	0.184	0.119	0.000	-0.020	-0.097	-0.126	-0.167	-0.180
6000	5.25	-0.5	0.262	0.186	0.160	0.099	0.000	-0.027	-0.087	-0.120	-0.158	-0.173
6000	5.25	-1.0	0.260	0.183	0.143	0.086	0.000	-0.035	-0.081	-0.116	-0.153	-0.170
6000	5.25	-2.0	0.261	0.185	0.128	0.070	0.000	-0.047	-0.079	-0.115	-0.152	-0.171
6500	3.00	0.0	0.165	0.103	0.097	0.069	0.000	-0.022	-0.044	-0.050	-0.066	-0.067
6500	3.00	-0.5	0.146	0.092	0.081	0.054	0.000	-0.022	-0.039	-0.047	-0.061	-0.062
6500	3.00	-1.0	0.135	0.087	0.069	0.045	0.000	-0.021	-0.035	-0.045	-0.057	-0.059
6500	3.00	-2.0	0.124	0.085	0.058	0.034	0.000	-0.019	-0.032	-0.044	-0.054	-0.056
6500	3.75	0.0	0.181	0.117	0.107	0.073	0.000	-0.024	-0.052	-0.062	-0.082	-0.085
6500	3.75	-1.0	0.164	0.107	0.091	0.058	0.000	-0.025	-0.046	-0.059	-0.076	-0.080
6500	3.75	-1.0	0.154	0.103	0.079	0.049	0.000	-0.025	-0.042	-0.057	-0.073	-0.076
6500	3.75	-2.0	0.145	0.101	0.069	0.039	0.000	-0.024	-0.039	-0.055	-0.070	-0.075
6500	4.50	0.0	0.194	0.129	0.117	0.078	0.000	-0.022	-0.059	-0.073	-0.095	-0.100
6500	4.50	-0.5	0.179	0.120	0.100	0.063	0.000	-0.024	-0.052	-0.069	-0.088	-0.093
6500	4.50	-1.0	0.171	0.116	0.088	0.054	0.000	-0.027	-0.048	-0.066	-0.084	-0.090
6500	4.50	-2.0	0.163	0.115	0.078	0.043	0.000	-0.028	-0.045	-0.064	-0.081	-0.088
7000	3.00	0.0	0.072	0.036	0.043	0.038	0.000	-0.001	-0.008	0.004	0.009	0.021
7000	3.00	-0.5	0.059	0.028	0.030	0.027	0.000	0.000	-0.004	0.005	0.013	0.025
7000	3.00	-1.0	0.050	0.025	0.020	0.019	0.000	0.001	-0.001	0.007	0.016	0.028
7000	3.00	-2.0	0.039	0.024	0.013	0.010	0.000	0.003	0.001	0.007	0.018	0.029
7000	3.75	0.0	0.095	0.057	0.058	0.044	0.000	-0.007	-0.019	-0.013	-0.013	-0.005
7000	3.75	-0.5	0.083	0.050	0.044	0.033	0.000	-0.006	-0.014	-0.011	-0.009	0.000
7000	3.75	-1.0	0.075	0.047	0.035	0.026	0.000	-0.005	-0.012	-0.010	-0.006	0.002
7000	3.75	-2.0	0.066	0.046	0.028	0.017	0.000	-0.004	-0.010	-0.009	-0.004	0.004
7000	4.50	0.0	0.116	0.076	0.070	0.050	0.000	-0.009	-0.027	-0.027	-0.031	-0.026
7000	4.50	-0.5	0.105	0.069	0.056	0.039	0.000	-0.010	-0.023	-0.025	-0.027	-0.021
7000	4.50	-1.0	0.099	0.066	0.047	0.031	0.000	-0.010	-0.020	-0.023	-0.024	-0.019
7000	4.50	-2.0	0.090	0.065	0.040	0.023	0.000	-0.010	-0.018	-0.022	-0.022	-0.017

Table 14c. The Oke fluxes for dwarfs.

T_{eff}	log g	[A/H]	Wavelength 7530	7850	8080	8400	8805	9700	9950	10250	10400	10800
4500	3.00	0.0	-0.540	-0.599	-0.573	-0.622	-0.697	-0.730	-0.806	-0.843	-0.855	-0.854
4500	3.00	-0.5	-0.541	-0.598	-0.591	-0.637	-0.701	-0.745	-0.811	-0.841	-0.851	-0.858
4500	3.00	-1.0	-0.543	-0.598	-0.609	-0.651	-0.705	-0.760	-0.816	-0.841	-0.850	-0.861
4500	3.00	-2.0	-0.553	-0.607	-0.637	-0.675	-0.719	-0.783	-0.825	-0.845	-0.854	-0.868
4500	3.75	0.0	-0.560	-0.617	-0.608	-0.650	-0.711	-0.761	-0.829	-0.862	-0.871	-0.873
4500	3.75	-0.5	-0.553	-0.610	-0.615	-0.655	-0.708	-0.766	-0.826	-0.854	-0.862	-0.870
4500	3.75	-1.0	-0.550	-0.605	-0.621	-0.660	-0.707	-0.771	-0.824	-0.848	-0.856	-0.867
4500	3.75	-2.0	-0.564	-0.617	-0.647	-0.685	-0.726	-0.791	-0.832	-0.851	-0.859	-0.872
4500	4.50	0.0	-0.583	-0.639	-0.646	-0.680	-0.727	-0.794	-0.857	-0.885	-0.893	-0.895
4500	4.50	-0.5	-0.571	-0.627	-0.642	-0.676	-0.719	-0.789	-0.846	-0.871	-0.878	-0.886
4500	4.50	-1.0	-0.567	-0.622	-0.644	-0.679	-0.719	-0.790	-0.840	-0.862	-0.869	-0.879
4500	4.50	-2.0	-0.589	-0.643	-0.674	-0.711	-0.750	-0.813	-0.852	-0.869	-0.877	-0.887
5000	3.00	0.0	-0.382	-0.425	-0.388	-0.426	-0.479	-0.475	-0.539	-0.565	-0.573	-0.559
5000	3.00	-0.5	-0.387	-0.426	-0.417	-0.448	-0.486	-0.500	-0.549	-0.566	-0.571	-0.565
5000	3.00	-1.0	-0.390	-0.428	-0.437	-0.463	-0.492	-0.518	-0.556	-0.569	-0.573	-0.571
5000	3.00	-2.0	-0.396	-0.431	-0.452	-0.475	-0.501	-0.530	-0.560	-0.570	-0.574	-0.576

Table 14c – *continued*

T_{eff}	log g	[A/H]	7530	7850	8080	8400	8805	9700	9950	10250	10400	10800
5000	3.75	0.0	-0.388	-0.431	-0.400	-0.436	-0.481	-0.487	-0.548	-0.573	-0.580	-0.566
5000	3.75	-0.5	-0.391	-0.430	-0.423	-0.453	-0.487	-0.506	-0.555	-0.572	-0.577	-0.570
5000	3.75	-1.0	-0.393	-0.431	-0.439	-0.466	-0.492	-0.521	-0.560	-0.572	-0.577	-0.574
5000	3.75	-2.0	-0.402	-0.437	-0.458	-0.481	-0.506	-0.535	-0.565	-0.574	-0.579	-0.579
5000	4.50	0.0	-0.400	-0.442	-0.423	-0.453	-0.486	-0.507	-0.564	-0.585	-0.592	-0.576
5000	4.50	-0.5	-0.399	-0.438	-0.436	-0.463	-0.489	-0.528	-0.570	-0.584	-0.587	-0.578
5000	4.50	-1.0	-0.398	-0.436	-0.446	-0.471	-0.493	-0.526	-0.565	-0.578	-0.582	-0.577
5000	4.50	-2.0	-0.415	-0.451	-0.472	-0.495	-0.517	-0.546	-0.576	-0.584	-0.588	-0.587
5500	3.00	0.0	-0.266	-0.290	-0.275	-0.293	-0.314	-0.300	-0.340	-0.349	-0.349	-0.329
5500	3.00	-0.5	-0.265	-0.288	-0.290	-0.303	-0.318	-0.315	-0.345	-0.348	-0.348	-0.334
5500	3.00	-1.0	-0.266	-0.288	-0.296	-0.308	-0.322	-0.323	-0.348	-0.350	-0.350	-0.339
5500	3.00	-2.0	-0.268	-0.289	-0.301	-0.312	-0.328	-0.328	-0.351	-0.352	-0.353	-0.346
5500	3.75	0.0	-0.273	-0.299	-0.281	-0.300	-0.318	-0.307	-0.349	-0.358	-0.359	-0.338
5500	3.75	-0.5	-0.272	-0.296	-0.296	-0.311	-0.322	-0.322	-0.353	-0.358	-0.358	-0.342
5500	3.75	-1.0	-0.272	-0.294	-0.302	-0.315	-0.326	-0.329	-0.355	-0.357	-0.358	-0.346
5500	3.75	-2.0	-0.275	-0.296	-0.308	-0.320	-0.333	-0.334	-0.357	-0.359	-0.360	-0.352
5500	4.50	0.0	-0.280	-0.307	-0.290	-0.308	-0.320	-0.317	-0.359	-0.368	-0.370	-0.345
5500	4.50	-0.5	-0.278	-0.303	-0.302	-0.317	-0.324	-0.329	-0.361	-0.366	-0.367	-0.348
5500	4.50	-1.0	-0.279	-0.301	-0.309	-0.322	-0.328	-0.335	-0.361	-0.364	-0.364	-0.351
5500	4.50	-2.0	-0.285	-0.306	-0.318	-0.330	-0.341	-0.342	-0.364	-0.365	-0.366	-0.357
6000	3.00	0.0	-0.155	-0.163	-0.159	-0.161	-0.171	-0.144	-0.166	-0.163	-0.158	-0.131
6000	3.00	-0.5	-0.155	-0.163	-0.163	-0.164	-0.174	-0.151	-0.169	-0.164	-0.160	-0.137
6000	3.00	-1.0	-0.155	-0.163	-0.166	-0.166	-0.177	-0.154	-0.171	-0.166	-0.163	-0.143
6000	3.00	-2.0	-0.158	-0.166	-0.170	-0.170	-0.183	-0.159	-0.176	-0.171	-0.168	-0.152
6000	3.75	0.0	-0.168	-0.178	-0.173	-0.176	-0.178	-0.155	-0.179	-0.176	-0.172	-0.145
6000	3.75	-0.5	-0.168	-0.177	-0.178	-0.180	-0.182	-0.163	-0.182	-0.177	-0.174	-0.151
6000	3.75	-1.0	-0.168	-0.177	-0.180	-0.181	-0.186	-0.166	-0.183	-0.178	-0.176	-0.156
6000	3.75	-2.0	-0.171	-0.180	-0.185	-0.186	-0.194	-0.171	-0.188	-0.184	-0.181	-0.166
6000	4.50	0.0	-0.180	-0.191	-0.185	-0.190	-0.184	-0.167	-0.191	-0.190	-0.186	-0.156
6000	4.50	-0.5	-0.177	-0.188	-0.188	-0.192	-0.188	-0.173	-0.192	-0.188	-0.186	-0.161
6000	4.50	-1.0	-0.177	-0.188	-0.191	-0.193	-0.192	-0.175	-0.192	-0.188	-0.185	-0.165
6000	4.50	-2.0	-0.180	-0.190	-0.195	-0.197	-0.201	-0.179	-0.196	-0.191	-0.189	-0.174
6000	5.25	0.0	-0.189	-0.203	-0.195	-0.201	-0.188	-0.178	-0.204	-0.203	-0.199	-0.164
6000	5.25	-0.5	-0.186	-0.198	-0.198	-0.202	-0.191	-0.182	-0.202	-0.198	-0.195	-0.167
6000	5.25	-1.0	-0.186	-0.197	-0.200	-0.202	-0.196	-0.182	-0.200	-0.195	-0.192	-0.169
6000	5.25	-2.0	-0.190	-0.200	-0.205	-0.207	-0.208	-0.186	-0.203	-0.198	-0.195	-0.179
6500	3.00	0.0	-0.057	-0.051	-0.045	-0.036	-0.056	-0.010	-0.023	-0.014	-0.005	0.029
6500	3.00	-0.5	-0.055	-0.051	-0.046	-0.035	-0.055	-0.012	-0.023	-0.012	-0.005	0.025
6500	3.00	-1.0	-0.055	-0.053	-0.048	-0.036	-0.062	-0.014	-0.024	-0.012	-0.006	0.017
6500	3.00	-2.0	-0.055	-0.051	-0.047	-0.036	-0.058	-0.014	-0.024	-0.013	-0.007	0.017
6500	3.75	0.0	-0.078	-0.076	-0.070	-0.063	-0.066	-0.026	-0.041	-0.032	-0.024	0.009
6500	3.75	-1.0	-0.077	-0.075	-0.070	-0.062	-0.067	-0.028	-0.040	-0.031	-0.024	0.005
6500	3.75	-1.0	-0.076	-0.074	-0.071	-0.062	-0.068	-0.029	-0.040	-0.030	-0.024	0.002
6500	3.75	-2.0	-0.076	-0.075	-0.072	-0.063	-0.071	-0.031	-0.042	-0.031	-0.026	-0.004
6500	4.50	0.0	-0.096	-0.096	-0.089	-0.085	-0.075	-0.042	-0.057	-0.049	-0.042	-0.007
6500	4.50	-0.5	-0.093	-0.093	-0.089	-0.083	-0.077	-0.043	-0.055	-0.046	-0.040	-0.011
6500	4.50	-1.0	-0.092	-0.092	-0.089	-0.082	-0.079	-0.043	-0.055	-0.045	-0.040	-0.014
6500	4.50	-2.0	-0.092	-0.092	-0.090	-0.083	-0.083	-0.044	-0.056	-0.046	-0.041	-0.020
7000	3.00	0.0	0.047	0.066	0.078	0.100	0.055	0.118	0.112	0.128	0.141	0.182
7000	3.00	-0.5	0.048	0.065	0.078	0.101	0.055	0.116	0.113	0.130	0.141	0.180
7000	3.00	-1.0	0.048	0.065	0.077	0.101	0.055	0.115	0.113	0.131	0.140	0.177
7000	3.00	-2.0	0.048	0.064	0.076	0.101	0.054	0.115	0.112	0.130	0.140	0.173
7000	3.75	0.0	0.017	0.032	0.043	0.061	0.046	0.101	0.095	0.108	0.119	0.159
7000	3.75	-0.5	0.018	0.032	0.042	0.062	0.046	0.100	0.095	0.109	0.119	0.155
7000	3.75	-1.0	0.018	0.031	0.041	0.062	0.044	0.098	0.094	0.110	0.118	0.152
7000	3.75	-2.0	0.018	0.030	0.040	0.061	0.042	0.097	0.093	0.109	0.117	0.147
7000	4.50	0.0	-0.008	0.004	0.014	0.029	0.034	0.083	0.076	0.088	0.098	0.137
7000	4.50	-0.5	-0.007	0.004	0.013	0.030	0.031	0.082	0.076	0.090	0.098	0.133
7000	4.50	-1.0	-0.006	0.004	0.013	0.030	0.029	0.081	0.075	0.090	0.097	0.130
7000	4.50	-2.0	-0.007	0.003	0.011	0.029	0.026	0.079	0.074	0.088	0.096	0.124

Table 15a. The Oke fluxes for giants.

			Wavelength									
T_{eff}	Log g	[A/H]	3390	3448	3509	3571	3636	3704	4032	4167	4255	4464
4000	0.75	-0.0	4.631	4.562	4.333	4.788	3.912	4.160	2.431	2.255	1.925	1.312
4000	0.75	-0.5	4.496	4.296	4.020	4.392	3.553	3.701	2.201	2.034	1.796	1.249
4000	0.74	-1.0	4.508	4.185	3.854	4.079	3.403	3.436	2.104	1.894	1.729	1.218
4000	0.75	-2.0	4.518	4.089	3.799	3.761	3.404	3.248	2.138	1.873	1.783	1.284
4000	0.75	-3.0	4.656	4.199	3.951	3.753	3.510	3.287	2.300	1.992	1.887	1.393
4000	1.50	-0.0	4.120	4.011	3.779	4.299	3.484	3.676	2.104	1.955	1.776	1.207
4000	1.50	-0.5	3.973	3.756	3.470	3.905	3.151	3.271	1.919	1.746	1.609	1.123
4000	1.50	-1.0	3.948	3.633	3.305	3.607	2.985	3.011	1.830	1.637	1.550	1.073
4000	1.50	-2.0	4.133	3.651	3.315	3.350	2.981	2.861	1.838	1.613	1.579	1.104
4000	1.50	-3.0	4.320	3.829	3.532	3.371	3.157	2.953	2.044	1.776	1.726	1.228
4000	2.25	-0.0	3.773	3.639	3.388	3.938	3.218	3.350	1.933	1.747	1.681	1.137
4000	2.25	-0.5	3.675	3.451	3.152	3.631	2.908	2.996	1.763	1.571	1.525	1.057
4000	2.25	-1.0	3.631	3.318	2.989	3.354	2.774	2.809	1.656	1.451	1.434	1.002
4000	2.25	-2.0	3.805	3.321	2.972	3.091	2.709	2.637	1.637	1.427	1.444	0.987
4000	2.25	-3.0	4.024	3.497	3.196	3.090	2.865	2.698	1.829	1.589	1.568	1.102
4500	0.75	-0.0	3.689	3.442	3.340	3.733	2.943	2.964	1.782	1.856	1.443	0.984
4500	0.75	-0.5	3.567	3.242	3.076	3.352	2.739	2.628	1.642	1.612	1.367	0.922
4500	0.75	-1.0	3.508	3.132	2.929	3.063	2.645	2.444	1.556	1.432	1.319	0.906
4500	0.75	-2.0	3.373	2.996	2.819	2.718	2.544	2.301	1.504	1.322	1.280	0.904
4500	0.75	-3.0	3.073	2.856	2.715	2.569	2.420	2.195	1.471	1.277	1.186	0.890
4500	1.50	-0.0	3.342	3.110	2.948	3.383	2.643	2.665	1.604	1.711	1.357	0.922
4500	1.50	-0.5	3.194	2.888	2.713	3.040	2.449	2.366	1.440	1.441	1.251	0.849
4500	1.50	-1.0	3.113	2.749	2.542	2.732	2.324	2.168	1.371	1.264	1.192	0.808
4500	1.50	-2.0	3.069	2.654	2.451	2.404	2.227	2.029	1.332	1.183	1.184	0.801
4500	1.50	-3.0	2.870	2.563	2.409	2.283	2.153	1.968	1.334	1.163	1.116	0.805
4500	2.25	-0.0	3.090	2.867	2.716	3.182	2.483	2.510	1.493	1.564	1.295	0.882
4500	2.25	-0.5	2.934	2.637	2.446	2.803	2.256	2.199	1.345	1.327	1.195	0.808
4500	2.25	-1.0	2.855	2.508	2.292	2.525	2.117	1.995	1.253	1.172	1.137	0.760
4500	2.25	-2.0	2.811	2.392	2.184	2.184	2.004	1.854	1.215	1.080	1.106	0.733
4500	2.25	-3.0	2.718	2.362	2.198	2.091	1.978	1.826	1.252	1.097	1.089	0.757
4500	3.00	-0.0	2.985	2.762	2.578	3.070	2.424	2.444	1.431	1.431	1.259	0.862
4500	3.00	-0.5	2.844	2.558	2.342	2.730	2.208	2.184	1.301	1.239	1.170	0.790
4500	3.00	-1.0	2.739	2.400	2.172	2.440	2.052	1.992	1.212	1.114	1.118	0.742
4500	3.00	-2.0	2.728	2.297	2.077	2.125	1.924	1.798	1.163	1.038	1.093	0.709
4500	3.00	-3.0	2.641	2.269	2.099	2.016	1.897	1.767	1.212	1.064	1.075	0.739
5000	1.50	-0.0	2.710	2.433	2.351	2.616	2.148	1.935	1.186	1.213	1.001	0.679
5000	1.50	-0.5	2.599	2.293	2.178	2.278	1.993	1.762	1.065	0.997	0.919	0.629
5000	1.50	-1.0	2.460	2.166	2.054	2.049	1.894	1.643	0.983	0.881	0.854	0.593
5000	1.50	-2.0	2.164	1.968	1.895	1.814	1.713	1.486	0.887	0.781	0.731	0.546
5000	1.50	-3.0	1.988	1.878	1.795	1.707	1.612	1.409	0.845	0.735	0.674	0.520
5000	2.25	-0.0	2.533	2.270	2.179	2.489	1.998	1.856	1.114	1.173	0.976	0.654
5000	2.25	-0.5	2.375	2.087	1.969	2.136	1.833	1.651	1.005	0.965	0.902	0.602
5000	2.25	-1.0	2.261	1.943	1.825	1.871	1.703	1.516	0.930	0.849	0.845	0.566
5000	2.25	-2.0	1.983	1.748	1.671	1.616	1.524	1.364	0.846	0.754	0.736	0.525
5000	2.25	-3.0	1.761	1.650	1.574	1.497	1.413	1.283	0.811	0.708	0.659	0.503
5000	3.00	-0.0	2.423	2.170	2.063	2.412	1.915	1.821	1.080	1.136	0.969	0.646
5000	3.00	-0.5	2.274	1.989	1.857	2.075	1.747	1.622	0.978	0.944	0.901	0.592
5000	3.00	-1.0	2.143	1.837	1.708	1.807	1.610	1.475	0.908	0.837	0.854	0.556
5000	3.00	-2.0	1.931	1.652	1.560	1.529	1.434	1.312	0.848	0.759	0.770	0.523
5000	3.00	-3.0	1.689	1.561	1.479	1.408	1.328	1.231	0.820	0.717	0.678	0.507
5500	1.50	-0.0	2.341	2.121	2.057	2.091	1.907	1.582	0.865	0.778	0.698	0.501
5500	1.50	-0.5	2.165	1.984	1.926	1.885	1.781	1.444	0.750	0.656	0.601	0.449
5500	1.50	-1.0	2.013	1.871	1.825	1.763	1.678	1.343	0.664	0.585	0.526	0.410
5500	1.50	-2.0	1.837	1.738	1.688	1.622	1.541	1.225	0.574	0.509	0.457	0.361
5500	1.50	-3.0	1.760	1.686	1.612	1.551	1.479	1.169	0.547	0.476	0.438	0.340
5500	2.25	-0.0	2.148	1.929	1.863	1.947	1.732	1.501	0.820	0.770	0.695	0.484
5500	2.25	-0.5	1.979	1.783	1.721	1.716	1.601	1.367	0.726	0.649	0.613	0.439
5500	2.25	-1.0	1.816	1.657	1.611	1.573	1.489	1.265	0.653	0.582	0.545	0.406
5500	2.25	-2.0	1.600	1.508	1.467	1.412	1.340	1.141	0.573	0.510	0.464	0.363
5500	2.25	-3.0	1.514	1.452	1.387	1.334	1.272	1.084	0.549	0.479	0.442	0.343
5500	3.00	-0.0	2.008	1.791	1.719	1.853	1.607	1.442	0.800	0.770	0.703	0.478
5500	3.00	-0.5	1.852	1.641	1.570	1.608	1.471	1.308	0.718	0.654	0.637	0.438

Table 15a – *continued*

T_{eff}	Log g	[A/H]	3390	3448	3509	3571	3636	3704	4032	4167	4255	4464
			Wavelength									
5500	3.00	-1.0	1.694	1.506	1.453	1.445	1.353	1.197	0.655	0.590	0.577	0.408
5500	3.00	-2.0	1.441	1.342	1.301	1.256	1.189	1.061	0.586	0.522	0.484	0.370
5500	3.00	-3.0	1.340	1.281	1.221	1.172	1.114	1.002	0.564	0.492	0.455	0.352
6000	2.25	-0.0	1.913	1.784	1.747	1.714	1.625	1.341	0.568	0.495	0.438	0.336
6000	2.25	-0.5	1.778	1.674	1.647	1.599	1.530	1.238	0.481	0.425	0.369	0.296
6000	2.25	-1.0	1.675	1.588	1.564	1.514	1.449	1.165	0.421	0.380	0.328	0.267
6000	2.25	-2.0	1.561	1.500	1.455	1.408	1.351	1.083	0.368	0.327	0.295	0.233
6000	2.25	-3.0	1.512	1.459	1.401	1.359	1.306	1.041	0.352	0.305	0.281	0.218
6000	3.00	-0.0	1.739	1.604	1.565	1.562	1.461	1.267	0.571	0.508	0.462	0.341
6000	3.00	-0.5	1.597	1.485	1.457	1.430	1.357	1.165	0.496	0.441	0.399	0.307
6000	3.00	-1.0	1.482	1.391	1.370	1.335	1.270	1.089	0.443	0.399	0.355	0.281
6000	3.00	-2.0	1.355	1.299	1.259	1.218	1.166	1.004	0.398	0.352	0.321	0.251
6000	3.00	-3.0	1.301	1.255	1.202	1.165	1.117	0.960	0.383	0.332	0.306	0.238

Table 15b. The Oke fluxes for giants.

T_{eff}	Log g	[A/H]	4566	4785	5000	5263	5882	6055	6370	6800	7100
			Wavelength								
4000	0.75	-0.0	1.046	0.737	0.663	0.411	-0.009	-0.322	-0.370	-0.583	-0.611
4000	0.75	-0.5	0.988	0.708	0.597	0.358	-0.094	-0.307	-0.388	-0.584	-0.635
4000	0.75	-1.0	0.988	0.702	0.557	0.322	-0.146	-0.304	-0.415	-0.601	-0.672
4000	0.75	-2.0	1.073	0.763	0.555	0.300	-0.208	-0.331	-0.485	-0.675	-0.773
4000	0.75	-3.0	1.196	0.853	0.596	0.307	-0.249	-0.375	-0.559	-0.770	-0.889
4000	1.50	-0.0	0.946	0.739	0.654	0.374	-0.005	-0.312	-0.386	-0.577	-0.630
4000	1.50	-0.5	0.889	0.689	0.585	0.330	-0.081	-0.294	-0.390	-0.569	-0.637
4000	1.50	-1.0	0.861	0.654	0.533	0.297	-0.124	-0.285	-0.399	-0.571	-0.649
4000	1.50	-2.0	0.910	0.661	0.489	0.266	-0.175	-0.293	-0.431	-0.603	-0.696
4000	1.50	-3.0	1.046	0.748	0.523	0.271	-0.217	-0.330	-0.493	-0.681	-0.788
4000	2.25	-0.0	0.872	0.764	0.669	0.348	0.015	-0.312	-0.405	-0.581	-0.653
4000	2.25	-0.5	0.820	0.707	0.602	0.310	-0.055	-0.292	-0.399	-0.568	-0.647
4000	2.25	-1.0	0.789	0.655	0.543	0.282	-0.098	-0.279	-0.396	-0.561	-0.644
4000	2.25	-2.0	0.805	0.613	0.472	0.251	-0.147	-0.274	-0.405	-0.568	-0.658
4000	2.25	-3.0	0.937	0.676	0.477	0.247	-0.195	-0.304	-0.456	-0.633	-0.734
4500	0.75	-0.0	0.813	0.511	0.468	0.297	-0.089	-0.258	-0.269	-0.441	-0.428
4500	0.75	-0.5	0.756	0.500	0.425	0.258	-0.115	-0.237	-0.291	-0.437	-0.461
4500	0.75	-1.0	0.741	0.501	0.396	0.229	-0.132	-0.229	-0.313	-0.447	-0.495
4500	0.75	-2.0	0.764	0.532	0.380	0.205	-0.154	-0.235	-0.347	-0.479	-0.550
4500	0.75	-3.0	0.769	0.545	0.374	0.190	-0.161	-0.240	-0.359	-0.493	-0.570
4500	1.50	-0.0	0.751	0.494	0.448	0.286	-0.076	-0.242	-0.267	-0.425	-0.428
4500	1.50	-0.5	0.689	0.469	0.403	0.247	-0.102	-0.222	-0.281	-0.418	-0.449
4500	1.50	-1.0	0.657	0.457	0.368	0.217	-0.117	-0.213	-0.294	-0.420	-0.469
4500	1.50	-2.0	0.670	0.470	0.341	0.188	-0.136	-0.213	-0.315	-0.438	-0.504
4500	1.50	-3.0	0.692	0.492	0.340	0.175	-0.146	-0.220	-0.330	-0.455	-0.527
4500	2.25	-0.0	0.703	0.492	0.443	0.278	-0.063	-0.231	-0.274	-0.418	-0.440
4500	2.25	-0.5	0.645	0.457	0.395	0.241	-0.089	-0.214	-0.281	-0.410	-0.451
4500	2.25	-1.0	0.610	0.436	0.357	0.212	-0.104	-0.205	-0.287	-0.408	-0.461
4500	2.25	-2.0	0.608	0.434	0.321	0.179	-0.124	-0.201	-0.297	-0.415	-0.479
4500	2.25	-3.0	0.647	0.463	0.321	0.167	-0.138	-0.209	-0.315	-0.435	-0.505
4500	3.00	-0.0	0.665	0.503	0.456	0.273	-0.041	-0.225	-0.286	-0.418	-0.457
4500	3.00	-0.5	0.615	0.461	0.403	0.239	-0.070	-0.210	-0.286	-0.409	-0.459
4500	3.00	-1.0	0.583	0.433	0.361	0.212	-0.088	-0.201	-0.286	-0.404	-0.460
4500	3.00	-2.0	0.582	0.422	0.317	0.177	-0.113	-0.197	-0.292	-0.407	-0.471
4500	3.00	-3.0	0.632	0.455	0.317	0.165	-0.134	-0.208	-0.313	-0.433	-0.503
5000	1.50	-0.0	0.556	0.352	0.326	0.201	-0.087	-0.184	-0.216	-0.318	-0.333
5000	1.50	-0.5	0.511	0.338	0.287	0.172	-0.091	-0.163	-0.216	-0.306	-0.339
5000	1.50	-1.0	0.487	0.330	0.260	0.152	-0.094	-0.155	-0.218	-0.303	-0.344
5000	1.50	-2.0	0.465	0.323	0.233	0.128	-0.097	-0.148	-0.220	-0.303	-0.349
5000	1.50	-3.0	0.452	0.321	0.222	0.115	-0.096	-0.146	-0.219	-0.301	-0.348

Table 15b – *continued*

T_{eff}	Log g	[A/H]	4566	4785	5000	5263	5882	6055	6370	6800	7100
			Wavelength								
5000	2.25	-0.0	0.531	0.347	0.321	0.198	-0.079	-0.180	-0.215	-0.315	-0.331
5000	2.25	-1.0	0.486	0.329	0.282	0.170	-0.084	-0.161	-0.214	-0.303	-0.336
5000	2.25	-2.0	0.460	0.317	0.254	0.149	-0.088	-0.152	-0.215	-0.299	-0.339
5000	2.25	-3.0	0.443	0.311	0.226	0.125	-0.093	-0.145	-0.215	-0.297	-0.342
5000	2.25	-3.0	0.436	0.311	0.215	0.112	-0.094	-0.143	-0.215	-0.296	-0.343
5000	3.00	-0.0	0.514	0.348	0.320	0.201	-0.067	-0.175	-0.215	-0.313	-0.334
5000	3.00	-0.5	0.470	0.327	0.282	0.171	-0.076	-0.160	-0.215	-0.303	-0.337
5000	3.00	-1.0	0.446	0.313	0.254	0.150	-0.081	-0.150	-0.214	-0.298	-0.338
5000	3.00	-2.0	0.437	0.310	0.226	0.125	-0.091	-0.144	-0.215	-0.296	-0.342
5000	3.00	-3.0	0.438	0.314	0.217	0.113	-0.094	-0.144	-0.216	-0.297	-0.344
5500	1.50	-0.0	0.403	0.252	0.228	0.148	-0.063	-0.119	-0.149	-0.210	-0.231
5500	1.50	-0.5	0.364	0.235	0.196	0.122	-0.064	-0.109	-0.146	-0.202	-0.227
5500	1.50	-1.0	0.339	0.223	0.175	0.105	-0.065	-0.103	-0.145	-0.199	-0.225
5500	1.50	-2.0	0.310	0.213	0.153	0.086	-0.063	-0.097	-0.143	-0.195	-0.223
5500	1.50	-3.0	0.298	0.211	0.145	0.075	-0.062	-0.095	-0.142	-0.193	-0.222
5500	2.25	-0.0	0.389	0.250	0.228	0.144	-0.063	-0.123	-0.154	-0.216	-0.237
5500	2.25	-0.5	0.355	0.234	0.197	0.121	-0.064	-0.111	-0.150	-0.207	-0.232
5500	2.25	-1.0	0.334	0.224	0.176	0.105	-0.064	-0.105	-0.149	-0.203	-0.230
5500	2.25	-2.0	0.310	0.215	0.155	0.086	-0.064	-0.099	-0.146	-0.200	-0.229
5500	2.25	-3.0	0.300	0.214	0.147	0.076	-0.063	-0.097	-0.145	-0.198	-0.228
5500	3.00	-0.0	0.380	0.251	0.230	0.144	-0.060	-0.126	-0.160	-0.222	-0.243
5500	3.00	-0.5	0.350	0.237	0.200	0.121	-0.061	-0.113	-0.155	-0.213	-0.238
5500	3.00	-1.0	0.332	0.227	0.179	0.106	-0.063	-0.107	-0.152	-0.208	-0.236
5500	3.00	-2.0	0.314	0.220	0.158	0.087	-0.065	-0.101	-0.150	-0.205	-0.234
5500	3.00	-3.0	0.306	0.219	0.151	0.078	-0.065	-0.100	-0.149	-0.204	-0.234
6000	2.25	-0.0	0.265	0.165	0.152	0.102	-0.039	-0.074	-0.091	-0.125	-0.136
6000	2.25	-0.5	0.238	0.151	0.129	0.083	-0.040	-0.068	-0.089	-0.120	-0.132
6000	2.25	-1.0	0.220	0.142	0.113	0.070	-0.040	-0.064	-0.088	-0.118	-0.130
6000	2.25	-2.0	0.200	0.137	0.097	0.055	-0.038	-0.060	-0.087	-0.115	-0.129
6000	2.25	-3.0	0.190	0.135	0.092	0.047	-0.038	-0.059	-0.086	-0.114	-0.128
6000	3.00	-0.0	0.269	0.174	0.158	0.103	-0.041	-0.080	-0.101	-0.137	-0.149
6000	3.00	-0.5	0.246	0.161	0.136	0.085	-0.042	-0.073	-0.098	-0.132	-0.145
6000	3.00	-1.0	0.230	0.153	0.120	0.073	-0.042	-0.069	-0.096	-0.129	-0.143
6000	3.00	-2.0	0.214	0.149	0.105	0.059	-0.042	-0.065	-0.095	-0.127	-0.143
6000	3.00	-3.0	0.206	0.148	0.100	0.051	-0.041	-0.064	-0.095	-0.126	-0.142

Table 15c. The Oke fluxes for giants.

T_{eff}	Log g	[A/H]	7530	7850	8080	8400	8805	9700	9950	10250	10400	10800
			Wavelength									
4000	0.75	-0.0	-0.761	-0.842	-0.803	-0.875	-1.008	-1.076	-1.163	-1.224	-1.238	-1.253
4000	0.75	-0.5	-0.774	-0.856	-0.838	-0.905	-1.026	-1.108	-1.184	-1.236	-1.248	-1.274
4000	0.75	-1.0	-0.804	-0.885	-0.888	-0.954	-1.060	-1.157	-1.222	-1.267	-1.279	-1.311
4000	0.75	-2.0	-0.906	-0.991	-1.029	-1.095	-1.178	-1.302	-1.347	-1.384	-1.397	-1.435
4000	0.75	-3.0	-1.034	-1.126	-1.181	-1.250	-1.328	-1.466	-1.501	-1.535	-1.550	-1.588
4000	1.50	-0.0	-0.764	-0.842	-0.829	-0.890	-1.007	-1.096	-1.169	-1.222	-1.233	-1.256
4000	1.50	-0.5	-0.763	-0.842	-0.845	-0.904	-1.010	-1.110	-1.174	-1.221	-1.231	-1.262
4000	1.50	-1.0	-0.771	-0.851	-0.869	-0.928	-1.022	-1.132	-1.189	-1.230	-1.240	-1.276
4000	1.50	-2.0	-0.819	-0.899	-0.939	-1.000	-1.078	-1.203	-1.245	-1.281	-1.294	-1.332
4000	1.50	-3.0	-0.921	-1.005	-1.056	-1.121	-1.194	-1.327	-1.359	-1.393	-1.408	-1.445
4000	2.25	-0.0	-0.775	-0.851	-0.859	-0.913	-1.015	-1.121	-1.184	-1.230	-1.240	-1.269
4000	2.25	-0.5	-0.765	-0.843	-0.863	-0.915	-1.010	-1.123	-1.179	-1.221	-1.231	-1.266
4000	2.25	-1.0	-0.761	-0.839	-0.869	-0.923	-1.009	-1.128	-1.179	-1.218	-1.228	-1.266
4000	2.25	-2.0	-0.776	-0.854	-0.897	-0.954	-1.029	-1.156	-1.195	-1.230	-1.244	-1.283
4000	2.25	-3.0	-0.860	-0.940	-0.990	-1.051	-1.121	-1.247	-1.277	-1.308	-1.322	-1.356
4500	0.75	-0.0	-0.542	-0.604	-0.532	-0.597	-0.708	-0.712	-0.796	-0.845	-0.859	-0.852
4500	0.75	-0.5	-0.558	-0.616	-0.580	-0.637	-0.725	-0.757	-0.819	-0.857	-0.866	-0.872
4500	0.75	-1.0	-0.583	-0.641	-0.637	-0.687	-0.753	-0.810	-0.853	-0.882	-0.889	-0.903
4500	0.75	-2.0	-0.639	-0.697	-0.728	-0.771	-0.819	-0.901	-0.922	-0.943	-0.951	-0.970
4500	0.75	-3.0	-0.662	-0.720	-0.756	-0.800	-0.847	-0.931	-0.950	-0.969	-0.978	-0.999

Table 15c – *continued*

T_{eff}	Log g	[A/H]	7530	7850	8080	8400	8805	9700	9950	10250	10400	10800
			Wavelength									
4500	1.50	-0.0	-0.532	-0.593	-0.539	-0.596	-0.697	-0.716	-0.789	-0.834	-0.846	-0.845
4500	1.50	-0.5	-0.541	-0.599	-0.573	-0.625	-0.706	-0.748	-0.804	-0.839	-0.848	-0.857
4500	1.50	-1.0	-0.554	-0.611	-0.611	-0.659	-0.721	-0.783	-0.824	-0.851	-0.859	-0.874
4500	1.50	-2.0	-0.588	-0.643	-0.673	-0.715	-0.761	-0.842	-0.865	-0.886	-0.894	-0.914
4500	1.50	-3.0	-0.615	-0.670	-0.705	-0.747	-0.792	-0.875	-0.893	-0.912	-0.921	-0.942
4500	2.25	-0.0	-0.534	-0.594	-0.558	-0.608	-0.697	-0.733	-0.796	-0.835	-0.844	-0.849
4500	2.25	-0.5	-0.537	-0.595	-0.582	-0.629	-0.701	-0.755	-0.804	-0.836	-0.844	-0.856
4500	2.25	-1.0	-0.543	-0.599	-0.606	-0.650	-0.709	-0.777	-0.814	-0.841	-0.848	-0.865
4500	2.25	-2.0	-0.561	-0.615	-0.644	-0.685	-0.731	-0.812	-0.835	-0.856	-0.864	-0.884
4500	2.25	-3.0	-0.589	-0.643	-0.676	-0.717	-0.762	-0.843	-0.860	-0.879	-0.888	-0.908
4500	3.00	-0.0	-0.542	-0.600	-0.584	-0.627	-0.701	-0.755	-0.808	-0.842	-0.849	-0.858
4500	3.00	-0.5	-0.540	-0.597	-0.598	-0.640	-0.702	-0.768	-0.811	-0.840	-0.846	-0.861
4500	3.00	-1.0	-0.540	-0.596	-0.610	-0.651	-0.705	-0.780	-0.814	-0.839	-0.846	-0.864
4500	3.00	-2.0	-0.552	-0.605	-0.634	-0.675	-0.719	-0.802	-0.824	-0.844	-0.853	-0.873
4500	3.00	-3.0	-0.587	-0.641	-0.674	-0.715	-0.758	-0.836	-0.853	-0.871	-0.879	-0.898
5000	1.50	-0.0	-0.387	-0.427	-0.391	-0.430	-0.487	-0.493	-0.538	-0.562	-0.566	-0.560
5000	1.50	-0.5	-0.389	-0.426	-0.421	-0.452	-0.491	-0.520	-0.547	-0.563	-0.565	-0.566
5000	1.50	-1.0	-0.395	-0.431	-0.443	-0.470	-0.500	-0.542	-0.558	-0.569	-0.572	-0.576
5000	1.50	-2.0	-0.404	-0.439	-0.459	-0.484	-0.512	-0.559	-0.569	-0.578	-0.582	-0.589
5000	1.50	-3.0	-0.405	-0.439	-0.461	-0.486	-0.515	-0.561	-0.570	-0.580	-0.584	-0.593
5000	2.25	-0.0	-0.386	-0.427	-0.394	-0.431	-0.486	-0.497	-0.540	-0.564	-0.568	-0.563
5000	2.25	-0.5	-0.387	-0.425	-0.420	-0.451	-0.488	-0.520	-0.547	-0.563	-0.566	-0.567
5000	2.25	-1.0	-0.390	-0.427	-0.438	-0.465	-0.495	-0.538	-0.555	-0.567	-0.570	-0.574
5000	2.25	-2.0	-0.397	-0.432	-0.453	-0.478	-0.505	-0.553	-0.563	-0.572	-0.576	-0.584
5000	2.25	-3.0	-0.399	-0.433	-0.455	-0.481	-0.508	-0.555	-0.564	-0.574	-0.578	-0.588
5000	3.00	-0.0	-0.388	-0.429	-0.402	-0.437	-0.486	-0.504	-0.545	-0.567	-0.571	-0.567
5000	3.00	-0.5	-0.389	-0.427	-0.424	-0.454	-0.490	-0.525	-0.552	-0.567	-0.570	-0.572
5000	3.00	-1.0	-0.390	-0.427	-0.438	-0.465	-0.494	-0.539	-0.556	-0.568	-0.572	-0.576
5000	3.00	-2.0	-0.396	-0.431	-0.452	-0.477	-0.503	-0.551	-0.561	-0.571	-0.575	-0.583
5000	3.00	-3.0	-0.400	-0.435	-0.456	-0.482	-0.509	-0.555	-0.564	-0.573	-0.577	-0.586
5500	1.50	-0.0	-0.250	-0.269	-0.264	-0.279	-0.308	-0.310	-0.326	-0.332	-0.328	-0.315
5500	1.50	-0.5	-0.250	-0.269	-0.275	-0.287	-0.310	-0.323	-0.329	-0.332	-0.330	-0.321
5500	1.50	-1.0	-0.252	-0.271	-0.280	-0.292	-0.314	-0.330	-0.333	-0.335	-0.334	-0.327
5500	1.50	-2.0	-0.254	-0.273	-0.284	-0.295	-0.318	-0.335	-0.337	-0.338	-0.338	-0.335
5500	1.50	-3.0	-0.254	-0.273	-0.284	-0.296	-0.320	-0.336	-0.338	-0.339	-0.339	-0.338
5500	2.25	-0.0	-0.259	-0.280	-0.273	-0.289	-0.311	-0.316	-0.333	-0.339	-0.337	-0.325
5500	2.25	-0.5	-0.258	-0.278	-0.283	-0.297	-0.314	-0.329	-0.336	-0.339	-0.338	-0.330
5500	2.25	-1.0	-0.259	-0.279	-0.288	-0.301	-0.318	-0.336	-0.340	-0.342	-0.341	-0.336
5500	2.25	-2.0	-0.261	-0.281	-0.293	-0.305	-0.323	-0.341	-0.344	-0.345	-0.346	-0.344
5500	2.25	-3.0	-0.261	-0.281	-0.293	-0.306	-0.325	-0.343	-0.345	-0.347	-0.347	-0.347
5500	3.00	-0.0	-0.267	-0.290	-0.282	-0.298	-0.317	-0.325	-0.342	-0.349	-0.347	-0.335
5500	3.00	-0.5	-0.265	-0.287	-0.291	-0.306	-0.320	-0.337	-0.345	-0.349	-0.348	-0.339
5500	3.00	-1.0	-0.266	-0.287	-0.296	-0.310	-0.323	-0.344	-0.348	-0.350	-0.350	-0.345
5500	3.00	-2.0	-0.268	-0.289	-0.301	-0.314	-0.329	-0.349	-0.352	-0.354	-0.354	-0.353
5500	3.00	-3.0	-0.269	-0.289	-0.302	-0.316	-0.332	-0.351	-0.353	-0.355	-0.356	-0.356
6000	2.25	-0.0	-0.138	-0.142	-0.140	-0.142	-0.163	-0.150	-0.151	-0.148	-0.141	-0.120
6000	2.25	-0.5	-0.138	-0.144	-0.144	-0.145	-0.166	-0.157	-0.155	-0.150	-0.145	-0.127
6000	2.25	-1.0	-0.140	-0.146	-0.148	-0.148	-0.169	-0.162	-0.158	-0.153	-0.149	-0.134
6000	2.25	-2.0	-0.143	-0.149	-0.152	-0.152	-0.173	-0.167	-0.162	-0.157	-0.153	-0.142
6000	2.25	-3.0	-0.142	-0.149	-0.152	-0.153	-0.175	-0.168	-0.163	-0.158	-0.154	-0.145
6000	3.00	-0.0	-0.154	-0.160	-0.158	-0.161	-0.171	-0.162	-0.164	-0.161	-0.155	-0.135
6000	3.00	-0.5	-0.154	-0.162	-0.163	-0.165	-0.175	-0.170	-0.168	-0.164	-0.159	-0.143
6000	3.00	-1.0	-0.155	-0.163	-0.166	-0.168	-0.178	-0.175	-0.171	-0.166	-0.163	-0.150
6000	3.00	-2.0	-0.158	-0.167	-0.170	-0.172	-0.184	-0.180	-0.177	-0.172	-0.169	-0.159
6000	3.00	-3.0	-0.159	-0.167	-0.171	-0.173	-0.186	-0.182	-0.178	-0.173	-0.171	-0.162

for each colour (note that the set of stars involved in each such mean is different for the different colours). The results are given in Table 16, where the standard deviations in δ are also given.

There is a tendency for many colours to suggest a slight revision of the IRFM temperature scale downwards, at least for the giants with $T_{eff} < 5000$ K. In particular, we note that the $V-K$

Table 16. Mean deviations $\delta(K)$ between T_{eff}(colour) and T_{eff}(IRFM), as well as standard deviations in δ.

Colour	$\delta(K)$	s.d. (K)
$(V-K)_J$	−50	70
$(J-K)_J$	130	70
$(J-H)_W$	−140	60
$(J-K)_W$	−80	70
$(J-H)_G$	190	60
$(J-K)_G$	70	70
$(J-L)_G$	−240	120
$(R-I)_C$	−170	80
$(V-R)_C$	−220	60
$(58-99)_{JML}$	−40	110
$(72-110)_{JML}$	130	180
$(78-110)_{Wing}$	−50	50
$(593-780)_F$	−120	140
$(593-1064)_F$	−50	150

The subscripts refer to the Johnson, Wennfors, Glass, Cousins, Johnson and Mitchell 13 colour, Wing and Frisk systems, respectively.

indices, the Cousins *VRI*, the JML 58–99 index and the Wing 78–110 index, as well as the IRFM with the Glass *K*-band or the revised *K*-band response function of Bessell & Brett (1987) (see the discussion in the appendix) as the reference band, together suggest a downward revision of between 40 and 100 K. It is true that other indices give evidence for an upward revision of the T_{eff}(IRFM) scale but we consider this evidence to be considerably weaker. Additional evidence for the reduction of our T_{eff}(IRFM) values comes from the comparison with Blackwell and collaborators (see above). Thus, we have adopted

$$T_{eff}(\text{adopted}) = T_{eff}(\text{IRFM}) - 80\ \text{K}, \tag{1}$$

for all the stars. Alternatively, a temperature correction factor slightly decreasing from 0 K at $T_{eff}=5500$ K to −100 K at $T_{eff}=4000$ K could be anticipated. However, a temperature-dependent systematic error in, for example, T_{eff} $(V-K)$ seems at least as possible as a corresponding error in T_{eff}(IRFM). A correction according to equation (1) would also bring the solar-type dwarfs into fair agreement with the reddest end of the colour – T_{eff} calibration of SH85. The particular choice of correction term is in fact close to the mean zero-point shift one would derive from the results given in Table 16.

The revised temperatures are given in Table 3. This table also contains temperatures for a few stars for which there are insufficient data to obtain values from the IRFM. These have been found from colours, as described above.

In order to test the possibility that the colours of particular stars might all indicate effective temperatures systematically different from those derived according to equation (1), indicating spurious errors in T_{eff}(IRFM), we have adopted the zero-point shifts z_i of Table 16, derived individual effective temperatures from each colour i and for each star and thus formed the differences

$$\delta_i = T_{eff}(\text{colour}_i) - T_{eff}(\text{IRFM}) - z_i.$$

The resulting differences, divided by the standard deviations of Table 16, were summed for each star and these numbers were found to have a roughly Gaussian distribution, with a standard deviation close to what would be expected if the δ_i values were stochastically independent. Thus, we did not find any signs of significant systematic errors in T_{eff}(IRFM) for any of the stars. For the few stars in the wings of the distribution, where the individual colours rather systematically seem to suggest temperatures different from those adopted in Table 3, we have indicated the effects as footnotes to Table 3.

We note in passing that the resulting temperature scale agrees very well in the high-temperature end with the V–K calibration of Carney (1983). The latter was based on model atmospheres by Kurucz (1979).

7 Comparison with effective temperatures from angular diameters

The most direct effective-temperature determinations for giant stars are based on angular diameter measurements, which in combination with limb-darkening estimates and apparent bolometric fluxes give effective temperatures. The most extensive set of angular diameter measurements for normal red giants has been obtained with the lunar occulation technique – such a set was used by Ridgway *et al.* (1980) to establish a temperature scale. Their set contained nine G and K giants with estimated errors varying from about 100 to 500 K. These errors are, however, only formal errors in the differential corrector reduction of the angular diameter measurements; in addition, important systematic errors may exist in the measurements and in the analysis. Ridgway *et al.* emphasize that these sources of error all will lead to underestimated T_{eff}s. In Fig. 17 we compare the V–K calibration of Ridgway *et al.* with ours. It is seen that our temperatures tend to be about 100 K hotter. In view of the considerable errors in the individual angular diameters and the direction of the systematic errors mentioned above, we conclude that the result of the comparison is acceptable.

Two of the stars in our sample, α Tau and α Boo, have relatively large angular diameters. Di Benedetto & Foy (1986) have discussed α Boo. From a Michelson interferometer, they find an angular diameter of 20.95 ± 0.20 milliarcsec. With our bolometric flux of 5.16 E − 12 W cm^{-2}, this gives $T_{\mathrm{eff}} = 4335 \pm 30$ K. The angular diameter of 20.88 ± 0.10 milliarcsec found by Ridgway *et al.* (1984) for α Tau on the basis of all their measurements, including the IR ones, gives 3917 K. The small error is overly reassuring, since White & Kreidl (1984) give an angular diameter of 20.45 ± 0.46 milliarcsec and Ridgway *et al.*, excluding their IR data, find 20.13 milliarcsec. This last value gives $T_{\mathrm{eff}} = 3990$ K. The value of the present paper is 3943 K.

Two other stars in the sample, β Gem and γ Dra, have been observed by Di Benedetto & Rabbia (1987). Using their angular diameters and our bolometric fluxes gives $T_{\mathrm{eff}} = 4938$ and 4017 K, respectively, for these two objects, compared with the values of 4896 and 3955 K given in Table 3.

Angular diameters (ϕ) have been computed for the standard stars, using the equation

$$\phi = 2^* F^{0.5} / T_{\mathrm{eff}}^2$$

These are given in Table 3, as well as the integrated fluxes (F).

8 The spectral type–T_{eff} – (B–V) relation for G–K Population I stars

From the adopted T_{eff} values of Table 3 we have obtained a relation between effective temperature and spectral type, basically derived from the standards of Keenan & McNeil (1976) but complemented with stars from the rest of the sample. We have avoided stars with [Fe/H] values known to be less than −0.3 dex. The resulting temperature calibration of spectral type is given in Table 17 and illustrated in Fig. 18. The scatter in T_{eff} and the small number of stars result in a weak calibration for subgiants (IV) and bright giants (II). Among the K stars, the

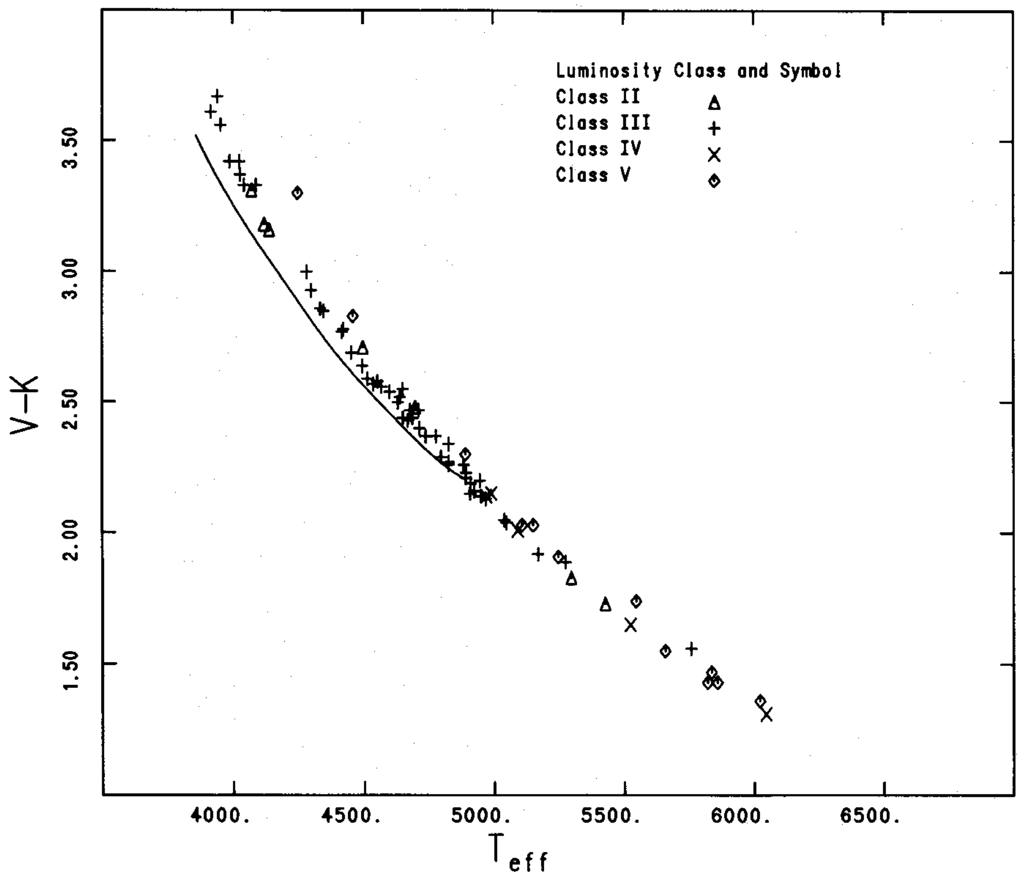

Figure 17. The observed $V-K$ colours of the stars are plotted versus the adopted values of T_{eff}. The line is the $V-K$, T_{eff} relation of Ridgway *et al.* (1984).

subgiants and bright giants are, however, about 150 K hotter and 400 K cooler, respectively, than the corresponding giant stars (III).

The $(B-V)$, T_{eff} diagram is given as Fig. 19 for the stars in the sample. The relationship is less tight than for the $(V-K)$, T_{eff} diagram. This is caused partly by gravity effects – at a given temperature the bright giants are generally redder than the giants, in agreement with the computations by BG78. It is also partly caused by abundance effects; α Boo, ϕ^2 Ori, μ Psc and, to a lesser extent, ρ Boo, all of which have [Fe/H] < -0.5, have blue $B-V$ colours for their T_{eff}, also in agreement with the BG78 calculations.

One point which is suggested by the data in Table 3 is that abundance differences can affect the spectral type versus T_{eff} relation to a significant degree. For example, both β CVn and β Com are classified as G0V stars, although β Com is 160 K hotter. The fact that it is more metal rich by 0.5 in [Fe/H] presumably explains this. For this reason, our K0V and K1V dwarfs σ Dra and o^2 Eri may be anomalously cool, by perhaps 100 K (note that o^2 Eri is 40 K cooler than the K2 V star ε Eri). Other stars which are metal poor and cooler than stars of similar spectral type are ϕ^2 Ori, α Boo and ρ Boo, all of which have [Fe/H] $\cong -0.5$.

9 Conclusions

The temperature scale for Population I G and K stars suggested by Tables 3 and 17 and Fig. 17 is estimated to be correct within 100 K, at least when applied to stars in the luminosity-class interval III–V. The differential effects in T_{eff} should be even better known.

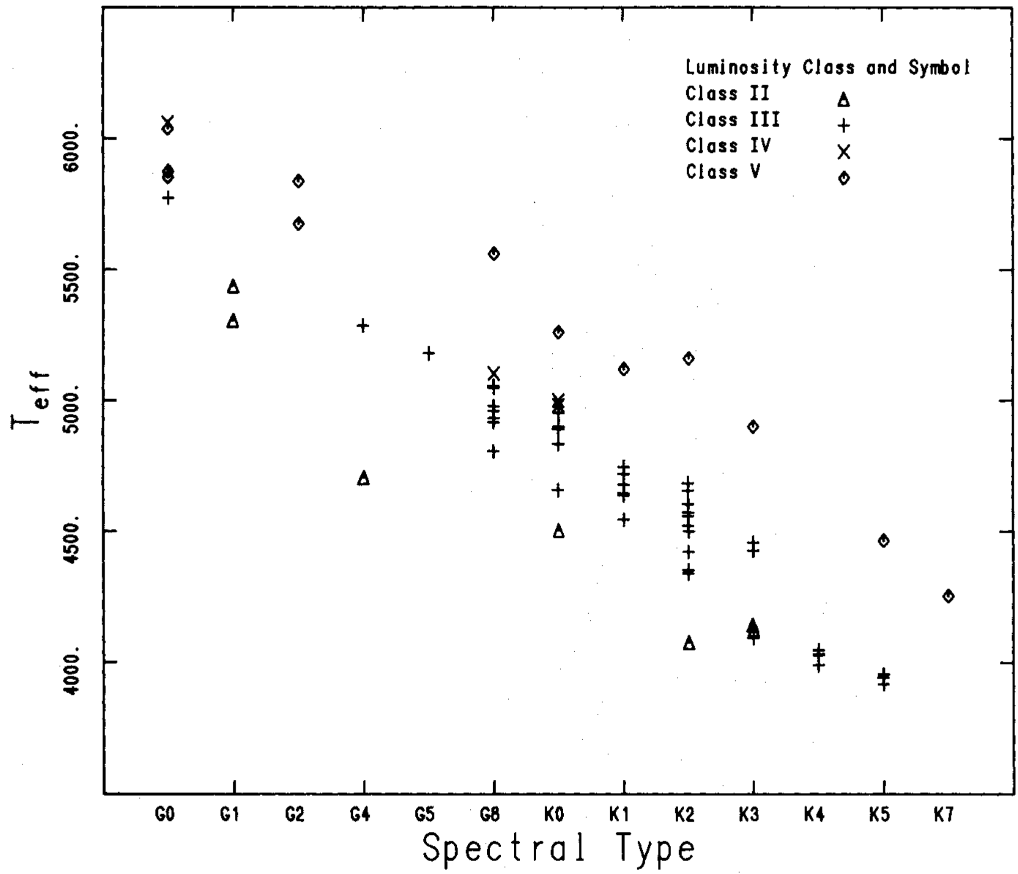

Figure 18. The adopted T_{eff} values of the stars are plotted versus their spectral types and luminosity classes.

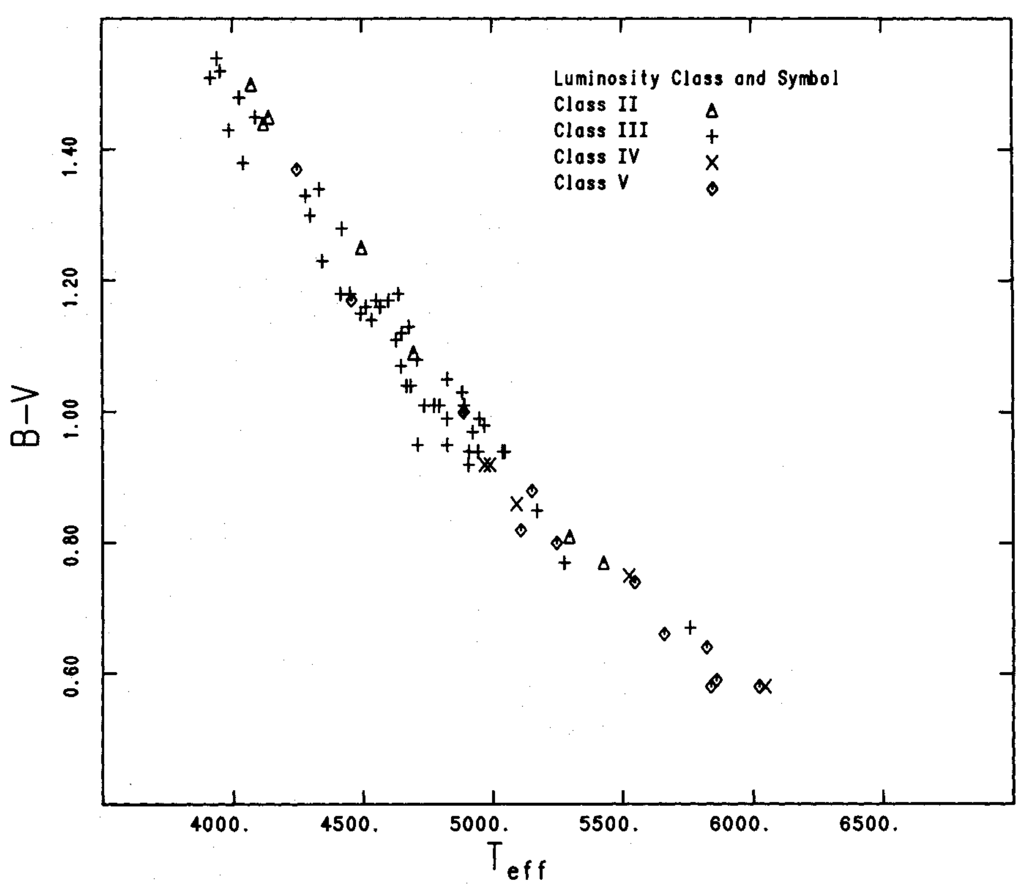

Figure 19. The observed $B-V$ colours of the stars are plotted versus the adopted values of T_{eff}. The stellar luminosity classes are indicated.

Table 17. Spectral type – luminosity class – temperature relation derived from the present sample of standard stars.

Spectral Type	Luminosity Class II	III	III-IV	IV	V
G0		5760(1)		6050(1)	5890(4)
G1	5360(2)				
G1.5					5830(1)
G2.5				5650(1)	5630(2)
G4	4700(1)				
G5		5180(1)	5600(1)		5650(1)
G6					5650(1)
G7					-
G8		4970(8)	4960(1)	5100(1)	5550(1)
K0	4500(1)	4820(5)	4820(2)	4990(1)	5250(1)
K1		4625(6)	4820(2)	4920(1)	5150:(1)
K2	4100:(1)	4520(10)			5100:(1)
K3	4100:(1)	4370(4)			4830(2)
K4		4050(5)			4450(1)
K5					4250(1)

The number in brackets is the number of stars used to find the effective temperature, while a colon indicates some smoothing was carried out.

The general agreement between the different $T_{\rm eff}$(colour) determnations and that of the IRFM is satisfactory also, as an indication that the mean temperature of the flux-forming regions in the model atmospheres is reasonably correct; the sensitivity of the IRFM to the detailed structure of the model atmospheres is less than and different to the corresponding sensitivity of the colour temperatures. The different tendencies for different colours traced in Figs 6–16 might contain information on shortcomings in the model atmospheres and synthetic spectra. However, in view of the problems with the proper definition of the colour systems as regards transmission functions (including that of the atmosphere) and calibrations, this possibility should not be overemphasized. Detailed flux curves at intermediate resolution with a calibration accurate to about 1 per cent would instead be relevant means for such important studies.

Acknowledgments

We are grateful for the assistance of Mr M. Briley, Dr K. Eriksson and Mr J. T. Ohlmacher. We thank Dr M. S. Bessell for sending a preprint of his work with Dr J. M. Brett. We wish to thank P. Williams and the anonymous referee. Special thanks are due to Dr Sandra Leggett for a detailed reading of the manuscript and for many constructive critical points and suggestions. Our work was supported by the Swedish Natural Science Research Council and by the National Science Foundation, under grants AST80-19570 and AST85-13872. Some of the calculations were made using the CRAY X-MP of the San Diego Supercomputer Center, the time being supplied under NSF grant AST85-09915. The interpretation of the results was materially assisted by the use of a RIDGE 32C computer and CHROMATICS CX-1536 image display system, purchased under the above grants.

References

Auman, J. R., 1967. *Astrophys. J. Suppl.,* **14,** 171.

Aumann, H. H., Gillett, F. C., Beichman, C. A., de Jong, T., Houck, J. R., Low, F. J., Neugebauer, G., Walker, R. G. & Wesselius, P. R., 1984. *Astrophys. J.,* **278,** L15.

Balfour, W. J. & Cartwright, H. M., 1977. *Astr. Astrophys. Suppl.,* **26,** 389.

Bell, K. L., Kingston, A. E. & McIlveen, W. A., 1975. *J. Phys. B. Atom. Mol. Phys.,* **8,** 358.

Bell, R. A. & Dreiling, L. A., 1981. *Astrophys. J.,* **248,** 1031.

Bell, R. A. & Gustafsson, B., 1978. *Astr. Astrophys. Suppl.,* **34,** 229.

Bell, R. A. & VandenBerg, D. A., 1987. *Astrophys. J. Suppl.,* **63,** 335.

Bell, R. A., Dwivedi, P. H., Branch, D. R. & Huffaker, J. N., 1979. *Astrophys. J. Suppl.,* **41,** 593.

Bell, R. A., Eriksson, K., Gustafsson, B. & Nordlund, A., 1976. *Astr. Astrophys. Suppl.,* **23,** 37.

Bessell, M. S., 1983. *Publs. astr. Soc. Pacif.,* **95,** 480.

Bessell, M. S., 1986a. *Publs. astr. Soc. Pacif.,* **98,** 354.

Bessell, M. S., 1986b. *Publs. astr. Soc. Pacif.,* **98,** 1303.

Bessell, M. S. & Brett, J. M., 1987. Preprint.

Blaauw, A., 1963. In: *Basic Astronomical Data,* p. 383, ed. Strand, K. Aa., University of Chicago Press.

Blackwell, D. E. & Shallis, M. J., 1977. *Mon. Not. R. astr. Soc.,* **180,** 177.

Blackwell, D. E., Petford, A. D. & Shallis, M. J., 1980. *Astr. Astrophys.,* **82,** 249.

Blackwell, D. E., Shallis, M. J. & Selby, M. J., 1979. *Mon. Not. R. astr. Soc.,* **188,** 847.

Blackwell, D. E., Petford, A. D. & Shallis, M. J., 1980. *Astr. Astrophys.,* **82,** 249.

Blackwell, D. E., Booth, A. J., Petford, A. D., Leggett, S. K., Mountain, C. M. & Selby, M. J., 1986. *Mon. Not. R. astr. Soc.,* **221,** 427.

Branch, D. R., Lambert, D. L. & Tomkin, J., 1980. *Astrophys. J.,* **241,** L83.

Carney, B. W., 1983. *Astr. J.,* **88,** 623.

Cayrel, R., Cayrel de Strobel, G. & Campbell, B., 1985. *Astr. Astrophys.,* **146,** 249.

Cayrel de Strobel, G., Bentolila, C., Hauck, B. & Duguennoy, A., 1985. *Astr. Astrophys. Suppl.,* **59,** 145.

Clegg, R. E. S., Lambert, D. L. & Tomkin, J., 1981. *Astrophys. J.,* **250,** 262.

Cochran, A. L., 1980. *Publs. Astr.,* **16,** The University of Texas, Austin.

Cousins, A. W. J., 1980. *S. Afr. astr. Obs. Circ.,* **1,** 234.

Cousins, A. W. J., 1981. *S. Afr. astr. Obs. Circ.,* **6,** 4.

Davis, S. P., Littleton, J. E. & Phillips, J. G., 1986. *Astrophys. J.,* **309,** 449.

Day, R. W., Lambert, D. L. & Sneden, C., 1973. *Astrophys. J.,* **185,** 213.

Di Benedetto, G. P. & Rabbia, Y., 1987. *Astr. Astrophys.,* **188,** 114.

Di Benedetto, G. P. & Foy, R., 1986. *Astr. Astrophys.,* **166,** 204.

Doughty, N. A. & Fraser, P. A., 1966. *Mon. Not. R. astr. Soc.,* **132,** 267.

Doughty, N. A., Fraser, P. A. & McEachran, R. P., 1966. *Mon. Not. R. astr. Soc.,* **132,** 255.

Dreiling, L. A. & Bell, R. A., 1980. *Astrophys. J.,* **241,** 736.

Edmonds, F. N., Schluter, H. & Wells, D. C., 1967. *Mem. R. astr. Soc.,* **71,** 271.

Frisk, U., 1983. *PhD Thesis,* Stockholm University.

Frisk, U., Bell, R. A., Gustafsson, B., Nordh, H. L. & Olofsson, S. G., 1982. *Mon. Not. R. astr. Soc.,* **199,** 471.

Frogel, J. A., Persson, S. E., Aaronson, M. & Matthews, K., 1978. *Astrophys. J.,* **220,** 75.

Geltman, S., 1962. *Astrophys. J.,* **136,** 935.

Gigas, D., 1986. *Astr. Astrophys.,* **165,** 170.

Glass, I. S., 1973. *Mon. Not. R. astr. Soc.,* **164,** 155.

Glass, I. S., 1974a. *Mon. Notes astr. Soc. Sth Afr.,* **33,** 54.

Glass, I. S., 1974b. *Mon. Notes astr. Soc. Sth. Afr.,* **33,** 71.

Gray, D. F., 1976. *The Observation and Analysis of Stellar Photospheres,* John Wiley and Sons.

Gunn, J. E. & Stryker, L. L., 1983. *Astrophys. J. Suppl. Ser.,* **52,** 121.

Gustafsson, B., Bell, R. A., Eriksson, K. & Nordlund, Å., 1975. *Astr. Astrophys.,* **42,** 407.

Gustafsson, B. & Bell, R. A., 1979. *Astr. Astrophys.,* **74,** 313.

Gustafsson, B., Kjærgaard, P. & Andersen, S., 1974. *Astr. Astrophys.,* **34,** 99.

Hansen, L. & Kjærgaard, P., 1971. *Astr. Astrophys.,* **15,** 123.

Hayes, D. S., 1985. *Calibration of Fundamental Stellar Quantities, IAU Symp. No. 111,* p. 225, ed. Hayes, D. S., Pasinetti, L. E. & Philip, A. G. D., Reidel, Dordrecht.

Hayes, D. S. & Latham, D. W., 1975. *Astrophys. J.,* **197,** 593.

Hoffleit, D., 1982. *Catalogue of Bright Stars,* Yale University Press, New Haven, Conn.

Johnson, H. L., 1965. *Astrophys. J.,* **141,** 923.

Johnson, H. L., 1966. *Ann. Rev. Astr. Astrophys.,* **4,** 193.

Johnson, H. L. & Mitchell, R. I., 1975. *Rev. Mex. Astr. Astrofis.,* **1,** 299.

Johnson, H. L., Mitchell, R. I. & Latham, A S., 1967. *Communs Lunar planet. Lab.*, **6**, 85.
Johnson, H. L., Mitchell, R. I., Iriarte, B. & Wisniewski, W., 1966. *Communs Lunar planet. Lab.*, **4**, 99.
Keenan, P. C., 1985. *Calibration of Fundamental Stellar Quantities, IAU Symposium No. 111*, p. 121, eds Hayes, D. S., Pasinetti, L. E. & Philip, A. G. D., Deidel, Dordrecht.
Keenan, P. C. & McNeil, R. C., 1976. *An Atlas of Spectra of the Cooler Stars*, Ohio State University Press.
Kjærgaard, P., Gustafsson, B., Walker, G. A. H. & Hultquist, L., 1982. *Astr. Astrophys.*, **115**, 145.
Kurucz, R. L., 1979. *Astrophys. J. Suppl. Ser.*, **40**, 1.
Kurucz, R. L., 1986. *Highlights of Astronomy*, **7**, 827.
Kurucz, R. L. & Peytremann, E., 1975. *SAO Special Report No. 362.*
Lambert, D. L. & Ries, L. M., 1981. *Astrophys. J.*, **248**, 228.
Leggett, S. K., Batholomew, M., Mountain, C. M. & Selby, M. J., 1986a. *Mon. Not. R. astr. Soc.*, **223**, 443.
Leggett, S. K., Mountain, C. M., Selby, M. J., Blackwell, D. E., Booth, A. J., Haddock, D. J. & Petford, A. D., 1986b. *Astr. Astrophys.*, **159**, 217.
Lengyel-Frey, D., 1977. *PhD Thesis*, University of Maryland.
Magain, P., 1983. *Astr. Astrophys.*, **122**, 225.
Manduca, A. & Bell, R. A., 1979. *Publs. astr. Soc. Pacif.*, **91**, 848.
Manduca, A., Bell, R. A. & Gustafsson, B., 1981. *Astrophys. J.*, **243**, 883.
Matthews, T. A. & Sandage, A. R., 1963. *Astrophys. J.*, **138**, 30.
Mountain, C. M., Leggett, S. K., Selby, M. J., Blackwell, D. E. & Petford, A. D., 1985. *Astr. Astrophys.*, **151**, 399.
McClatchey, R. A., Benedict, W. S., Slough, S. A., Burch, D. E., Calfee, R. F., Fox, K., Rothman, L. S. & Garing, J. S., 1973. *AFCRL Atmospheric Absorption Line Parameter Compilation*, **AFCRL-TR-73-0096**, Bedford, Mass.
Neckel, T. & Chini, R., 1980. *Astr. Astrophys. Suppl.*, **39**, 411.
Nissen, P. E., 1981. *Astr. Astrophys.*, **97**, 145.
Nissen, P. E., Edvardsson, B. & Gustafsson, B., 1985. *Production & Distribution of C, N, O Elements, Proc. of ESO workshop*, p. 131, eds Danziger, I. J., Matteucci, F. & Kjar, K., ESO, Garching.
Oke, J. B., 1964. *Astrophys. J.*, **140**, 689.
Piccirillo, J., Bernat, A. P. & Johnson, H. R., 1981. *Astrophys. J.*, **246**, 246.
Ridgway, S. T., Joyce, R. R., White, N. M. & Wing, R. F., 1980. *Astrophys. J.*, **235**, 126.
Ridgway, S. T., Jacoby, G. H., Joyce, R. R., Siegel, M. J. & Wells, D. C., 1984. *Astr. J.*, **87**, 1044.
Saxner, M. & Hammarbäck, G., 1985. *Astr. Astrophys.*, **151**, 372.
Selby, M. J., Mountain, C. M., Blackwell, D. E., Petford, A. D. & Leggett, S. K., 1983, *Mon. Not. R. astr. Soc.*, **203**, 795.
Shallis, M. J. & Blackwell, D. E., 1979. *Astr. Astrophys.*, **79**, 48.
Smith, P. L., 1976. *Mon. Not. R. astr. Soc.*, **177**, 275.
Sopar, A. & Malyuto, V., 1974. *Publs. Tartu Obs.*, **42**, 91.
Stilley, J. L. & Calloway, J., 1970. *Astrophys. J.*, **160**, 245.
Strecker, D. W., Erickson, E. F. & Witteborn, F. C., 1979. *Astrophys. J. Suppl.*, **41**, 501.
Sturch, C., 1966. *Astrophys. J.*, **143**, 774.
Swensson, J. S., Benedict, W. S., Delbouille, L. & Roland, G., 1970. *Mem. Soc. Roy. Liège*, Special Vol. No. **5**.
Tomkin, J., Lambert, D. L. & Balachandra, S., 1985. *Astrophys. J.*, **290**, 289.
Traub, W. A. & Stier, M. T., 1976. *Appl. Optics*, **15**, 364.
VandenBerg, D. A. & Bell, R. A., 1985. *Astrophys. J. Suppl.*, **58**, 561.
Wennfors, B., 1986. *PhD Thesis*, Stockholm Observatory, Sweden.
White, N. M. & Kreidl, T. J., 1984. *Astr. J.*, **89**, 424.
Wing, R. F., 1967. *PhD Thesis*, University of California, Berkeley, CA, USA.
Wing, R. F., 1971. *Kitt Peak Nat'l Obs. Contrib. No. 554*, p. 145, Proc. Conf. Late-Type Stars, ed. Lockwood, G. W. & Dyck, H. M., Tucson.
Wing, R. F., Gustafsson, B. & Eriksson, K., 1985. *Calibration of Fundamental Stellar Quantities, IAU Symposium No. 111*, p. 571, eds Hayes, D. S., Pasinetti, L. E. & Philip, A. G. D., Reidel, Dordrecht.
Wishart, A. W., 1979. *Mon. Not. R. astr. Soc.*, **187**, 59P.
Wu, C.-C., Ake, T. B., Boggess, A., Bohlin, R. C., Imhoff, C. L., Holm, A. V., Levay, G., Panek, R. J., Schiffer, F. H. & Turnrose, B. E., 1983. *The* IUE *Ultraviolet Spectral Atlas*, IUE *NASA Newsletter No. 22.*

Appendix A: Transformation equations

Bessell & Brett (1987, hereafter BB87) have discussed transformation equations between various colour systems. From their work we have:

$K_J = K_G + 0.013 - 0.007\,(V-K)$,

and

$$K_{CIT} = K_G - 0.018 + 0.002\,(V-K).$$

Similar very small colour terms are found in the synthetic colour results, namely

$$K_J = K_G + 0.003\,(V-K)$$

and

$$K_{CIT} = K_G - 0.005\,(V-K),$$

from the models 4000/1.5/0.0, 4500/2.25/0.0, 5000/3.0/0.0 and 5500/3.0/0.0, based on the Vega zero point.

Similarly, BB87 find

$$(V-K)_G = 0.013 + 0.993\,(V-K)_J,$$

and

$$(V-K)_{CIT} = 0.018 + 0.998\,(V-K)_G.$$

The data presented in Tables 9 and 10 give

$$(V-K)_G = -0.002 + 1.003\,(V-K)_J$$

and

$$(V-K)_{CIT} = -0.006 + 1.005\,(V-K)_G.$$

In other words, both the calculated and observed $(V-K)$ colours of the three systems are very similar.

There is also good agreement between the calculated and observed $(J-K)$ colours of the three systems. BB87 find the Glass and Johnson systems to be identical, whereas the CIT system gives colours which are about 0.05 mag bluer. We find the calculated Glass colours to be intermediate between the Johnson and CIT colours, with a difference of about 0.02 mag between each. The Glass and CIT $H-K$ colours are also predicted to be very similar, but we do not find the CIT $J-H$ colours to be much redder than the Glass ones. The difference quoted by BB87 is nearly 0.1 mag for the 4000 K models, whereas Tables 9 and 10 show a difference of only about 0.02 mag. Finally, we see that the Johnson system is predicted to give rather bluer $K-L$ colours than do the other two systems, by about 0.02 mag at $T_{eff} = 4000$ K. This difference is small but was seen by BB87. BB87 also found $K-L = 0.03 + 0.040\ (V-K)$, whereas the models predict a smaller coefficient of $V-K$, about 0.03.

BB87 present a Table of mean colours for giant and dwarf stars. In addition to the infrared colours, they include Cousins $V-I$. Comparison of the giant star colours with those of the models 5500/3.0/0.0, 5000/3.0/0.0, 4500/2.25/0.0 and 4000/1.50/0.0, which are intended to represent a Population I giant branch, and using $V-K$ as the independent variable, shows that the $V-I$ colours of Table 11 are about 0.03 mag bluer than the colours of BB87 for the three hotter models. However, the synthetic colour of 4000/1.50/0.0 is at least 0.10 mag and probably about 0.13 mag bluer than the observed value. The comparison of temperatures derived from $V-I$ with those from the IRFM also showed that the synthetic Cousins colours are too blue. Some of this may be due to a zero point shift and, indeed, Vega (the zero point star) was observed by Bessell and not Cousins, but the reason for the excessive blueness of the coolest model is unknown.

As noted earlier, Sopar & Malyuto (1974) have suggested new sensitivity profiles for the Johnson RI bands. The synthetic colours predicted using these profiles can be compared with

Table A 1. Johnson system colours.

	Sopar and Malyuto response functions		Johnson response functions		Transformed from Cousins	
Model	$V-R$	$R-I$	$V-R$	$R-I$	$V-R$	$R-I$
4000/1.5/0.0	1.00	0.81	0.92	0.60	1.06	0.78
4500/2.25/0.0	0.76	0.63	0.69	0.47	0.83	0.61
5000/3.0/0.0	0.62	0.51	0.57	0.39	0.68	0.50
5500/3.0/0.0	0.50	0.41	0.46	0.32	0.56	0.41
9650/3.9/0.0	−0.04	0.00	−0.04	0.00	0.06	−0.05

Johnson colours obtained from the transformation of observed Cousins colours. To do this, we use Bessell's (1983) transformation equations derived from observations by Neckel & Chini (1980). Bessel states that these data resemble the Johnson system very closely in the F0–K5 region. The results for the Population I giant branch models are given in Table A1.

A comparison of the $(V-R)_J$ and $(R-I)_J$ colours predicted using Bessell's transformation of the Cousins colours shows that there is much better agreement with the Sopar & Malyuto version of the Johnson R and I response functions than with the original Johnson response functions. There does, however, seem to be some problems with the zero point. This may be partly due to the normalization of our colours to the curiously blue $V-R$ $(=-0.04)$ colour of Vega.